OPEN ACCESS
IOP Publishing | IMMT
International Journal of Extreme Manufacturing
Int. J. Extrem. Manuf. **4** (2022) 022003 (43pp)
https://doi.org/10.1088/2631-7990/ac5f78

Topical Review

The fabrication, characterization and functionalization in molecular electronics

Yi Zhao[1], Wenqing Liu[1], Jiaoyang Zhao[1], Yasi Wang[2], Jueting Zheng[1], Junyang Liu[1,2,*], Wenjing Hong[1,2] and Zhong-Qun Tian[1,2]

[1] State Key Laboratory of Physical Chemistry of Solid Surfaces, College of Chemistry and Chemical Engineering, Xiamen University, Xiamen 361005, People's Republic of China
[2] Innovation Laboratory for Sciences and Technologies of Energy Materials of Fujian Province (IKKEM), Xiamen 361005, People's Republic of China

E-mail: jyliu@xmu.edu.cn

Received 11 November 2021, revised 4 January 2022
Accepted for publication 21 March 2022
Published 8 June 2022

Abstract

Developments in advanced manufacturing have promoted the miniaturization of semiconductor electronic devices to a near-atomic scale, which continuously follows the 'top-down' construction method. However, huge challenges have been encountered with the exponentially increased cost and inevitably prominent quantum effects. Molecular electronics is a highly interdisciplinary subject that studies the quantum behavior of electrons tunneling in molecules. It aims to assemble electronic devices in a 'bottom-up' manner on this scale through a single molecule, thereby shedding light on the future design of logic circuits with new operating principles. The core technologies in this field are based on the rapid development of precise fabrication at a molecular scale, regulation at a quantum scale, and related applications of the basic electronic component of the 'electrode–molecule–electrode junction'. Therefore, the quantum charge transport properties of the molecule can be controlled to pave the way for the bottom-up construction of single-molecule devices. The review firstly focuses on the collection and classification of the construction methods for molecular junctions. Thereafter, various characterization and regulation methods for molecular junctions are discussed, followed by the properties based on tunneling theory at the quantum scale of the corresponding molecular electronic devices. Finally, a summary and perspective are given to discuss further challenges and opportunities for the future design of electronic devices.

Keywords: molecular electronics, molecular junction, molecular electronic device, fabrication and functionalization

* Author to whom any correspondence should be addressed.

2631-7990/22/022003+43$33.00

1. Introduction

The pursuit of higher performance and lower cost silicon-based electronic devices has been the best motivation for continuous miniaturization and integration, with the developments of state-of-art manufacturing technologies in the semiconductor industry [1, 2]. With the approach of sub-5 nm nodes in the complementary metal-oxide-semiconductor (CMOS) chip manufacturing, the size and machining accuracy of CMOS-based devices gradually enter molecular and even atomic scales [2–7] (left in figure 1). However, to keep pushing the limit into this scale, the quantum tunneling effect especially that between source and drain electrodes will ultimately become obvious and nonnegligible [8, 9]. Therefore, to further extend Moore's Law and even surpass it, new operating principles of electronic devices based on quantum tunneling effects need to be considered. At this point, molecular electronics and the corresponding developed research tools may offer future opportunities, demonstrating a new operating strategy for 'Beyond CMOS' [10, 11] (right in figure 1). Molecular electronics is a highly interdisciplinary subject that studies charge tunneling behavior through single molecules [12, 13], supramolecules [14] and even clusters [15]. With precise sub-nanometer and even atomic structural adjustments on molecular electronic devices, their electric properties can be highly controlled and manipulated [12, 16]. Firstly, since the size of a molecule is usually sub-3 nm and even at the atomic scale, using molecular electronic devices to replace traditional silicon semiconductor devices may bring a new revolution in device miniaturization [16–19]. Secondly, molecules with various chemical structures exhibiting various properties can be designed and synthesized in large quantities through organic synthesis. Thus some new functional molecular devices such as sensors [18], actuators [20] and optoelectronic devices [21, 22] can be developed [12]. Thirdly, some novel quantum effects emerge at the scale of the molecular electronic device, which can be used as new working principles for the construction of quantum devices that are different from semiconductor devices working on conventional principles, such as the tunneling field-effect transistor (FET), spintronic devices and so on [17–19], demonstrating a new operating strategy for 'Beyond CMOS' [23].

In the study of molecular electronics, how to realize the connection between single-molecule and external measuring circuits to form the stable 'electrode–molecule–electrode junction' (abbreviated as molecular junction) [24, 25], how to accurately obtain and regulate the electric signal of the molecular junction [26, 27], and how to fabricate the corresponding high-performance devices [12, 16, 18] are the key scientific issues that need to be solved (figure 2). On the one hand, understanding the charge transport through single-molecule junctions is the first step in establishing single-molecule electronics. This requires reliable contact between the atomic-scale electrodes with the target molecules: firstly, the electrodes require precise control to fit the size of molecules and even tune their conformation; secondly, the molecules should be modified with anchoring groups at both ends for a better connection. Both requirements demand a certain degree of atomic precision control. Since the 1980s, many experimental approaches for the preparation of atomic-scale metal point contacts and the technologies of single-molecule manipulation have been proposed, such as the scanning tunneling microscope break junction (STM-BJ) [28–32], conductive probe atomic force microscope break junction (cpAFM-BJ) [33–38], mechanically controllable break junction (MCBJ) [39–45], micro-electromechanical systems-based break junction (MEMS-BJ) [46, 47], electromigration junction (EMJ) [48–52], on-wire photolithography [53], carbon nanotubes (CNTs) [54–57] and graphene-based electrodes [58–60], etc, offering unique platforms to connect single-molecule into measuring circuits. Besides, with the developments of organic synthesis, researchers are able to add the anchoring groups, such as thiol, methylthiol, pyridyl, amino, etc, onto different connection sites of the functional molecular backbone, which enables covalent or coordinate bonding to the electrodes [61, 62]. On the other hand, from the perspective of the application, the developed platforms for molecular junctions provide technical advantages for manipulating and regulating the properties of single-molecule, offering single-molecule sensing and recognition [63, 64], single-molecule electrochemical behavior [19], chemical reactions at the single-molecule scale [65, 66] and other frontier directions and fields. Some new concepts of charge transport based on quantum mechanisms have also been discovered, such as Coulomb blockade [67, 68], the Kondo effect [69], quantum interference (QI) [70–73], thermoelectricity [74–77], thermoconductance [78–81] and spintronics [82]. In addition, the study of charge transport properties at the single-molecule scale will also help us deepen our understanding of the electrical properties of organic electronics and optoelectronic materials, which assists in the optimization of the properties of these materials for applications to organic electronics [83, 84] or organic light emitting diodes [85] and other fields.

In this review, we will focus on the basic concept of molecular electronics to provide a comprehensive summary of the manufacturing and regulation approaches even to the molecular/atomic scale in this field. In section 1, we briefly introduce the research background of molecular electronics. In section 2, we briefly describe the theoretical background of the charge transport mechanism in molecular electronics. In section 3, we comprehensively summarize the fabrication methods of molecular junctions, divided into three categories, including static junctions, dynamic junctions and large-scale array junctions. Section 4 discusses the characterization and regulation of molecular electronics at the atomic scale. Section 5 is the functionalization of molecular junctions, that is, various molecular devices including molecular rectifiers, optical switches, transistors, etc. Finally, we briefly summarize some challenges and opportunities in this field. This review aims to provide researchers with basic knowledge about the fabrication, characterization and regulation of molecular junctions to help their further research on the molecular and even atomic scale.

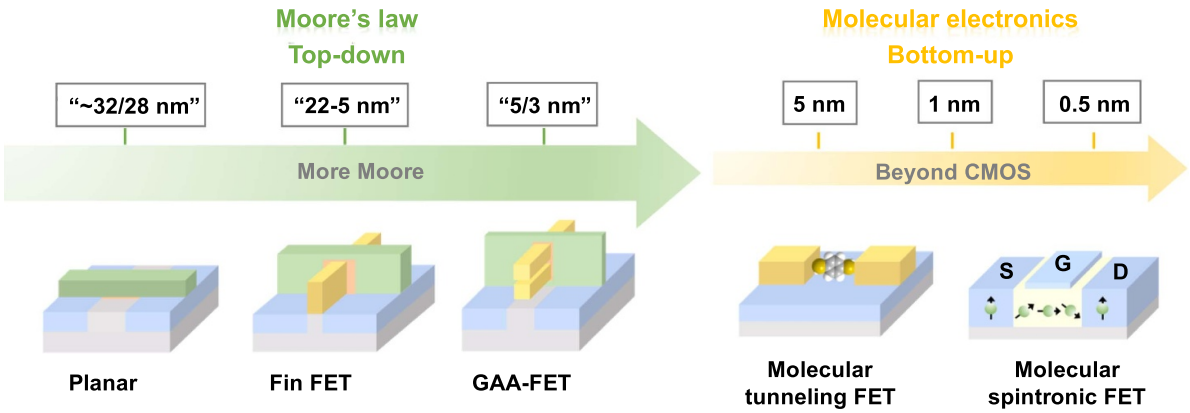

Figure 1. Molecular electronics, a potential candidate for 'Beyond CMOS'. The Fin FET was named because the source/drain region forms structures like fins on the silicon surface. The GAA-FET means 'Gate-All-Around FET'.

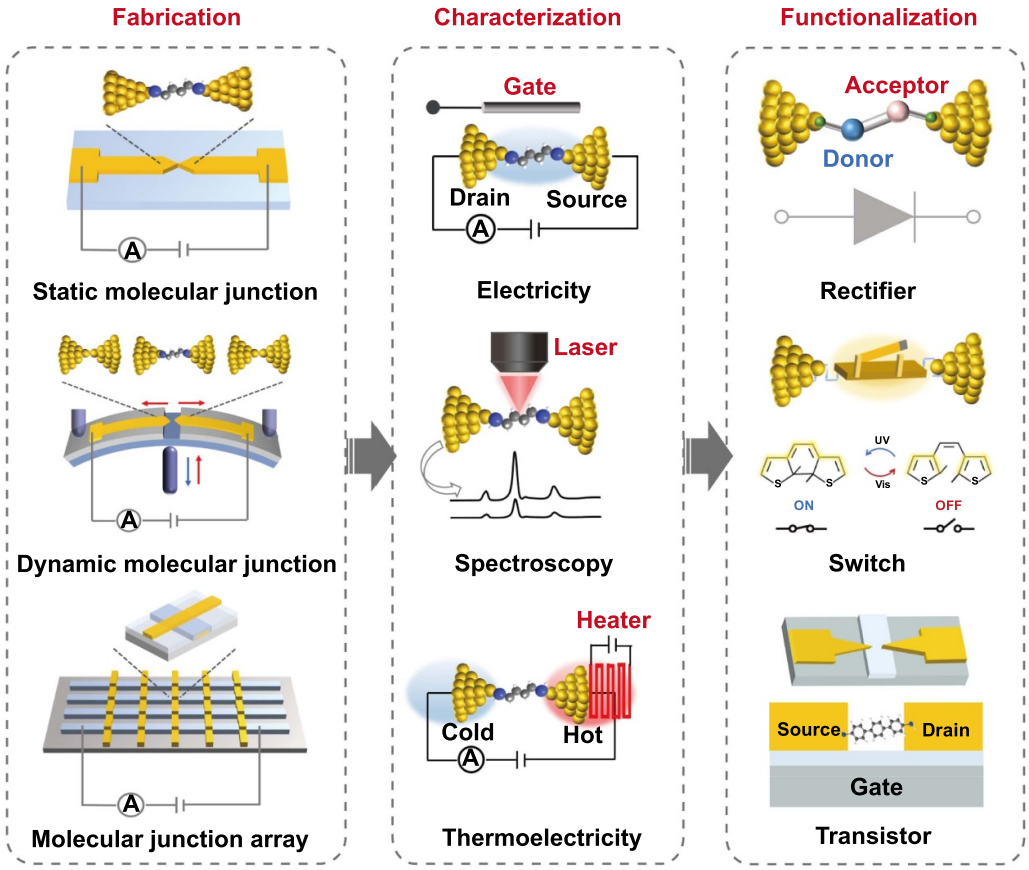

Figure 2. Three essential aspects of molecular electronics: fabrication, characterization and functionalization.

2. Research background

Since the scale of molecules is generally below 3 nm, the electrical properties of molecules in this case no longer follow Ohm's law from conventional macroscopic conductors. At this scale, the quantum effects start to play a leading role in the charge transport of molecules. In this section, the theoretical background of charge transport mechanisms of nanoscale conductors, such as the atomic point contact of metal electrodes and molecular junctions, is briefly described.

2.1. Electric transport mechanism of the molecular junction

When the point contact of the metal atoms is broken, two electrodes with atomic-scale tips are formed, and the gap between the electrode pairs can be adjusted by a particular method to match the target molecule. The two ends of the target molecule are designed with anchoring groups, and the electrode and molecule are connected by the interaction between the anchoring groups and the metal electrode. Thus, the molecular junction can be constructed to obtain the connection between molecules and external measuring circuits [24].

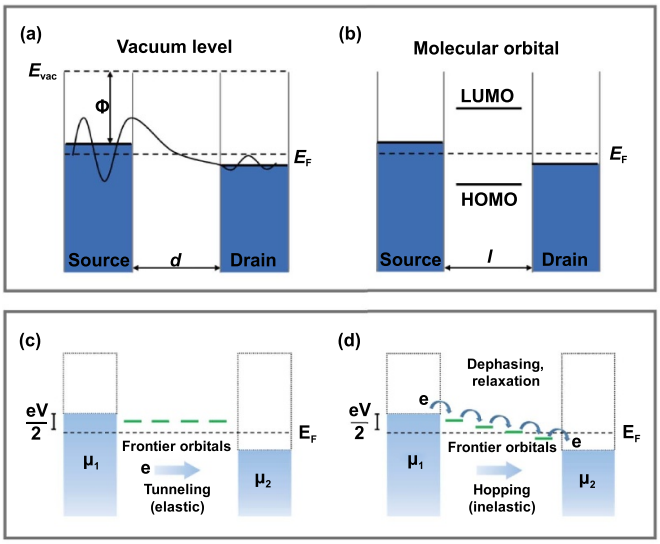

Figure 3. Schematic of electron tunneling through (a) vacuum and (b) (1, 4-benzenedithiol) BDT molecule junction and schematic of transport mechanisms in molecular junctions: (c) direct tunneling and (d) hopping tunneling.

It is worth noting that the transport mechanism of electrons in molecular junctions is more complex than that in metal atomic point contact, depending not only on the transport properties of the electrons on the molecular framework itself but also on the coupling degree between the anchoring group and the metal electrode. Therefore, charge transport in molecular junctions may follow different mechanisms.

In the case of metal contact with no molecules, as shown in figure 3(a), electrons tunnel through a vacuum barrier between two electrodes and the tunneling conductance generated by the vacuum tunneling of electrons in the nanogap can be obtained from:

$$G = G_0 \mathrm{e}^{-\beta_T d} \tag{1}$$

where d is the distance traveled by the electron tunneling, and β_T represents the tunneling decay constant, which is determined by the height of the barrier between the energy states.

For the case of the tunneling through molecular junction, as illustrated in figure 3(b), analogous to the equation of tunneling current in the absence of molecular, its conductance can be described by the following equation:

$$G = A\mathrm{e}^{-\beta_1 l} \tag{2}$$

where G is the conductance of the molecular junction, A corresponds to G_0 in vacuum tunneling, which can be analogous to contact resistance and is related to the coupling degree of molecules and electrodes, l is the length of the molecular junction and β_1 is the tunneling decay constant of the molecule. In experiments, the value of β_1 is usually determined by testing the conductance of the same type of molecules with different lengths. Generally, for molecules with a larger highest occupied molecular orbital–lowest unoccupied molecular orbital (HOMO–LUMO) gap, the β_T is also larger, and for conjugated molecules, the HOMO–LUMO gap is smaller, and β_T is also smaller [86].

According to the interaction between electrons and molecules, the transport mechanism of electrons in molecular junctions can be separated into two types: coherent transport (the coherence of electrons is preserved during transport through molecules) and incoherent transport (the coherence of electrons is destroyed when passing through molecules).

For short molecules such as 1,4-benzenedithiol (BDT), due to their relatively large HOMO–LUMO gap, electrons have a high probability to directly pass through the molecule in the way shown in figure 3(c) without inelastic interaction with the molecule, so that the coherence of electrons is maintained. For long molecules (usually >3 nm) with a smaller HOMO–LUMO gap or a small energy barrier between the transport orbit and the Fermi level, the electrons are more likely to be scattered by the electrons or atoms in the molecule, so that the electron changes from one eigenstate to another. This inelastic scattering process destroys the coherence of the electronic phase and changes the phase of the electron (figure 3(d)). Under this condition, the charge transport will be dominated by a hopping mechanism [87, 88].

2.2. QI in electric transport in the single-molecule junction

Coherent transport maintains the phase of electrons passing through the molecular junction, which makes QI possible in the process of single-molecule electron transport. The phenomenon of QI brings opportunities to the development of high-performance molecular devices. In this section, we will introduce the QI effect in single-molecule charge transport.

Interference is a characteristic of propagating waves. Similarly, in molecular electronics, scientists have also found the QI effect, which is caused by the interaction of electron wave functions from different paths through the molecule during propagation. As shown in figure 4(a), taking the benzene ring molecule as an example which is a common model in molecular electronics, when electrons pass through the *meta*-connected benzene (right column of figure 4(a)), the wave function of the transport paths indicated by the red arrow and the blue arrow are in opposite phases after superposition. Therefore, the transmission probability of electrons will drop sharply to form a dip around the electrode Fermi level (green line in figure 4(b)). That is, an anti-resonance transport feature with ultralow conductance will be formed. This phenomenon is called destructive quantum interference (DQI). In contrast, when the wave functions of electrons pass through the *para*-connected benzene (left column of figure 4(a)), the two paths have the same phase, therefore the transmission probability of electrons is relatively smooth after superposition (red line in figure 4(b)), which is known as constructive quantum interference (CQI) [89].

The QI effects were first predicted by theorists [90]. However, the single-molecule conductance value is often below 10^{-5} G_0 when the DQI effect exists. It is not easy to experimentally test those molecular systems exhibiting DQI. It was not until 2011 that the Wandlowski group experimentally observed this phenomenon for the first time [91]. The

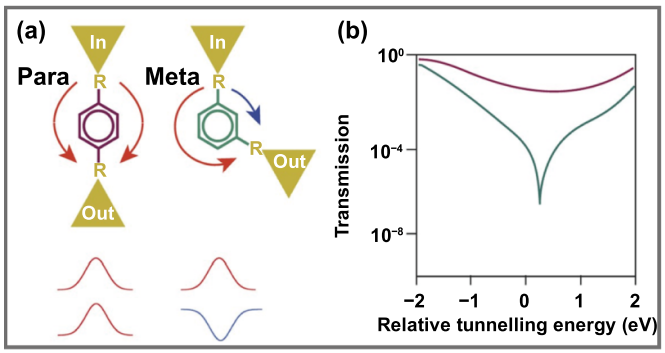

Figure 4. Explanatory diagrams for quantum interference phenomena: (a) phase diagram of wave functions passing through two transport paths of benzene ring molecules (R represents the anchoring group bound to the electrode) and (b) electron transmission probability curves of *para*-linked molecules (red) and *meta*-linked molecules (green). Reproduced from [89], with permission from Springer Nature.

phenomenon of QI enables conductance modulation at a large scale, which brings opportunities for the development of high-performance molecular devices. Since then, different research groups have used different methods to control the QI effect to achieve different molecular device functions [43, 60, 71, 72, 92, 93]. The characterization and regulation of QI in charge transport through the single-molecule junction will be discussed in section 4.

3. Fabrication of molecular junctions

The molecular junction is the fundamental component of the molecular electronic device. Therefore, the construction of molecular junctions is the core issue in molecular electronics [24, 25]. The ideal construction method of an electrodes pair with a nanogap for wiring the molecule needs to meet many requirements at the same time: (a) the size of the prepared nanogap can be down to 0–5 nm; (b) the nanogap can be prepared and controlled to fit different target molecules; (c) the material of the electrode pair can be replaced; (d) the prepared electrode pair has strong interactions with the target molecule through anchoring groups and (e) the instrument is simple, low in cost and fast in processing [26].

The existing fabrication methods of molecular junctions are mainly divided into two major categories. The first is a series of 'static molecular junction' techniques prepared with fixed electrodes in which the distance cannot be adjusted directly. This kind of molecular junction can be simply fabricated by several steps of micro and nano fabrication, and it is flexible and convenient to use [48, 54, 58]. The second type is the 'dynamic molecular junction' based on the repeated opening and closing of metal electrodes to realize the multiple and repeated construction of single-molecule junctions. This kind of method can repeatedly open and close the electrodes pair a large number of times, which is helpful for the acquisition of a large number of conductance data for statistical analysis, thus obtaining highly reliable electrical transport properties of the molecular junction [31, 32, 37, 38]. We compared the typical molecular junction fabrication methods for these two types and summarized them in the radar diagram shown in figure 5. It is clear that each method has its own unique advantages and disadvantages. Furthermore, in the final part of this section, we also introduce some large-area array methods developed based on molecular junction construction methods. This type of molecular junction has realized the progress from one-dimensional (1D) isolated electrodes to two-dimensional (2D) cross-logic circuits, which is helpful for the final realization of large-scale molecular integrated circuits. Next, we will discuss these three fabrication categories in detail [94, 95].

3.1. Static molecular junction

The static molecular junction is composed of two parts: fixed nanogaps and self-assembled molecules. Therefore, the construction methods of static molecular junctions can be divided into two categories according to the sequence of the construction of nanogaps and the assembling of molecules. One is to assemble molecules on the metal substrate (one electrode) first and then construct another electrode [99, 100]. For example, liquid metal gallium indium eutectic alloy (EGaIn) electrode technology builds the molecular junction by pulling the EGaIn tip as the top electrode on the substrate which has assembled molecules in advance [101]. This kind of method does not rely on complex micro and nano manufacturing technology and has high yield and good repeatability. The other is to construct the electrode pair with the nanogap first and then assemble molecules within the gap [48, 54, 58]. For example, EMJs [50] and carbon-based junction methods [66, 102–104], etc, firstly form gaps on metal or carbon material wires through electromigration (EM), oxygen plasma, focused ion beam (FIB) and other fabrication techniques, and then assemble molecules inside the nanogap for measurement. In this section, we will briefly introduce several common methods for the construction of static molecular junctions.

3.1.1. EMJ. EM is usually a physical phenomenon in which some atoms in the conductor or semiconductor material move or diffuse under the action of an external electric field. This phenomenon occurs when scattering at a defect in the lattice causes momentum transfer between the electron and the atom, and then the atom is pushed in the opposite direction to the current, which results in cavities or whiskers (hillocks) in certain parts of the conductor, as the process in figures 6(a) and (b) shows [18]. EM has always been regarded as a serious failure mode of metal interconnections in integrated circuits since its discovery [105]. Nevertheless, considering the ability to break a metal conductor into a face-to-face electrode pair, EM has been adopted to construct nanoscale gaps on metal nanowires in molecular electronics [49, 50]. The general process of constructing a molecular junction through EM driven by an external electric field is shown in figures 6(c) and (d). At the beginning, a voltage is applied on either side of the electrode and its resistance is monitored. When the electrode is thinned enough for its resistance to change by of ΔR, the program will start scanning the voltage again from the low voltage

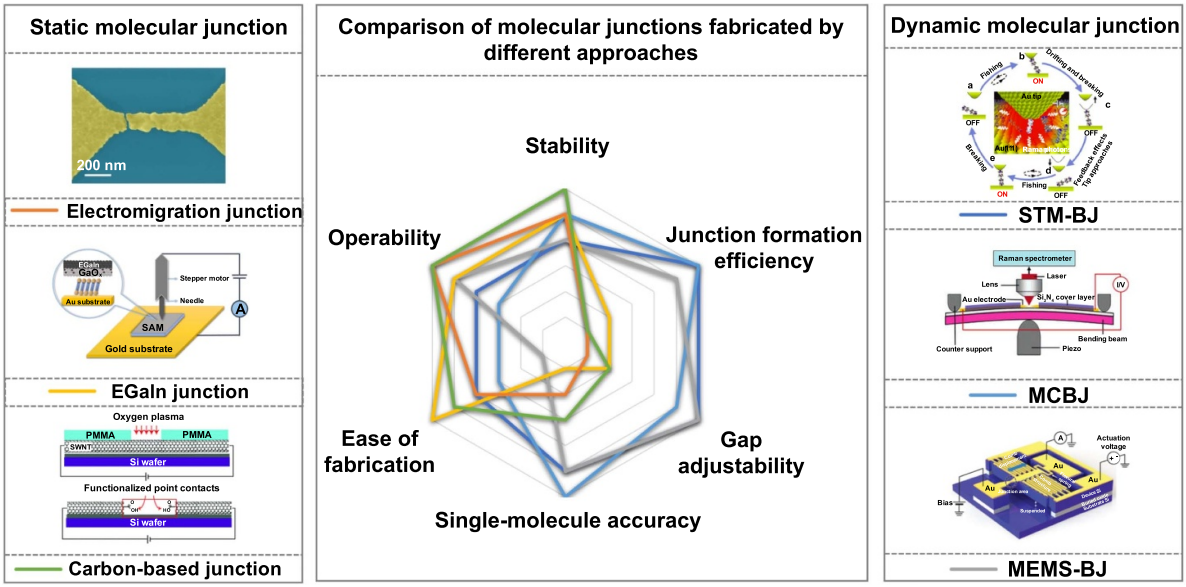

Figure 5. Comparison of different molecular junctions fabricated by different approaches (center column); several typical static molecular junctions such as the electromigration junction (left column). Reproduced from [52], with permission from Springer Nature. EGaIn junction and carbon-based junction; [96] John Wiley & Sons. © 2019 SIOC, CAS, Shanghai, & WILEY-VCH Verlag GmbH & Co. KGaA, Weinheim; [66] John Wiley & Sons. © 2021 SIOC, CAS, Shanghai, & WILEY-VCH GmbH. Several typical dynamic molecular junctions such as STM-BJ, MCBJ and MEMS-BJ (right column); Reproduced from [97]. CC BY-NC-SA 3.0. Reprinted with permission from [98]. Copyright (2006) American Chemical Society. [47] John Wiley & Sons. © 2020 WILEY-VCH Verlag GmbH & Co. KGaA, Weinheim.

(figure 6(c)); As the electrode is thinned to an atomic-scale size, it spontaneously breaks under a constant low-bias voltage (figure 6(d)) until the conductance plateaus near 1 G_0, indicating the formation of atomic-scale contacts [18].

The initial way to use EM to prepare a metal nanoelectrode pair is to break the metal nanowires by continuously increasing the applied bias voltage. In 1999, Park *et al* first reported the EM-fabricated molecular junction method [51], as shown in figure 6(e). Using this technique, they successfully prepared a metal electrode pair with a typical gap of ∼1 nm. However, since the migration process is uncontrollable, the fusion of nanowires usually occurs due to the excessive heat under high-bias voltage, leaving large gaps which are unable to wire molecules, causing a relative low success rate of generating molecular junctions. Therefore, how to effectively control the gap size of the EMJ is a crucial issue. Over the past years, researchers have tried many approaches to optimize the EM process.

At present, the most common and direct approach to control the gap distance of fracture is from the perspective of migration current control. The main control schemes include feedback-controlled electromigration (FBEM) [106–111], inversed-feedback-controlled electromigration (iFBEM) [112] and self-breaking [113, 114]. Strachan *et al* developed an FBEM method that simply controls the gap size by monitoring the resistance change during the repeatedly applied incremental voltage ramp [108] (figure 6(f)). Through this method, the width of the electromigrated nanogap was successfully controlled to as small as 1 nm. On this basis, Suga *et al* developed a new iFBEM technique combined with alternate polarity voltage operation [112] (figure 6(g)). Using this method, they have prepared Au nanogap electrodes with high crystallinity under low temperature and a hydrogen atmosphere. For the self-breaking scheme, the metal nanowire is first reduced to a few atoms through the FBEM method, and then the final breaking is spontaneously completed through the thermal fluctuation of the metal itself to avoid excessive heat generation. This method largely avoids the formation of metal clusters inside the nanogap. Through this method, O'Neill *et al* obtained extremely small nanogaps at sub-nanometer scale without residual metal clusters inside the gaps [113], as shown in figure 6(h).

In addition, there have been some attempts to improve the migration effect from the perspective of the feedback signal. First, noise analysis of the migration current signal has been introduced to determine the evolution stage of the conductor structure [115] (figure 6(i)). Wheeler *et al* observed in their experiments that for a large amount of molecular junction configuration, there are pronounced asymmetries between bias dependence and shot noise. This asymmetry demonstrates the critical role of nanoscale electron and ion heating in transport. Besides, to obtain better migration control effects by improving the response speed to the migration process, a programmable logic gate array (i.e. FPGA) chip was used to replace the traditional CPU processor to complete the measurement and control of the system [116] (figure 6(j)). Experiments showed that the cycle time of the control system based on FPGA is about 10^2 times shorter than that of the traditional FBEM process, so the heat can be well controlled without thermal runaway.

Since the EM process normally causes Joule heating, another way to realize the controllable preparation of an EM nanogap is to adjust the local temperature. Xiang *et al* found that the Joule heating power is linearly proportional to the

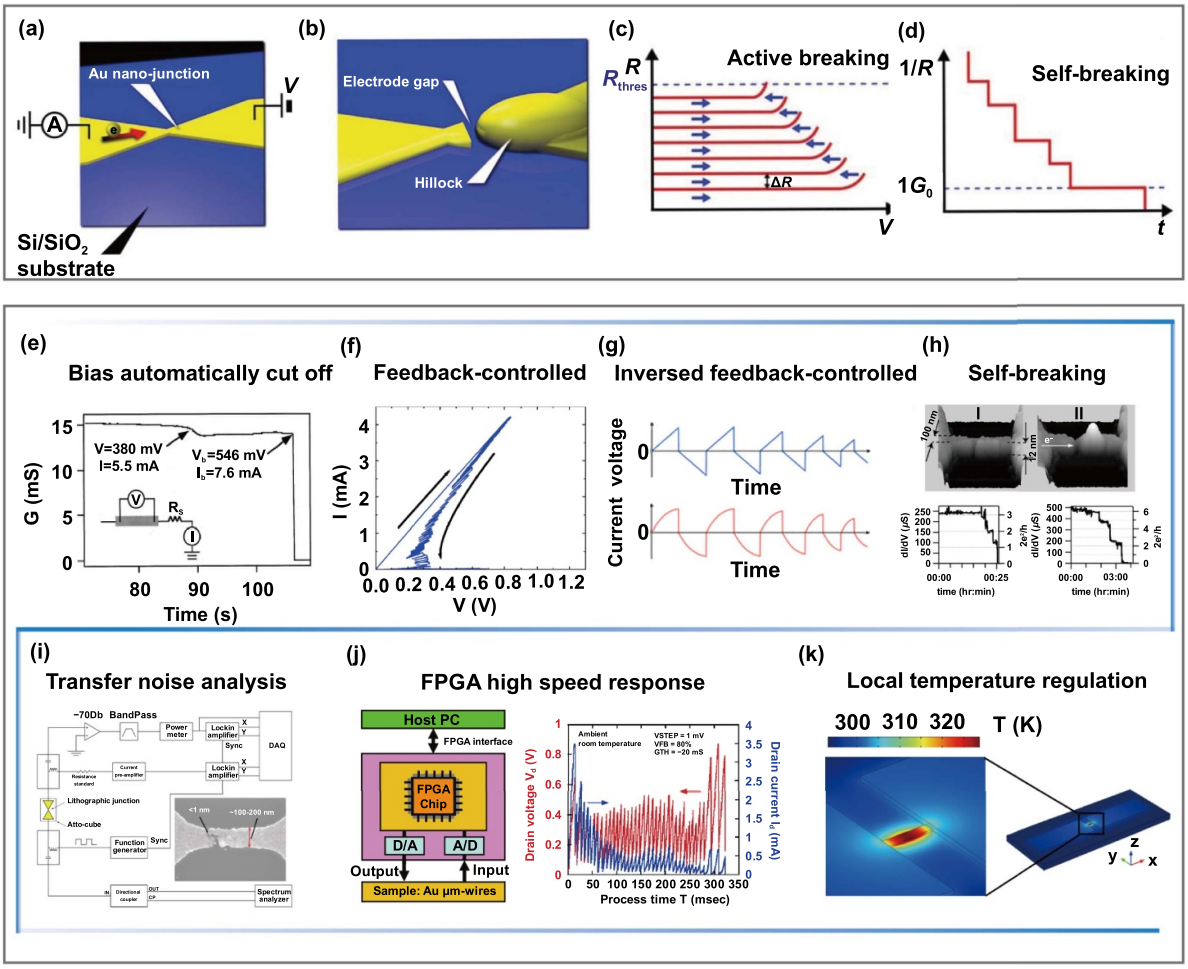

Figure 6. (a)–(d) Typical process of constructing a molecular junction through electromigration driven by an external electric field. Reproduced from [18]. CC BY-NC-SA 3.0. (a) Schematic of electrode before electromigration. (b) Schematic of electrode after electromigration. (c) The process of applying voltage repeatedly. (d) The process of self-breaking in low bias. (e)–(k) Electromigration process improvement route. (e) Bias automatically cut off. Reprinted with permission from [51]. Copyright (1999) AIP Publishing. (f) Feedback-controlled. Reprinted from [108], with the permission of AIP Publishing. (g) Inversed feedback-controlled. Reprinted with permission from [112]. Copyright (2020) American Chemical Society. (h) Self-breaking. Reprinted from [113], with the permission of AIP Publishing. (i) Transfer noise analysis. Reprinted figure with permission from [115], Copyright (2013) by the American Physical Society. (j) FPGA high-speed response. Reprinted with permission from [116]. Copyright (2014), American Vacuum Society. (k) Local temperature regulation method. Reprinted from [117], with the permission of AIP Publishing.

ambient temperature. More importantly, the local temperature in the nano-contraction depends in a parabolic manner on the ambient temperature. Through experiments, they finally realized the successful EM of gold nanowires at a variable temperature range from 4.2 K to room temperature [117], as shown in figure 6(k).

3.1.2. EGaIn junction. Another type of static molecular junction fabrication method is to firstly assemble the monolayer of the target molecule onto a bottom electrode, then cover the self-assembled monolayer (SAM) layer with another electrode to form the molecular junction. EGaIn technology is one such method using liquid metal as the top electrode, which has a large contact area, and is one of the common means of SAM electrical characterization. The construction methods of the EGaIn top electrode are mainly divided into two categories: one is the tapered tip formed by pulling the liquid metal [101, 118]. The second is a microfluidic solution based on micromachining technology [119–122].

For the measurement of electrical properties of molecular layers, the SAM is usually prepared on the surface of the bottom electrode, and then attached to the electrode on the other side to form a molecular junction [123, 124]. Therefore, to form a SAM junction, the upper electrode should be made onto the SAM layer. The traditional method normally uses metal sputtering or evaporation to deposit a metal layer (usually gold or titanium) on the surface of the SAM layer; however, this may destroy the intrinsic organic SAM layer, resulting in a short circuit [125].

To solve the problem of the possible damage to the SAM, researchers began to use liquid metal as the top electrode [100, 101]. At first, a liquid mercury drop as the top electrode was widely studied for its large electrode contact area, lack

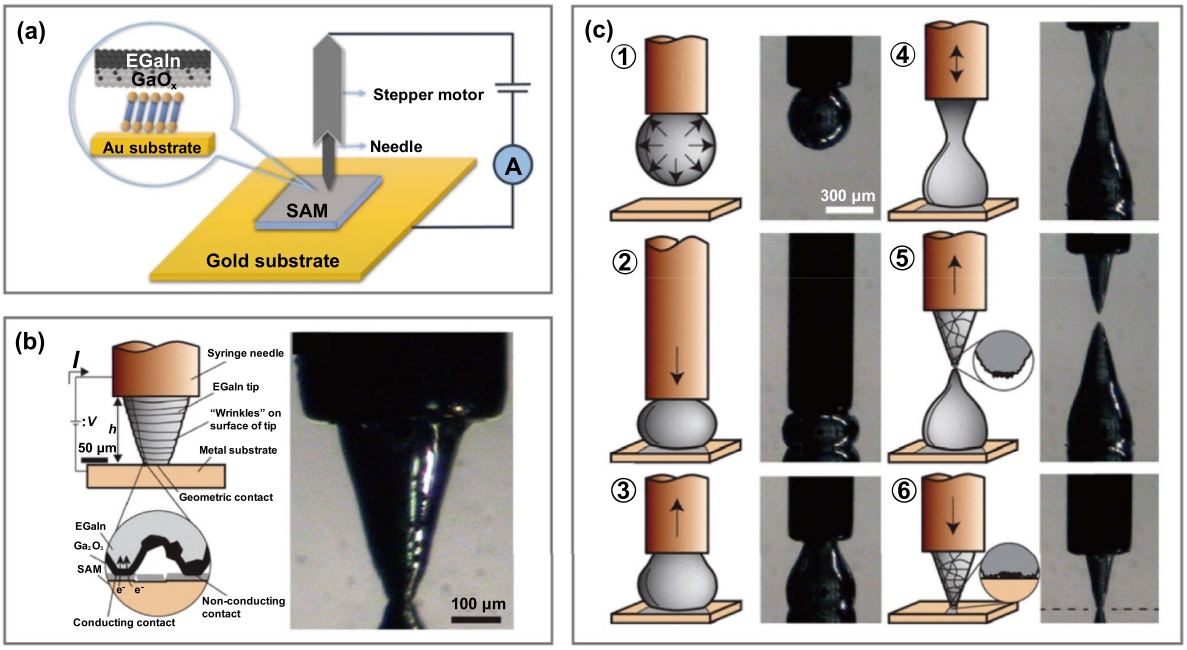

Figure 7. (a) Schematic of EGaIn testing device. [96] John Wiley & Sons. © 2019 SIOC, CAS, Shanghai, & WILEY-VCH Verlag GmbH & Co. KGaA, Weinheim. (b) Schematic diagram (left) and image (right) of EGaIn tapered tip; (c) schematic of fabrication of EGaIn tapered tip electrode and junction formation process. Reprinted with permission from [118]. Copyright (2018) American Chemical Society.

of damage to the sample surface and universality to different kinds of molecular systems [126]. For example, in 2001, Whitesides' group used the liquid metal mercury as the top electrode to construct an Ag–SAM–Hg sandwich structure, and measured the tunneling electron transfer rate of SAM [100]. However, there are great risks in experimental operation since Hg is a highly toxic substance. In addition, the fluidity of the Hg droplet is too strong thus causing dynamic changes of contact area, which easily lead to penetration into the bottom electrode from the defect of the SAM layer, also resulting in the short circuit of the device. To overcome this issue, a gallium indium eutectic alloy (eutectic GaIn, EGaIn) electrode has been developed. The EGaIn is a liquid at room temperature with its surface easily being oxidized to form Ga_2O_3, which can prevent metal penetration. Whitesides' group firstly adopted this non-toxic and non-volatile EGaIn material as the upper electrode to form the SAM junction [101], which has become widely used in recent years. Figure 7(a) gives the schematic of the EGaIn testing device [96]. They stretched a EGaIn droplet to form a needle tip, which greatly reduced the contact area between the tip and the SAM layer [118]. Thus, the short circuit rate during testing was significantly reduced, and the molecular junction (Ag–C_{10}SH–Ga_2O_3/EGaIn) was constructed, as shown in figures 7(b) and (c).

Due to the metallicity and fluidity of liquid metal, EGaIn can essentially be used and adjusted for various applications in microfluidics [127]. The use of microfluidic channels provides a convenient method for producing droplets in a controllable and repeatable manner. In 2010, Nijhuis *et al* designed and prepared a stabilized Ga_2O_3/EGaIn fluid in a microchannel in the transparent polymer polydimethylsiloxane (PDMS), which can be used to construct an SAM-based tunnel junction array [120, 121]. As shown in figure 8(a), the scheme is a cross-bar structure in which the bottom silver electrode is constructed by photolithography in advance, the top EGaIn electrode is constructed through the microchannel in the PDMS, and the SAM is placed between the two intersecting electrodes [120]. However, in this solution, since the bottom electrode needs to be patterned by photolithography, this may cause edge disorder and photoresist residue, which may lead to a defective SAM. In response to the above problems, Wan *et al* developed an EGaIn top electrode stabilized in a microscale through-hole PDMS mold, which is independent of the (non-patterned) bottom electrode, and additionally, the PDMS mould can be reused and recycled [122], as shown in figure 8(b). Karuppannan *et al* further optimized the bottom electrode in another way [119]. They reported a method for making micro-holes on an AlO_x-coated, template-stripped Au layer, based on a two-step etching process (figure 8(c)), which avoids direct contact between the Au surface and the photoresist during the manufacturing process.

3.1.3. Carbon-based molecular junction. So far, most molecular junctions are constructed from metals such as gold [30], silver [128, 129], platinum [130], etc. However, the contact formed between the metal and the molecule is likely to cause the molecular orbital to be broadened, leading to a strong coupling with the electrodes. Therefore, the intrinsic charge transport properties of the molecule may not be easily reflected. Carbon-based nanomaterials, for instance, CNTs and graphene, exhibit excellent electrical conductivity due to their π-conjugated framework [131–134], making them ideal candidates for constructing electrodes with atomic precision.

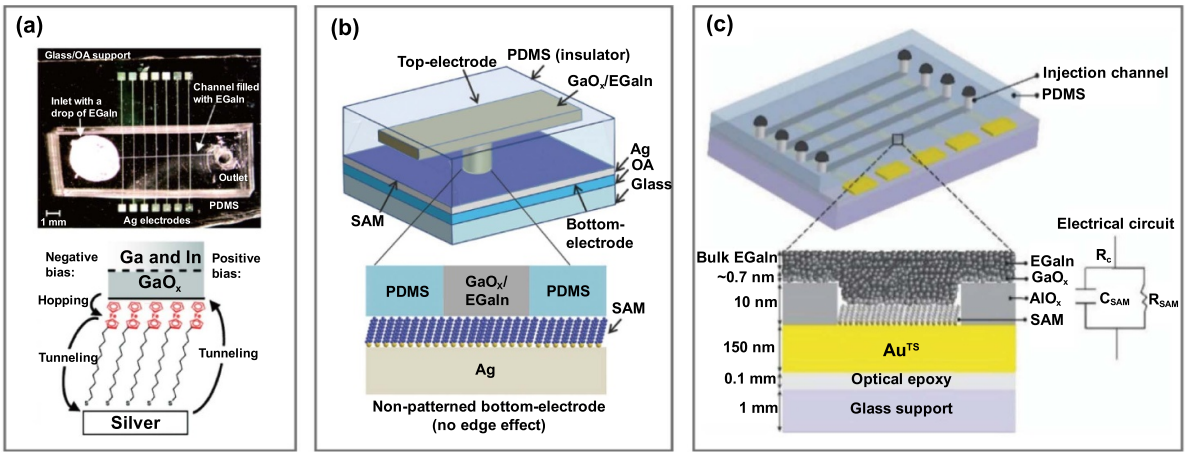

Figure 8. Schematic illustrations of microfluidic channels molecular junctions. (a) Cross-bar configuration, Reprinted with permission from [120]. Copyright (2010) American Chemical Society. (b) EGaIn top electrode stabilized in a microscale through-hole PDMS mould, [122] John Wiley & Sons. © 2014 WILEY-VCH Verlag GmbH & Co. KGaA, Weinheim. (c) AlO_x-coated micro-holes configuration. [119] John Wiley & Sons. © 2019 WILEY-VCH Verlag GmbH & Co. KGaA, Weinheim.

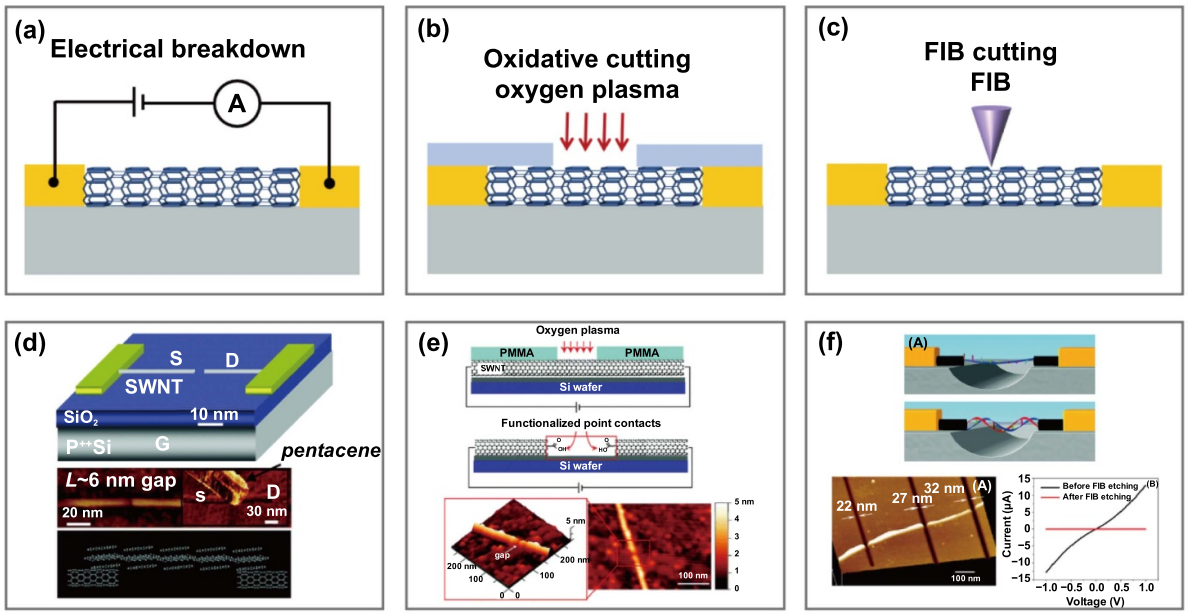

Figure 9. (a)–(c) Typical methods of fabricating carbon nanotube-based electrodes: schematic of (a) electrical breakdown, (b) oxygen plasma etching and (c) focused ion beam (FIB) etching schemes. (d) Schematic diagram of a cut SWNT with a sub-10 nm gap to be used as source (S) and drain (D) electrodes of an organic FET and the corresponding AFM image. Reprinted with permission from [56]. Copyright (2004) American Chemical Society. (e) Schematic demonstration of oxygen plasma etching and the AFM image of the interval cut into the SWNT. Reprinted with permission from [102]. Copyright (2008) American Chemical Society. (f) Schematic diagram of nanogap- bridging DNA molecules and high-resolution AFM image of the SWNT electrodes after FIB cutting. Reprinted with permission from [141]. Copyright (2008) American Chemical Society.

Compared with traditional metal electrodes, carbon-based nanomaterials have advantages of good chemical stability, easy chemical modification and relatively low contact resistance with molecules. Through π–π interactions and covalent bonds, carbon materials can be easily coupled with molecules. Since most of the molecules are carbon-based organic compounds, the greater compatibility between the carbon electrode and molecule leads to better construction of the molecular junction [66, 102–104].

3.1.3.1. CNT-based electrodes. The CNT is a kind of 1D ballistic conductor with easily regulated semiconductor characteristics, which is an ideal contact for building molecular electronic devices [133, 134]. In order to construct CNT electrodes to match the length of the target molecule, it is necessary to cut them to create nanogaps. Common processing methods include electrical breakdown (figure 9(a)) [56, 57, 135–138], oxygen plasma etching (figure 9(b)) [54, 55, 139] and FIB etching (figure 9(c)) [140, 141].

Similar to the EM process for metal electrodes, by applying a high-density current to the CNT, electrical breakdown will eventually occur, and the nanotube will be cut off to create a nanogap. In 2001, Avouris *et al* studied the current saturation and electrical breakdown in multi-walled carbon nanotubes (MWCNTs) [136]. They found that compared with metal wires, the MWCNT does not fail in the typical continuous acceleration pattern of EM in metal materials, instead, a stepwise breakdown will happen. Moreover, this breakdown process is very sensitive to the prescence of oxygen. On this basis, in 2004, Tsukagoshi *et al* used this method to cut MWCNTs with a controlled interval of less than 50 nm, and constructed a pentacene nano-transistor with CNT electrodes [135]. Similarly, Dai *et al* have performed electrical breakdown of single-walled carbon nanotubes to form nanogaps as small as 2 nm [56]. Thus, they constructed the smallest organic transistor, with an effective channel length of 1–3 nm and width of 2 nm. Figure 9(d) gives the schematic diagram of a cut single-walled carbon nanotube (SWNT) with a gap less than 10 nm served as source (S) and drain (D) electrodes in an organic FET and the corresponding atomic force microscope (AFM) image. In another study, Wei *et al* reported a new process combining electrical breakdown and electron beam-induced deposition (EBID) [57]. First, CNT was cut by the electrical breakdown method to obtain an initial large gap of 10–60 nm. Then, the gap size of CNT electrode was further reduced by SEM EBID. This method realizes the controllable fabrication and *in-situ* characterization of CNT nanoelectrodes.

The second method is local oxygen plasma etching. Guo *et al* first developed this method in 2006 [54]. They first used electron beam lithography (EBL) to open a small window on a polymethyl methacrylate (PMMA) mask. Through this window, the CNTs are cut by oxygen plasma ions to obtain an interval of less than 10 nm. Due to the oxidation, the carbon atom at the end of the CNT electrodes is oxidized and functionalized with carboxyl groups, and molecules anchored with amino ends can be linked to the electrodes via amide covalent bonds by forming a stable CNT–single-molecule–CNT junction, as shown in figure 9(e) [102].

In addition, FIB technology can use high-intensity FIBs to mill materials at the nanometer level, and thus can also be used for cutting CNTs [140]. By regulating the ion beam current and dose of FIB to form controllable gaps on CNTs, Roy *et al* prepared CNT-based nanoelectrodes for directly detecting the conductivity of DNA at the single-molecule level [141] (figure 9(f)).

3.1.3.2. Graphene-based electrodes. Graphene is one type of 2D carbon nanomaterial composed of sp^2-hybridized carbon atoms arranged in a hexagonal honeycomb lattice, with special electrical conductivity, high carrier mobility and the characteristics of ion doping. These excellent physical properties mean graphene has great potential application in building molecular devices [131, 132, 142]. Moreover, compared with 1D CNTs, large-area 2D graphene can be manufactured to nanogap arrays at the wafer level, which is more convenient for integrated processing. Similar to the abovementioned construction methods of CNT electrodes, the currently reported preparation methods of graphene-based electrodes also include electroburning [59, 143–146] and oxygen plasma etching [58, 146].

In 2011, Prins *et al* first reported the formation of graphene electrodes with a nanogap using feedback-controlled electroburning [59] (figure 10(a)); the width of produced nanogap is controlled by a feedback program, as shown in figure 10(b). Another control idea is to change the partial pressure of oxygen to achieve electroburning controllable gap preparation (figure 10(c)). Nef *et al* found that the control of oxygen partial pressure is critical to the creation of small gaps in graphene [143], as observed in the electrical breakdown of CNT [136]. Experiments have shown that the success rate of electroburning in vacuum conditions with reduced oxygen partial pressure is as high as 98% compared to ambient conditions.

As mentioned above, CNTs can be cut by oxygen plasma to form nanogaps with carboxyl modification [54, 55, 139]. Similarly, this method can also be utilized to form graphene-based nanogaps, as shown in figure 10(d). In 2012, Guo *et al* developed a 'dotted line lithography', then defined an oxygen plasma oxidative-etching process to introduce molecular-level gap arrays on the single-layer graphene sheets [58]. Specifically, the graphene sheet was first prepared by a chemical vapor deposition (CVD) method and transferred to a silicon substrate. Then a layer of PMMA was spin-coated and patterned by photolithography to form an array window (i.e. dotted line) with small holes less than 10 nm. Finally, the oxygen plasma accurately etched the graphene through the window to form a gap of less than 10 nm, as shown in figure 10(e). By this method, graphene point-contact arrays modified with terminal carboxyl groups can be obtained (with a yield of up to 50%).

Further, Lau *et al* combined the traditional lithography-defined plasma etching with feedback-controlled electroburning [146] (figures 10(f) and (g)). The schematics for the process flow of graphene-based electrode fabrication using this method are shown in figure 10(g). First, the graphene ribbons with notches are etched by oxygen plasma under the protection of a lithographic-defined electron beam photoresist, and then the electroburning is performed to open the notch into an electrod pair with a nanogap. The yield of graphene nanogap produced by this method can be increased to 71%. This scalable method paves the way for the use of graphene electrodes for large-scale integrated molecular circuits.

3.2. Dynamic molecular junction

The static molecular junction has the advantages of good stability and easy manufacture; however, since the electrodes are fixed, the size of the nanogap cannot be directly controlled and, therefore, the target molecule will not always be able to connect to the electrodes. Besides, the effect of configuration and conformation changes in the molecular junction, arising from changes to the nanogap, on the charge transport properties will also be unknown. The dynamic break junction technology, enabling molecular junction formation and breakage by dynamically controlling the distance between the electrodes pair, will be helpful for us to gain information from multi-dimensions of not only the electrical properties,

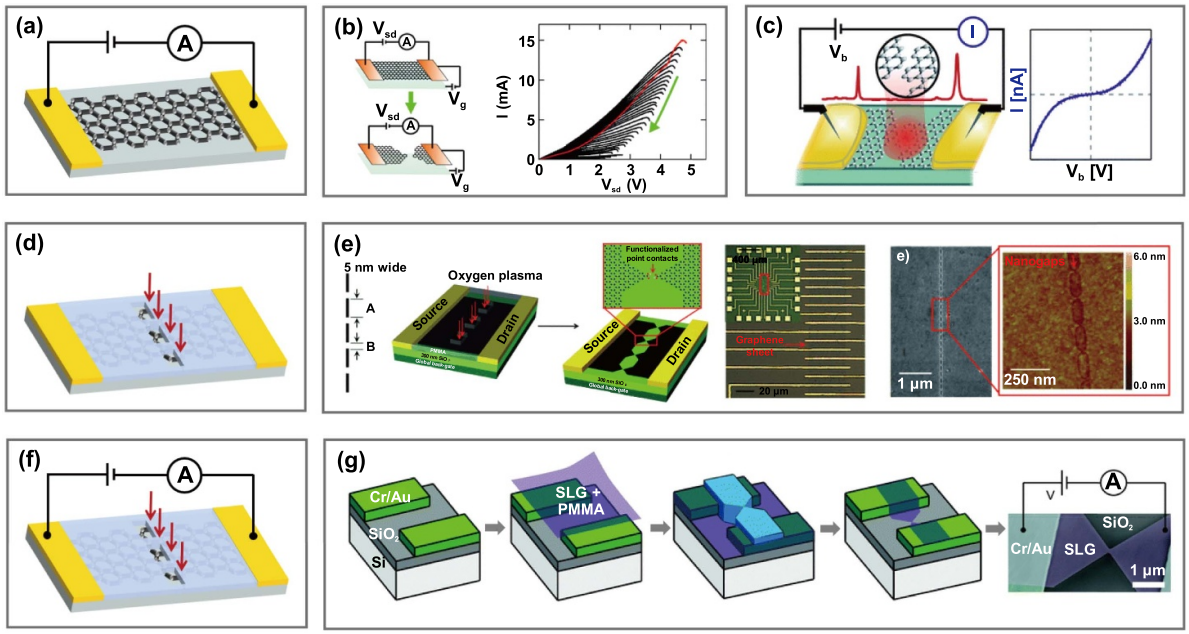

Figure 10. Typical methods of fabricating graphene-based electrodes. Schematic of (a) electroburning process (b) feedback-controlled electroburning and (c) oxygen partial pressure-controlled electroburning. Reprinted with permission from [59]. Copyright (2011) American Chemical Society. Reproduced from [143] with permission of The Royal Society of Chemistry. (d) Schematic of oxygen plasma oxidative-etching process. (e) Schematic of 'dotted line lithography'-defined oxygen plasma oxidative-etching process and SEM and AFM images of a prepared indented graphene point contact array. [58] John Wiley & Sons. © 2012 WILEY-VCH Verlag GmbH & Co. KGaA, Weinheim. (f) Schematic of electroburning and plasma etching composite process. (g) Schematics for the process flow of graphene-based electrode fabrication. Reproduced from [146]. CC BY 3.0.

but also the length properties in the molecular junction [26]. In addition, through the repeated opening and closing of the metal electrode, the multiple and repeated construction of a large number of single-molecule junctions can be realized. Therefore, considerable statistical data can be obtained, making the data of single-molecule electrical transport properties as reproducible and credible as possible [27]. With the growing developments and maturity of nanotechnology and micro/nano-machining technology in recent years, the main dynamic molecular junction technologies include STM-BJ [28–32], atomic force microscope break junction (AFM-BJ) [33–38] and MCBJ [48–51], as well as MEMS-BJ [46, 47] technology.

3.2.1. STM-BJ. Scanning probe microscope typically includes both STM and AFM. Correspondingly, based on this, researchers developed *in situ* break junction technique such as STM-BJ [28–32] and AFM-BJ [33–38]. As STM-BJ is one of the most commonly used methods for break junctions, in this part, we will focus on STM-BJ; more experimental details on AFM-BJ can be found in a recent review [147]. The STM technology has the ability to image and manipulate single molecules with atomic resolution, and the distance between tip and substrate is precisely controlled through piezoelectric actuators with angstrom resolution. Based on these advantages, Tao *et al* introduced STM into the conductance test of single-molecule junctions in and developed the STM-BJ technology. They successfully measured the conductance of a 4,4′-bipyridine (BPY) junction using this method [30].

3.2.1.1. Several construction strategies for STM-BJs. Figure 11(a) gives a schematic of a typical STM-BJ measurement set-up. According to whether the tip is in contact with the substrate during the break junction process, the STM-BJ method can be divided into hard-contact mode and soft-contact mode. For the hard-contact mode, the tip will penetrate into the substrate during the tip approach in the break junction process. Due to the ductility of gold, the contact area between the tip and the substrate gradually decreases during the tip pulling process, and will eventually experience a single-atom point contact. Then, continuous pulling will create a nanogap when the point contact breaks and molecular junction forms thereafter (figure 11(b)). The soft-contact mode means that the tip does not touch the substrate during the break junction process. The soft-contact mode can be divided into $I(s)$ and $I(t)$ modes (where I means current, s means distance and t means time). In the $I(s)$ method, the tip is suspended close to the substrate until the molecule moves into the gap to form a molecular junction, then the tip is pulled to break the junction with the current-distance information recorded at the same time [29] (figure 11(c)). For the $I(t)$ method, the distance between the tip and the substrate is kept constant, and the change of the current with time is recorded. When the molecular junction is formed and broken, the current will have a sudden jump and fall, respectively [28] (figure 11(d)).

3.2.1.2. Unconventional STM-BJ configurations. The traditional STM-BJ method is mainly applied using the same metal (such as Au, Ag or Pt) for tip and substrate, especially the most

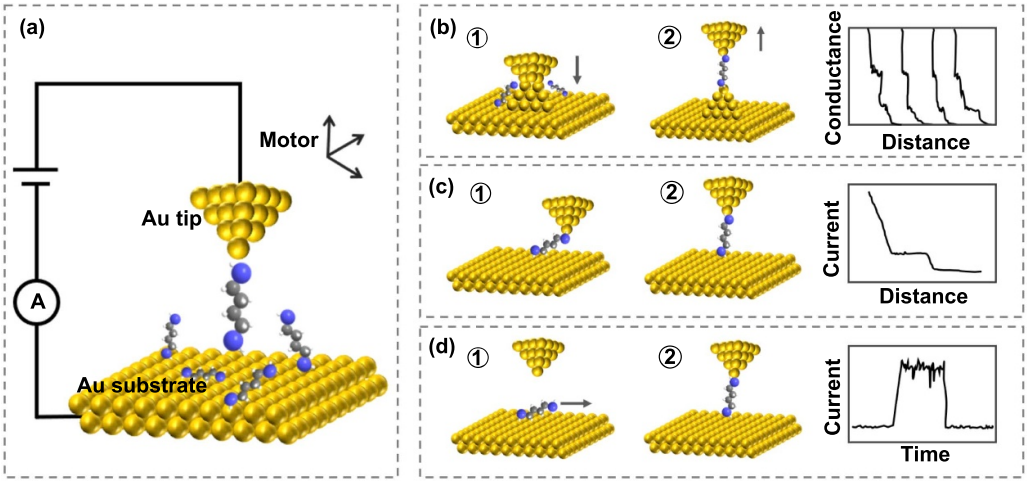

Figure 11. (a) Schematic of STM-BJ set-up; molecular junction evolution process of (b) hard-contact mode, (c) $I(s)$ mode and (d) $I(t)$ mode.

widely used Au–molecule–Au structure. The separate structure of STM-BJ makes it convenient to modify the materials of tip and substrate separately. Therefore, in recent years, to further expand the research scope of STM-BJ technology, different research groups have proposed a number of modification schemes for tip and substrate.

In view of the diversity of metal materials, scientists are working on the development of different metal electrodes to further expand the application range of the STM-BJ. However, it is still difficult for many metal materials to produce atomic-size contact by direct mechanical collisions of the tip into the substrate. Aiming at this problem, Mao's research group has developed an electrochemical-STM-BJ technology (EC-STM-BJ) [148]. Specifically, through electrochemical deposition, other kinds of metal can be electrodeposited on the tip. When the tip approaches the substrate, the heterogeneous metal at the tip will jump to the substrate under the induction of a high electric field. This process is called the 'jump-to-contact' mechanism. Using this method, they extended the available electrode materials for STM-BJ measurements to Cu, Ag, Fe, etc [128, 149].

On the other hand, the preparation of asymmetric molecular junctions with different metal electrodes is also challenging. Mao's group has developed a *z*-piezo pulse-modulated STM-BJ method to fabricate asymmetric molecular junctions with the tip and substrate electrodes made of different metals [150]. The process is shown in figure 12(a). By adjusting the pulse voltage, the position of the STM tip entering the substrate can be controlled: the high voltage is sufficient to make the tip impact the substrate surface and transfer some terminal cluster from the tip to the surface, resulting in a homogeneous Ag–molecular–Ag symmetric molecular junction, while under a small pulse voltage the tip quickly retracts and captures molecules to form an asymmetric molecular junction with an Ag tip and an Au substrate.

In addition to metal electrode materials, many groups have recently successfully constructed metal–molecular–semiconductor asymmetric molecular junctions using Si, gallium arsenide (GaAs) and other semiconductor materials. As shown in figure 12(b), Nichols' group constructed an Au–SAM–GaAS asymmetric molecular junction with a self-assembling molecular monolayer on GaAs substrate [151–153]. Through experiments and theoretical exploration, it has been proved that GaAs as a junction component endows a molecular junction with unique rectification characteristics and photoelectric response effect. Aragonès *et al* constructed the Au–molecular–Si molecular junction on STM [154] (figure 12(c)). The results show that the mechanical stability of the molecular junction on the silicon electrode can be increased by 30% when the silicon substrate is modified by hydrogenated silicon, compared with the same molecule but connected between two gold electrodes. Furthermore, Peiris *et al* found that thiols can form stable covalent bonds with H-terminated silicon [155, 156]. The Si–molecule–Si junctions have been constructed through a strong Si–S contact, and the stability of this kind of junction has been proved to be five times higher than those formed between typical gold electrodes.

In addition, in recent years, some researchers have combined gold tips with carbon-based material substrates (such as graphite [157], high-temperature oriented pyrolytic graphite [158] and few-layer graphene [159–161], etc) to construct nanogaps using STM-BJ technology. Kim *et al* developed an Au–molecule–graphite hybrid device structure and confirmed its high rectification characteristics, which extends the possibility of constructing STM-BJs with a variety of carbon-based electrodes [157] (figure 12(d)). Yang's group prepared a series of asymmetric metal–molecule–graphene molecular junctions by combining a metal electrode with a graphene electrode [161–164] (figure 12(e)). Experimental and theoretical calculations show that the use of graphene asymmetric junctions and coupling by appropriate anchoring groups may lead to higher conductivity values and smaller attenuation constants than metallic molecular junctions. In addition to Au/graphene electrode pairs, they also tried Pt/graphene electrode pairs [163]. Furthermore, they have constructed a completely metal-free molecular junction using an electrochemically etched carbon fiber as the STM tip [164] (figure 12(f)).

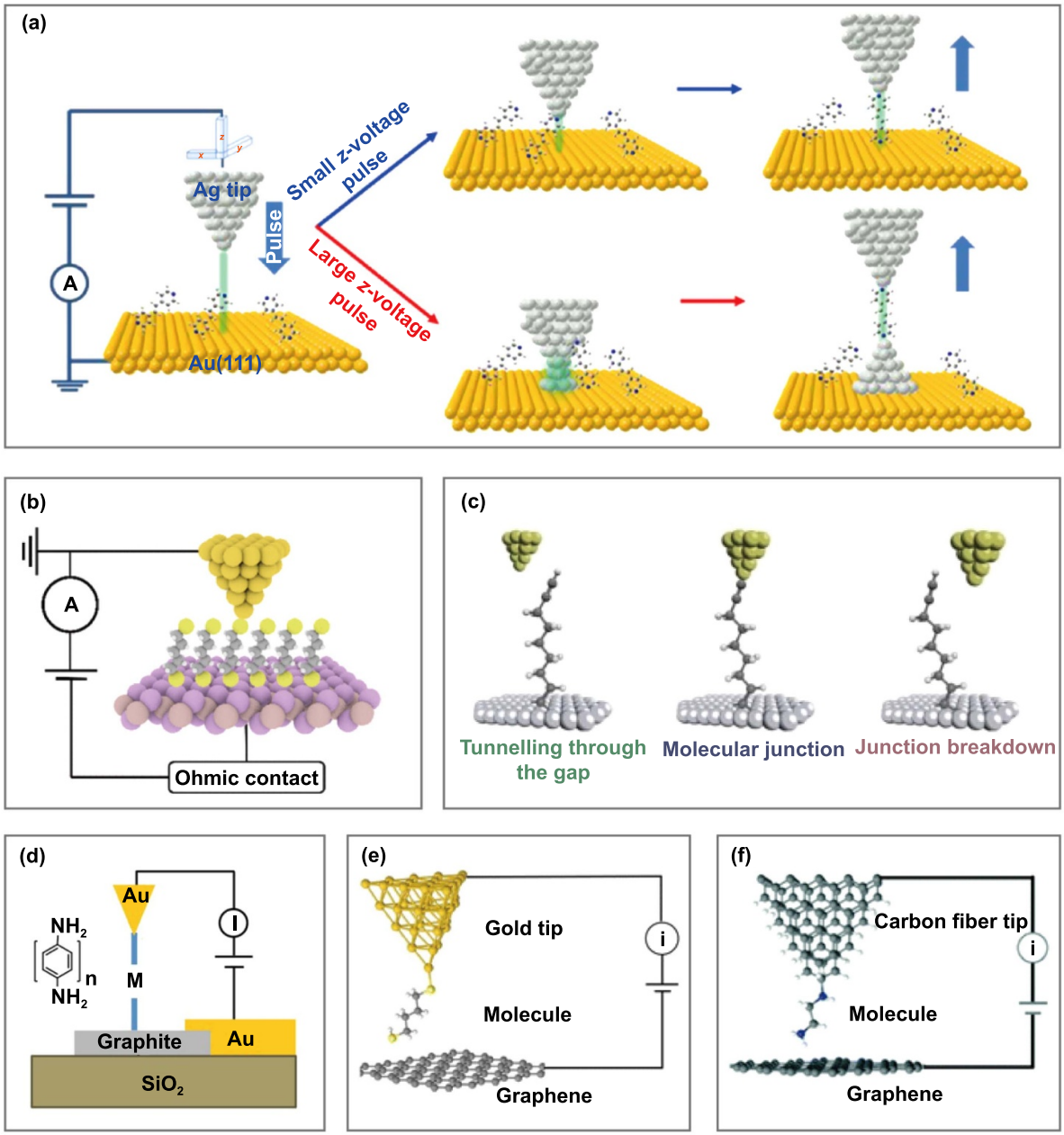

Figure 12. (a) Schematic of *z*-piezo pulse-modulated STM-BJ method to form Ag–molecular–Au asymmetric molecular junction (up) and Ag–molecule–Ag symmetric molecular junction (down). Reprinted with permission from [150]. Copyright (2021) American Chemical Society. (b)–(f) Schematic of (b) Au–SAM–GaAS, (c) Au–molecule–Si, (d) Au–molecule-graphite, (e) Au–molecule–graphene, (f) carbon fiber–molecule–graphene asymmetric molecular junction. Reprinted with permission from [152]. Copyright (2017) American Chemical Society. Reproduced from [154]. CC BY 4.0. Copyright (2014) National Academy of Sciences. Reprinted with permission from [161]. Copyright (2016) American Chemical Society. Reproduced from [164] with permission of The Royal Society of Chemistry.

3.2.2. MCBJ. Unlike the aforementioned STM-BJ and AFM-BJ technologies, which both produce break junctions through longitudinal electrode stretching, MCBJ technology is a strategy that transforms the longitudinal movement of a motor into horizontal electrode stretching [165]. In 1985, Moreland *et al* realized the breaking and spacing control of Nb−Sn metal wire through a model with three-point support, which became the prototype of MCBJ technology later [166]. In the early 1990s, van Ruitenbeek's group first proposed the concept of the MCBJ and used it to study atomic point contacts [167, 168]. In 1997, Reed *et al* began to use MCBJ technology to construct molecular junctions and study the electrical properties of molecules [39]. Since then, MCBJ technology has gradually developed into one of the mainstream testing techniques for molecular electronics due to its relatively simple working principle and unique advantages.

A typical MCBJ setup is shown in figure 13(a). A microchip with a suspended and notched micro-bridge structure is fixed in a three-point support structure, with a pushing rod in the center of the bottom and two counter supports on the left and

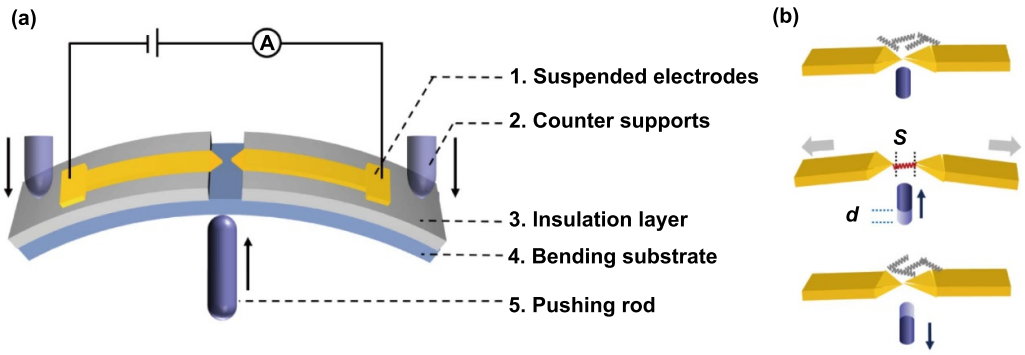

Figure 13. (a) Schematic of MCBJ set-up, (b) molecular junction evolution during MCBJ chip opening and closing.

right sides of the top. When the pushing rod moves upward, the substrate is subjected to a bending force, which stretches the suspended micro-bridge to both sides. The notched center of the metal bridge bears the strongest stretching force and finally breaks into an electrode pair with a nanogap. Benefiting from the flexible elastic substrate, the electrode pair can be merged back together when the pushing rod is pulled back. Therefore, owing to the reduction ratio between the movement of the pushing rod and the gap distance, the nanogap can be precisely controlled with even sub-angstrom resolution to accurately fit the target molecule and realize the repeated construction of molecular junctions, as shown in figure 13(b).

3.2.2.1. Construction of MCBJ chips. According to the principle of MCBJ technology introduced above, the structure of a suspended metal bridge with a notch in the middle on the surface of a microchip is the prerequisite for MCBJ technology. This ensures that the center of the metal bridge with stress concentration can be broken to form nanogaps before the chip is fractured or beyond elastic deformation during the deformation process. Therefore, the fabrication of microchips with a suspended and notched metal nanobridge is the key basis for MCBJ technology. With the developments of micro and nano-manufacturing technologies, this prerequisite can be realized. At present, the main preparation methods of MCBJ microchips include mechanical cutting [39, 167–170], electrochemical deposition [171–181] and EBL microfabrication [40–45, 182–186].

3.2.2.2. Notched-wire chip. The notched-wire sample was first adopted in MCBJ technology [39, 167, 168]. The principle of the notched wire is to fix the wire with epoxy resin and then manually cut the wire with a scalpel to form a notch in the center of the wire [169, 170], as shown in figure 14(a). The advantages of the notched-wire method are the short preparation cycle, low preparation cost and low equipment technology threshold. However, the precision and stability of the chips prepared by this macroscopic method are poor, and the reduction ratio of this chip is only about $10^{-2} \sim 10^{-3}$. This means that to realize the molecular-scale nanogap variation (about 1 nm), the movement resolution of the pushing rod should be around 10^{-11} m using a piezo stack.

Recently, Zhang *et al* discovered that the electrode distance of the notched-wire nano-contacts obtained can be further precisely adjusted with sub-angstrom precision through laser irradiation [187]. Through incident light position-adjustment experiments and theoretical simulations, they clarified that the main mechanism of atomic contact conductance modulation comes from the thermal expansion of the substrate under the suspended electrode caused by light irradiation. Furthermore, by modulating focus size and power of the laser beam, they extended the application of the scheme to miniaturized photolithographic electrode junctions, and found that it also has a modulation effect to the nano-gap size for the construction of molecular junction. This confirms the potential feasibility of light modulation construction of integrated molecular arrays.

3.2.2.3. Electrochemically assisted MCBJ chip. The idea of combining MCBJ technology with an electrochemical deposition method to construct atomic point contact was first proposed by Tao's group [172, 173]. Then Tian's group further improved and proposed the concept of electrochemically assisted MCBJ (EC-MCBJ) [176–180]. The EC-MCBJ method mainly includes three steps: (a) micromachining to prepare chips with a microscale-spaced electrode pair; (b) electrochemical deposition onto the electrode pair to reduce the gap and finally contact each other; (c) mechanically controllable breaking to realize atomic point contact and the corresponding nanogaps for molecular junction fabrication. Figure 14(b) gives a schematic and image of a typical EC-MCBJ chip. In addition to the traditional gold electrode, the method is also suitable for the preparation of other metal electrode pairs such as nickel and copper [188].

3.2.2.4. Nano-lithographic MCBJ chip. The traditional MCBJ chips tend to have a lower reduction ratio, so a pushing rod with high precision is required, and besides, the smaller ratio results in greater interference from external vibration. Therefore, how to develop a method for the preparation of MCBJ chips with a high reduction ratio is a very important issue. Micro- and nano-manufacturing methods, mainly nanolithographic technology, can significantly improve the high reduction ratio of MCBJ chips. In 1995, Zhou *et al* used a micro-manufacturing method for the first time to release the

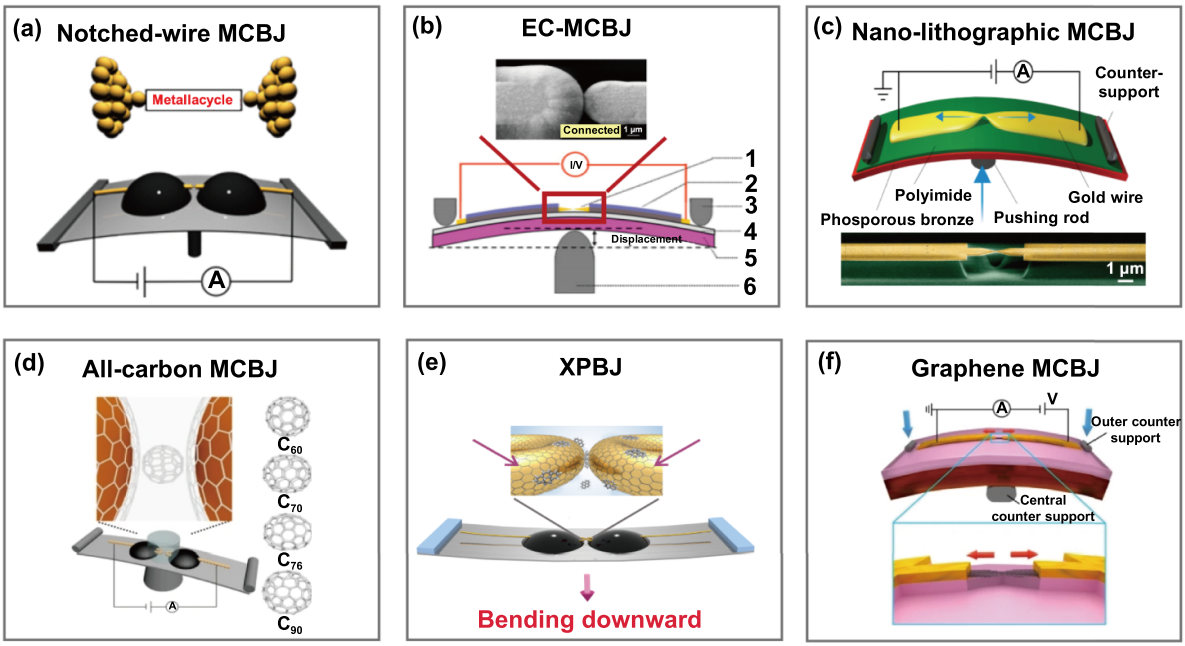

Figure 14. Schematic of different MCBJ chips. (a) Notched-wire MCBJ. Reprinted with permission from [169]. Copyright (2017) American Chemical Society. (b) EC-MCBJ. Reproduced from [176]. © IOP Publishing Ltd. All rights reserved. (c) Nano-lithographic MCBJ. Reproduced from [43], with permission from Springer Nature. (d) All-carbon MCBJ. Reproduced from [189]. CC BY 4.0. (e) XPBJ. Reproduced from [190]. CC BY 4.0. (f) Graphene MCBJ. Reproduced from [60], with permission from Springer Nature.

structure underneath the thin gold wire through anisotropic wet etching of silicon to form a suspension structure, and fabricated the first micro-machined MCBJ chip [40]. However, this method has not been widely used because of its complexity and low efficiency. In 1996, van Ruitenbeek's group introduced polyimide (PI) as an insulating and sacrificial layer for the first time, and combining this with EBL formed a suspended gold nanobridge with a width of about 100 nm and a thickness of about 80 nm by dry etching of PI [182]. This method can be mass-produced and stably repeated, thus becoming a common protocol [41–45, 183–185]. The typical nano-lithographic MCBJ chip is shown in figure 14(c). The traditional EBL micro-fabrication process mainly includes the following steps: insulation layer deposition (PI, silicon oxide, etc), preparation of the nanoscale wire with a notched profile by EBL, and dry etching of the isolation layer to free the nanowire into a suspended metal bridge. Therefore, the reduction ratio of this chip will reach about $10^{-4} \sim 10^{-5}$, the movement resolution of the pushing rod can be lowered to around 10^{-6} m, which is achievable using a step motor.

3.2.2.5. Carbon-based MCBJ chip. As mentioned above, carbon-based electrodes can be introduced to the single-molecule electronics measuring system in a STM-BJ configuration, and so can MCBJ technology. Recently, our group has developed a new method for graphene-based MCBJ chips. We introduced the CVD graphene on copper wire as the electrode pair, and used MCBJ technology to dynamically break and connect the graphene electrodes. Therefore fullerene-based molecules can be captured to build a series of tunable all-carbon molecular junctions [189], as shown in figure 14(d). In addition, we also defined this method as the cross-plane break junction (XPBJ) technique, which enables the measurement of some polyhydrocarbon molecules without anchoring groups by van der Waals interactions [190]. The scheme is shown in figure 14(e): two copper wires with graphene on the surface are bent into a curved surface, placed as close as possible and fixed on a flexible substrate with epoxy resin glue. During the test, the motor pulls the chip down so that the two electrodes will gradually approach until a tunnel junction is formed. In addition, Caneva *et al* prepared graphene MCBJ chips by photolithography and other micro-processing methods [60], as shown in figure 14(f). Specifically, first, the graphene is transferred to a polymer-coated metal substrate and a bowtie structure is formed by O_2 plasma etching. The polymer area around the bowtie is then etched away and the metal lead structure is evaporated. With the support of the polymer structure below, the graphene electrode can be repeatedly stretched without collapsing.

3.2.2.6. Other configurations of MCBJ chip. Since the electrode stretching configuration of the MCBJ method is planar with the corresponding chips produced through the planar micro- and nano-manufacturing technology, it is easy for researchers to continue to introduce other modules onto the MCBJ chips to achieve different functions. In recent years, with the requirement for the development of multi-dimensional detections, people have put forward higher requirements for the MCBJ chip [165].

The three-electrode system is helpful to study the charge transport characteristics of molecules at different energy levels, and has an important guiding role in the construction

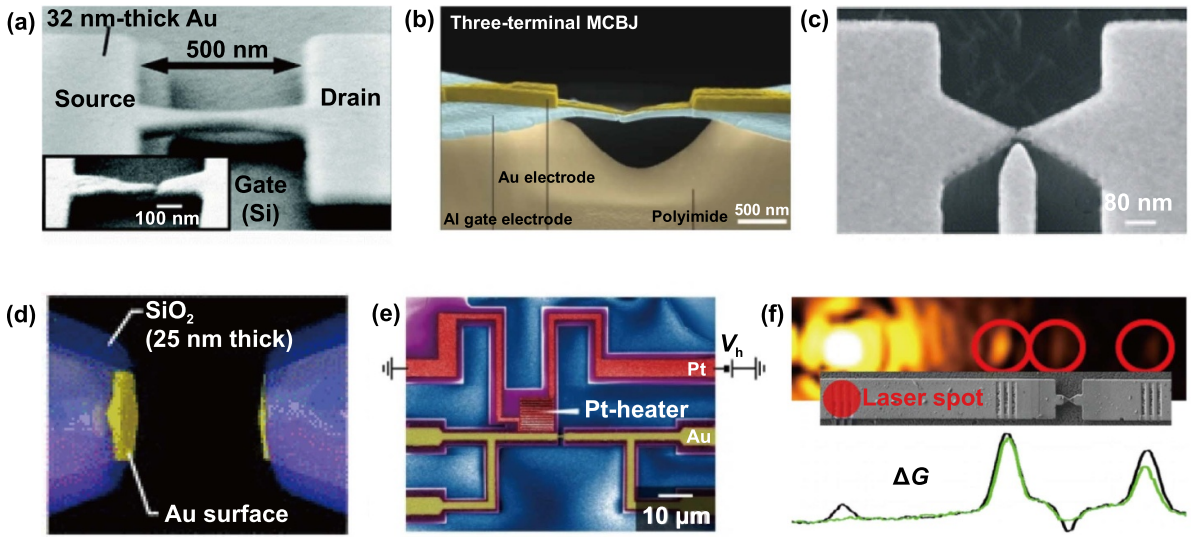

Figure 15. (a)–(c) SEM pictures of different types of three-electrode systems. (a) The structure of directly uses the silicon substrate itself as the back gate. Reprinted with permission from [191]. Copyright (2005) American Chemical Society. (b) Suspended sandwich back gate structure. Reproduced from [194], with permission from Springer Nature. (c) The structure has a third gold electrode close to the source and drain as the gate electrode. Reprinted with permission from [196]. Copyright (2013) American Chemical Society. (d) Schematic of SiO_2 coating protected MCBJ chip. Reprinted from [197], with the permission of AIP Publishing. (e) Schematic of a heater-embedded MCBJ chip. Reproduced from [80]. CC BY-NC-SA 3.0. With permission. (f) SEM picture of MCBJ chip with grating structure. Reprinted with permission from [200]. Copyright (2014) American Chemical Society.

of molecular electronics devices, which is a prototype of single-molecule transistor. In addition to forming a gold electrode pair on the top of the motor as the source and drain, the gate can also be easily introduced by means of micro and nano-manufacturing technologies [191–196]. The three-electrode system that has been developed so far mainly uses the doped silicon substrate itself as the back gate [191, 192] (figure 15(a)), the suspended sandwich back gate structure [193, 194] (figure 15(b)), and the structure that a third electrostatic gold electrode close to the source and drain as the gate electrode [195, 196] (figure 15(c)).

Measuring the conductivity of a single molecule in an electrolyte environment is often affected by the tunneling background and the ionic current in the electrolyte solution. To solve this problem, Arima *et al* prepared an MCBJ chip with SiO_2 coating on the electrodes by CVD (figure 15(d)) [197]. The ionic contribution enhances the conductance measuring background, which might influence the charge transport of intrinsic molecular junction through the electrode pairs, is inhibited by the formation of dielectric protective gold electrode region by SiO_2. Alternatively, Muthusubramanian *et al* also deposited a layer of Al_2O_3 on an MCBJ chip using plasma-enhanced atomic layer deposition to suppress the tunneling background in aqueous environments on charge transport [198].

By studying the thermoelectric effect of molecules, we can get the information of the dominated charge transport orbital of the molecular junction, and the nano-lithographic MCBJ method also shows its advantages in this field [78–81]. Makusu *et al* fabricated a snake-like Pt coil heater near a suspended nanobridge to study thermoelectric effects at the molecular scale [80] (figure 15(e)). By applying a bias voltage on the Pt wire to heat one side of the electrode pairs, the temperature difference between the electrode pairs can be realized and the Seebeck coefficient of the molecular junctions can be measured.

The construction of single-molecule optoelectronic devices through light stimulation on molecular junctions has attracted more and more interest. However, the integration of optical elements into molecular devices remains a challenge due to the large spatial size of the introduced external light source. Recently, Zhao *et al* innovatively introduced metal-coated tapered fibers to construct nano-electrodes based on MCBJ technology, and developed an optical fiber-based break junction technique [199]. In that technique, the tapered fiber is used as both an optical waveguide and a metal electrode after breaking, so as to process the electrical and optical signals of the single-molecule junction at the same time. Through testing, they proved that the conductance of imidazole monomer junction can be increased by about 40% under light irradiation. This method integrates optical and electronic components into molecular optoelectronic devices at the same time, which helps to understand the interaction between single molecules and confined light waves.

In addition, some special structures are needed to meet the needs of detecting tunnel junctions under the excitation of surface plasmon. For example, Benner *et al* made grating structures near the gold suspended nanobridge, so as to realize the long-distance transmission of surface plasmons, and then coupled the nanostructure of the nanobridge will produce a light-assisted tunneling [200] (figure 15(f)).

3.2.3. MEMS-BJ. Furthermore, in order to realize the array integration of molecular electronic chips, combining the integrated circuit manufacturing technologies of silicon-based semiconductors will be a trend in the future. Besides, in order

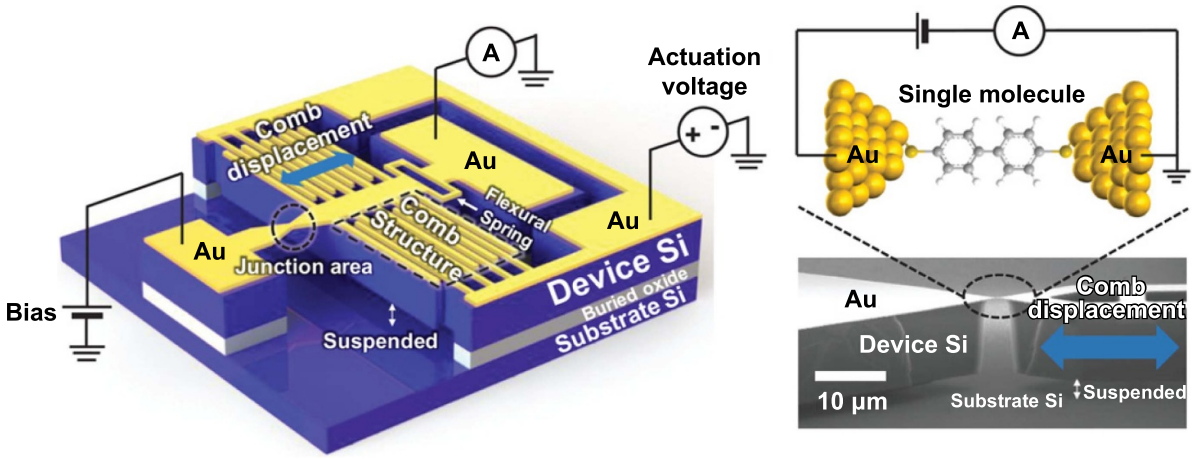

Figure 16. Schematic of MEMS-BJ (left) and SEM image of suspended gold nanobridge structure (right). [47] John Wiley & Sons. © 2020 WILEY-VCH Verlag GmbH & Co. KGaA, Weinheim.

to realize the controllable break junction of the electrode pair on the chip, we need to integrate the driving components like 'piezomotor' for STM and AFM, and 'pushing rod' for MCBJ, so as to truly realize the dynamic break junction on the surface of planar chip completely. MEMS can integrate various sensors and actuators on a single chip [201]. Thus, it is expected to use the MEMS-related technologies to realize molecular junction detection in a lab-on-chip device.

Hihath's group prepared a MEMS-based break junction system on chip by silicon manufacturing, which is called MEMS-BJ [47], as shown in figure 16. The chip is prepared on the silicon-on-insulator wafer through processes such as gold plating, photolithography, and etching. By integrating the suspended comb drive structure with sub-nanometer precision and the break junction on the one chip, a reliable and mass-produced single-molecule break junction system is realized. Using this system, they achieved simultaneous measurements of single-molecule Raman and conductance.

3.3. Large-scale molecular junction array

Molecular electronics designs electronic components at the level of atoms and molecules, and its ultimate goal is to prepare next-generation molecular electronic devices which might be capable of supporting silicon-based electronic devices. Compared with the isolated single-molecule junctions, molecular devices composed of SAMs have the advantage of large-scale stability to provide the possibility of large-area junction integration [94, 95, 125]. The cross-bar structure is a typical large-area SAM measuring tool, which can realize the electrical characterization of SAMs with complex interactions [202–205]. In addition, because the nanowires can be periodically assembled into evenly spaced parallel arrays, they are suitable for integrated circuit architectures. However, the manufacturing of such large-area junctions remains challenging due to the difficulty of forming electrical contact with SAM in a non-invasive manner and the density of the bars being limited by lithographic processing limits. Based on this, many research groups have carried out extensive researches to achieve the construction of a reliable device platform with large-scale molecular connections.

On the one hand, due to the highly integrated molecular junction array, the nanowires need to be assembled into a sufficiently narrow spaced bar structure without short-circuiting, which brings many challenges to lithographic processing [212, 213]. Green *et al* developed a method of superlattice nanowire-pattern transfer to fabricate super-dense, highly aligned crossbar circuits [206]. By combining the bistable rotaxane molecular monolayer as the data storage element and the fault-tolerant concept learned from the Teramac supercomputer, they realized the construction of a 160 000-bit molecular electronic storage circuit, as shown in figure 17(a).

On the other hand, to avoid the defects and damages of the SAM during the deposition of the top contacts, many research groups have proposed various novel and creative solutions to achieve damage-free packaging of large-area SAM monolayers [125]. For example, the use of polymer or carbon material soft interlayer [207, 208], nano-particle protective layer [209, 210], liquid metal top electrode [211] and other solutions.

Firstly, electrical short circuit can be avoided through the soft interlayer deposition process [207, 208]. Park *et al* introduced a highly conductive polymer PEDOT:PSS (poly(3,4-ethylenedioxythiophene):poly(styrenesulfonate)) layer between the top metal layer and the SAM [207], as shown in figure 17(b). They selected a PI with high thermal stability and low roughness as the flexible substrate, and reported the construction of molecular-level electronic devices based on the flexible substrate. Experimental results show that the devices based on an ultra-thin monolayer can reliably operate in various bending configurations. Najarian *et al* introduced electron-beam deposited carbon (eC) into the upper and lower electrodes to construct electrode contacts [208] (figure 17(c)). The molecular junction with eC layer on Au electrode can improve the roughness of the electrode, reduce the electric migration and provide covalent bonding of the molecular interconnection to improve the stability of the junction. Using this method, they realized the formation of a solid all-carbon molecular junction on a flexible or translucent substrate.

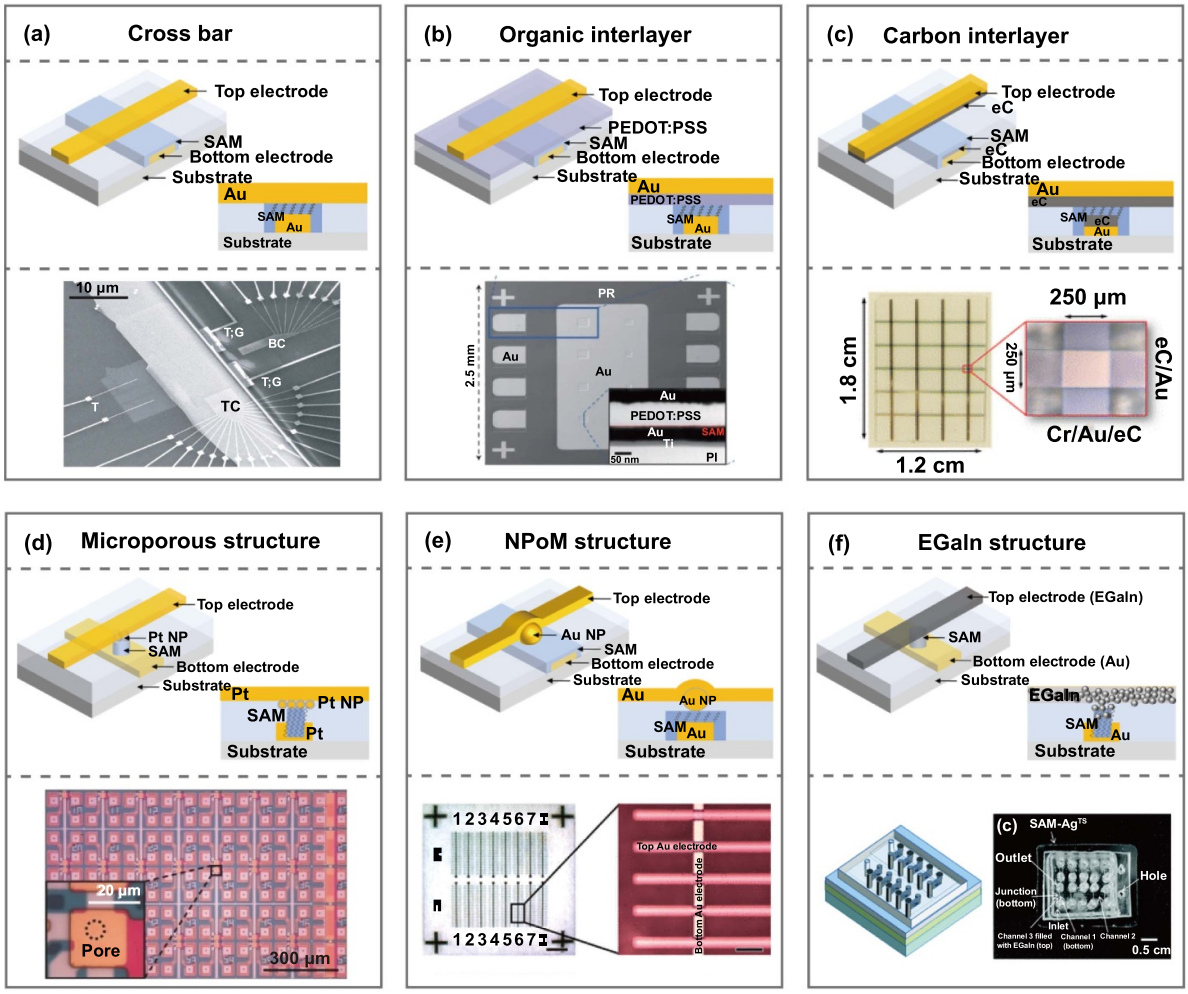

Figure 17. (a) Schematic of cross-bar configuration molecular junctions (up) and SEM images of the nanowire crossbar memory (down). Reproduced from [206], with permission from Springer Nature. (b) Schematic of cross-bar molecular junctions with organic interlayer (up) and SEMs of a flexible molecular device (down) (c) Schematic of cross-bar molecular junctions with carbon interlayer (up) and optical image of completed flexible all-carbon molecular junction device (down). Reprinted with permission from [208]. Copyright (2016) American Chemical Society. (d) Schematic of cross-bar molecular junctions with microporous structure (up) and photograph of molecular junctions device arrays (down) [209]. Reproduced from [209], with permission from Springer Nature. (e) Schematic of cross-bar molecular junctions with NPoM structure (up) and photograph of top and bottom electrodes arranged to form cross-bar devices (down). Reprinted with permission from [210]. Copyright (2021) American Chemical Society. (f) Schematic of EGaIn electrode (up) and photograph of a complete microchannel device (down). Reproduced from [211] with permission of The Royal Society of Chemistry.

Second, nanoparticles can be used to build reliable contacts, providing multiple functions such as metal contacts, protective layers and plasma antennas [209, 210]. Hellmann *et al* developed a new approach to SAM top contact construction based on microporous structures in crossbars, which avoids the damage caused by SAM during top deposition [209]. In this method, as shown in figure 17(d), the SAM is first restrictedly assembled on the Pt bottom electrode through the micro-vias technique. Then, the nanoparticle is bonded to the anchoring group on top of the SAM through a solution to form a nanoparticle film to protect the SAM. The top electrode is then further strengthened by directly evaporating the metal. This method can simultaneously produce thousands of stable molecular junctions in an individual hole, opening up a new way to integrate molecular compounds in solid-state devices. Kos *et al* constructed an optoelectronic device based on a nanoparticle-on-mirror (NPoM) geometric structure array [210]. The structure of the device is shown in figure 17(e). The SAM is trapped between the bottom Au electrode and a single AuNP to form a molecular junction. The top semi-transparent electrode is in contact with AuNP and intersects with the bottom electrode to form 300 independent crossbars to create molecular junctions with repeatable morphology and electrical response. The advantage of this structure is the use of plasmonic nanomaterials in combination, making it a strong candidate for optical detection and energy harvesting.

In addition, the EGaIn electrode mentioned above is another simple method for constructing the non-destructive contact of SAM, and it can also be used for the construction of large-area structures [119–122]. For example, Wan *et al* reported a SAM tunnel junction array based on the EGaIn top electrode [211]. As shown in figure 17(f), the top electrode

is composed of liquid metal GaO_x/EGaIn fixed in a micro-via array in PDMS. These top electrodes can be placed directly on the bottom electrode of the ultra-flat template to form a highly repeatable electrical contact with the SAM. Unlike some traditional techniques that form large-area junctions, this method uses liquid metal as a soft-top contact, and therefore avoids electrode defects such as edges, terraces and pits.

4. Precise characterization and regulation of molecular junction

After the accurate fabrication of the molecular junction, how to characterize and regulate the properties of the molecular junction becomes the next important issue. First of all, charge transport properties through the molecular junction characterized by electrical measurement are the top priority. What's more, the electrical responses by the outer stimulation such as optoelectronic signal or the spectroscopic information can be obtained under the photo-illumination, and the corresponding thermoelectric properties can be extracted when adding temperature control.

4.1. Electrical characterization

4.1.1. Statistical analysis of electrical characterization. The single molecule charge transport property, is one of the essential characteristics of molecules themselves, which enables fingerprint definition of molecules similar to the spectral properties [13, 27]. However, the conductance directly obtained by measurement is often not a definite value which many factors will lead to the existence of deviation. Therefore, the charge transport properties of molecules with minor structural changes may have significant changes. On the other hand, even for molecules with the same structure, different conformations and molecule-electrode adsorption configurations also cause significant charge transport properties changes [31, 62, 214]. Even in different research groups adopting different molecular junction construction methods, the transport properties of the same molecular junction might be different, which makes the reproducibility and accuracy of electrical data the most important challenge in this field. Therefore, it is necessary to conduct sufficient data analysis and data mining to extract reliable and reproducible information about molecular conductance.

In molecular electronics, the dynamic breaking junction technology (STM-BJ or MCBJ) can control the electrodes to continuously open and close, so as to achieve high reproducibility of the repeated construction and breakage of molecular junctions, thus obtaining a large amount of information in a short period for statistics [15]. In a break junction experiment, by applying a small bias voltage (10–100 mV) between the electrode pairs, the conductance-distance curve is obtained, which represents the change of the conductance with the variation of the stretching distance of the electrodes pair. Figure 18(a) describes an ideal break junction process (left column) and shows the conductance-distance curve corresponding to each stage (right column) [215]. At the beginning, as the gold electrode is stretched, the gold electrode changes from multiple atomic point contact to single atomic point contact, corresponding to the a–b processes shown in figure 18(a). When the gold electrode continues to be stretched, the point contact of gold atoms breaks, and then the nanogap is formed (processes b–d) due to the snap-back effect of the gold atomic contact, the electrode retreat process (the shadowed section 1 in the right column of figure 18(a)) is normally too fast to be directly detected. When the distance between the electrodes is close to the length of the target molecule, the target molecule may be connected to the two gold electrodes separately through the anchor group (the shadowed section 2), thereby forming a molecular junction (processes d–g). At the same time, it can be observed from the conductance distance curve that, after the formation of molecular junction, the measured conductivity value is almost in a constant value, called the conductance plateau, which

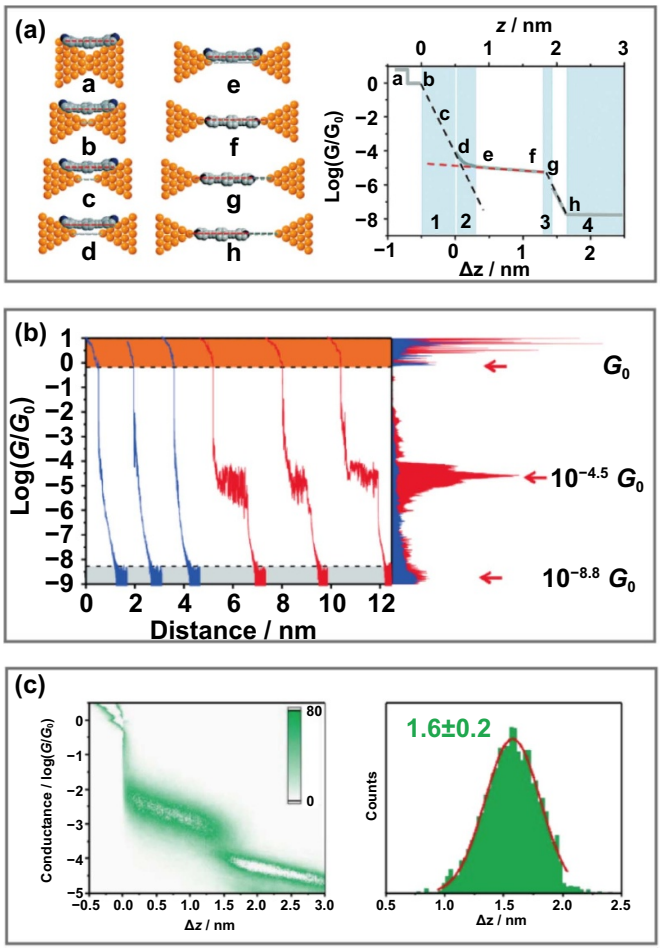

Figure 18. (a) Schematic of molecular junction formation and break during a test (left) and conductance-distance curve of molecular junction. Reproduced from [215] with permission of The Royal Society of Chemistry. (b) Individual conductance-distance trace and 1D conductance statistical histogram of OPE-type molecule. Reproduced from [91]. CC BY 2.0. (c) The conductance-distance histogram of phenothiazine based molecular junction (left) and the relative displacement distribution of molecular junction (right). [170] John Wiley & Sons. © 2017 Wiley-VCH Verlag GmbH & Co. KGaA, Weinheim.

suggests the conductance value of the target molecule. Subsequently, the gold electrodes continue to be pulled apart. When the gap width of the electrodes is greater than the molecular length by further stretching, the molecular junction breaks (the shadowed section 3 and processes g–h). At this point, the conduction-distance curve declines with a slope similar to b–d and reaches the tunneling background (the shadowed section 4).

According to the above discussion, with the continuous electrodes pair opening and closing during the test, the conductance will continuously break down to the background and then rise back to greater than G_0. In order to perform a large amount of data analysis, we extracted the conductance-distance curve of each individual break junction process so that a series of curves can be obtained for statistics. A large number of conductance data from the extracted conductance-distance curves are gathered to obtain a 1D conductance histogram, therefore to confirm the conductance value of molecular junction through the peak in the histogram. The typical conductance-distance traces with pure tunneling (blue lines) and molecular junction (red lines) and the corresponding conductance histograms are shown in figure 18(b) [91].

According to the above introduction, another dimension of distance information can be obtained from the conductance-distance curve, so we can make a 2D statistical graph. The method of combining conductance and distance statistics is called 2D conductance-distance histogram statistical method, which is referred to the left column of figure 18(c). Therefore, the 2D conductance-distance histogram will show the characteristics of the conductance intensity cloud of the molecular junction, which can better reflect the distribution of the conductance from molecular junctions. Furthermore, using the same method to calculate the distance difference between the junction formation and junction breakage in each conductance-distance curve, the accumulated lengths can also be gathered for histogram construction, which refers to the statistical length of molecular junction by Gaussian fitting, as shown in the right column in figure 18(c) [170].

4.1.2. Electrical transport properties of single-molecule junction. The development of molecular electronics experimental technology and data analysis methods has laid a good foundation for studying the electrical transport properties of molecular junctions. Since the birth of molecular electronics, how to establish the correlation between molecular structure and the electrical transport properties of molecular junction has been a key problem in molecular electronics [15, 27]. In section 2, we mentioned that for a molecular junction whose electrical transport mode is a tunneling mechanism, its conductance can be described by $G = Ae^{-\beta l}$ [12]. Thus, the tunneling resistance depends on the length l of molecules in the junction, the tunneling decay constant β, which is related to the molecular energy level, and the pre-exponential factor A, which is related to the coupling state between the electrodes. Therefore, the research on the electric transport properties of molecular junction can be carried out correspondingly around the influence of these parts.

Firstly, the effect of length on the transport properties of molecular junction has been studied extensively [216–221]. According to theoretical predictions, different molecular lengths will lead to different mechanisms for charge transport. That is to say, for short molecules, it conforms to the coherent transport mechanism and the molecular resistance changes exponentially with length [222, 223]. As the number of repeating units increases, for long molecular lines, the hopping mechanism will be dominant. Generally speaking, in the experimental process, the electron transport mechanism can be judged as coherent transport or hopping mechanism according to whether there is temperature dependence and length dependence in the molecular junction system. In fact, there is a competition between these two transport mechanisms. In other words, for molecules with repeating unit structures, charge transport will transition from direct tunneling mechanism to hopping mechanism as the number of repeating units increases [216–221]. Experiments have confirmed that many molecular systems with conjugated structures, such as oligophenyleneimine (OPI) [218] and oligophenyleneethynylene (OPE) [219], have such properties, as shown in figures 19(a) and (b). It can be seen that the shorter unit conforms to the coherent transport mechanism, and the conductance changes exponentially with distance, and does not change with temperature. When the number of units becomes larger, the tunneling decay constant becomes significantly smaller, and the conductance also changes with temperature. However, this length-dependent mechanism of molecular conductance does not always hold. In 2018, Garner *et al* reported an anomaly. They designed and synthesized bicyclo [2.2.2] octasilane molecule, and found that the system has lower direct tunneling electrical transport capacity than that of the same size under vacuum conditions [32]. Experiments and calculations confirm that this phenomenon is due to the destructive σ interference effect in the double ring structure. This, in turn, makes it possible to design a class of highly insulated molecules based on QI that breaks down the length constraint.

On the other hand, the electric transport properties of molecular junctions are also related to tunneling decay constant β. In general, the value of β is mainly associated with the HOMO-LUMO gap [214]. A simple classification is that the HOMO-LUMO gap of conjugated system molecules is small, and β is also small ($\sim$0.3 $Å^{-1}$) [223–225]. The HOMO-LUMO gap of saturated alkane molecules is larger, and β is also larger (0.8–1 $Å^{-1}$) [214, 226–228]. For example, Kaliginedi *et al* designed and studied the electric transport properties of a series of dithiol-terminated OPE molecules (figure 19(c)) [214]. Through the comprehensive verification of STM-BJ and MCBJ technologies, the effect of different molecular lengths and/or HOMO-LUMO gaps on conductance has been systematically studied. It is confirmed that increases in molecular length and/or HOMO-LUMO gaps lead to a decrease in the conductance of linearly conjugated benzene. In addition, people have also reported some work on regulation of conductance by molecular energy level [227–229]. For instance, Capozzi *et al* used an electrolytic gate to adjust the conductance of electrochemically inert molecules in the molecular junction, which can controllably adjust the energy

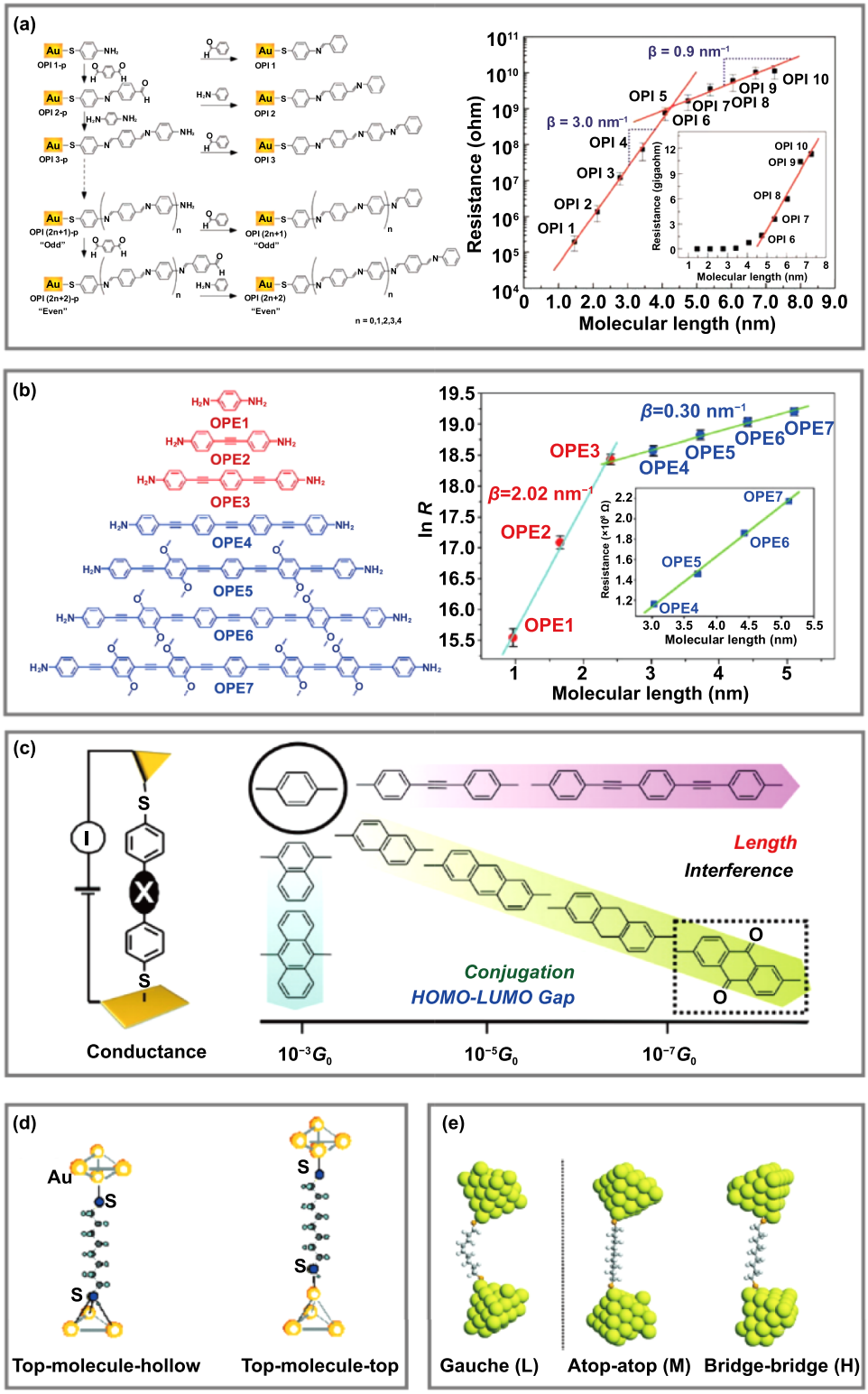

Figure 19. (a) Structure and preparation process of OPI molecular wires on gold substrate (left) and plot of ln$R$ versus molecular length of OPI molecules junction from tunneling to hopping mechanism (right). From [218]. Reprinted with permission from AAAS. (b) Structure of OPE molecular wires (left) and plot of ln$R$ versus molecular length of OPE molecules junction from tunneling to hopping mechanism (right). Reprinted with permission from [219]. Copyright (2009) American Chemical Society. (c) Schematic of research facility and OPE derivative structure with different length and HOMO-LUMO gap. Reprinted with permission from [214]. Copyright (2012) American Chemical Society. (d) Models of two different molecular-electrode contact geometry of alkanedithiol molecular junctions found by Tao's group. Reprinted with permission from [224]. Copyright (2006) American Chemical Society. (e) Three typical arrangement models of Au-alkanedithiol-Au junctions found by Wandlowski's group. Reprinted with permission from [231]. Copyright (2008) American Chemical Society.

level alignment of the system [230]. It was found in experiment that the conductance of molecules conducted through HOMO increases (decreases) at a positive (negative) gate potential, while molecules conducted through LUMO show the opposite trend.

In addition, the impact of coupling degree between molecule and electrode on the molecular junction electric transport process has also been extensively studied [224, 231, 232]. For example, in the measurements for the conductance of molecular junctions, the researchers found that many of them had multiple conductance values, which is due to the different molecular structures caused by the different contact angles or the different contact sites between molecule and electrode. In terms of contact angle, Venkataraman's group found that the electrical transport capacity of BPY molecule was relatively weak when the Au-N bond between the anchored group and the electrode is perpendicular to the plane of the conjugated component in the molecular structure. On the contrary, when the Au-N bond is parallel to the conjugated component in the molecular structure, the electric transport of the molecular junction is enhanced, which is due to the different coupling degree between the molecule and the electrode in the two configurations [232]. In terms of contact sites, for example, Tao's group found that the same single alkanedithiols may have multiple conductance values during the research on the electric transport properties of alkanedithiol junctions. They proposed for the first time that the high conductivity value may be contributed by the thiol group connected to the top or acupuncture point of the gold electrode, while the low conductance value may be contributed by the thiol group connected to the top of the gold electrode (figure 19(d)) [224]. For another example, Wandlowski's group studied the electric transport property of nonane molecules with two sulfhydryl anchored groups at both ends, and found that it had three different conductivity values of high, medium and low. They believe that this phenomenon is related to the possibility that molecules may bind to different sites of electrode, such as gauche, atop and bridge (figure 19(e)) [231].

4.1.3. QI properties of single-molecule junctions. In recent years, the QI effect has become a focus in the study of the structure-properties relationship between molecular structure and charge transport properties through single-molecule junction [73]. In section 2, we mentioned that QI effects can significantly change the conductance of single-molecule, especially DQI effects. This will bring new solutions to the preparation of high-performance molecular devices with a high ON/OFF ratio. Therefore, the current research on QI effect in single-molecule charge transport is mainly focused on developing the regulation methods of QI effects.

Firstly, the QI can be regulated by electrical method [70–72]. That is, the conjugated mode or energy level difference of molecular devices can be adjusted by the third gate electrode in electrochemical gating (reference electrode) and electrostatic gating (bottom gate electrode). For example, Tao's group used gate voltage to adjust the energy level difference between the electrode Fermi level and the frontier molecular orbitals, and observed extremely low conductance when the Fermi level matched the energy at the antiresonance transport of DQI [72] (figure 20(a)). Similarly, Zhou's group adjusted the energy level arrangement between the molecules and the electrodes by controlling the electrode potential. They found that the conductance of the meta-connected benzene molecules varied from $10^{-6.0}$ to $10^{-3.3}$ G_0 by more than 2 orders of magnitude, while the redox state of the molecule remained unchanged. Using this method, they also realized the regulation of DQI [71]. In addition, Hong's group developed a four-electrode electrochemical gating method, as shown in figure 20(b), to study the electrical transport process of 2,4-thiophene (2,4-TP-SAc) and 2,5-thiophene (2,5-TP-SAc) derivatives [70]. They found that 2,4-TP-SAc has a larger dependence on the bias voltage, with a 100-times change in conductance when the electrode potential was adjusted from −0.4 V to 1.3 V. For the first time, they clearly observed the anti-resonant characteristic peak of DQI on the electron transmission spectrum, realizing the regulation of QI by electrochemical methods.

Second, by adjusting the relative position of two molecules by mechanical force, the QI of charge transport in the π–π stacking system can be regulated [43, 60]. In 2016, van der Zant's group reported on the use of mechanical force to CQI [43]. As shown in figure 20(c), they used MCBJ technology to study the charge transport of OPE3 π–π stacking molecules. The overlapped conformations of two molecules can be manipulated by the movement of the electrodes. They found that when two π–π stacked molecules slide against each other, there is a significant decrease in conductance. Through theoretical calculations, it is found that the decrease in conductance is caused by DQI. Therefore, by using mechanical force to change the orbital coupling of π–π stacked molecules can realize the regulation of QI, and quasi-periodic changes in conductance can be observed.

In addition, using chemical methods to change the molecular structure are also common strategies to control QI [92, 93]. In 2017, Hong's group reported a chemical method for protonation regulation of QI [92]. As shown in figure 20(d), they used MCBJ technology to study the charge transport properties of the protonated azulene derivatives. The results showed that the conductance of protonated azulene derivative (red curve, figure 20(d)) was higher than that of neutral one (black curve, figure 20(d)). Theoretical results showed that the HOMO-LUMO gap changes after protonation, which weakens the DQI of the azulene system, thus realizing the chemical regulation of QI.

4.2. Spectroscopy characterization

There are many factors affecting the electrical properties of single-molecule. During the measurement, different connection states and structural changes caused by the reaction may both affect the charge transport properties [224, 231–233]. However, the direct clarification of structural information of molecular junction is still lacking. Vibration spectrum can provide molecular fingerprint information, so it can help to determine the microstructure of molecular junction and

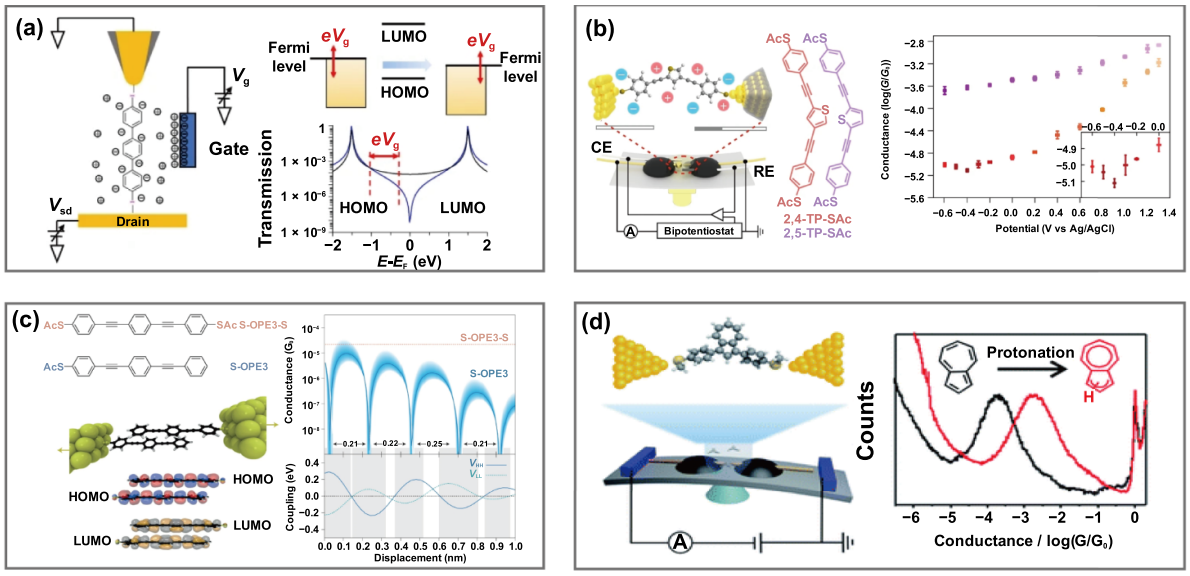

Figure 20. (a) Schematic of the electrochemical gate-controlled measurement setup (left) and energy level diagram and transmission spectrum of molecular junction under gate regulation. Reproduced from [72], with permission from Springer Nature. (b) Schematics of the four-electrode electrochemical gated MCBJ technique method (left) and the tendency of the molecular conductance of sample (right). Reproduced from [70], with permission from Springer Nature. (c) Diagram of molecular junction with π–π stacked molecules (left) and result of transport calculations combined with molecular dynamics simulations (right). Reproduced from [43], with permission from Springer Nature. (d) Schematic of the MCBJ setup (right) and conductance histograms of samples (left). Reproduced from [92]. CC BY 3.0.

clarify its structure-property relationship. With the development of tunneling electronics, high-resolution tunneling spectroscopy techniques, such as point-contact spectroscopy (PCS) and inelastic electron tunneling spectroscopy (IETS) have emerged [234]. PCS [235] and IETS [236, 237] have gradually developed into important tools for identifying intrinsic vibrations triggered by tunneling electron within molecular junctions. The principle is basically similar in that an inelastic electron tunneling process between two electrodes transferring energy into molecular vibration through electron–vibration interaction [234]. This effect is shown as a slight kink in the I–V curve, with a corresponding step in the first-order partial derivative spectrum and a peak in the second-order partial derivative curve, which corresponds to the vibrational fingerprint information of molecule. In 2002, Smit *et al* used PCS for the first time to characterize hydrogen junction [235]. Through PCS, they observed small changes in conductance caused by the electron–phonon interaction of the single-molecule junction, which clearly clarified the existence of molecules between metal electrodes. In 2006, Long *et al* used IETS to detect molecular changes within molecular junctions in anhydrous and hydrated environments, and found effects of hydration on molecular junction electrical transport [238]. Although PCS and IETS have been widely used for the detection of molecular junctions, the high vacuum and ultra-low temperature (~4 K) experimental conditions limit their wide applications.

Spectroscopic techniques, such as infrared spectroscopy and Raman spectroscopy, are expected to be used for structural characterization of molecular junctions at room temperature. In particular, Raman spectroscopy, due to the presence of nanostructures, can greatly enhance the signal and improve the detection sensitivity by surface enhanced Raman scattering (SERS), which can achieve high sensitivity to single-molecule level. The molecular junction fabricated by the metal nanoelectrode gap can effectively exhibit the properties of a face-to-face coupled antenna, and thus cleverly realize the SERS characterization of bridging molecules inside the nanogap as the 'hotspot' [98, 239]. Since Tian *et al* first reported the SERS study of molecular junctions by combining SERS with MCBJ, the combined characterization of single-molecule junctions by electrical and enhanced Raman spectroscopic methods has been applied more and more widely [98]. The experimental methods can be divided into two categories according to the construction of molecular junctions.

One type is static molecular junction in conjunction with SERS technique. For example, Ward *et al* developed a single-molecule SERS measurement using EM (EMJ-SERS), which realized the simultaneous monitoring of the electrical and spectral signal of the molecular junction in the prepared nanogap [240]. Experiments have shown that the change in conductance during the junction breaking process is related to the change in the intensity of the Raman mode vibration (figure 21(a)). David *et al* developed a cross-nanowire molecular junction (X-nWJ) platform that can simultaneously use IETS and SERS to directly measure the current–voltage-temperature characteristics of the same junction [241] (figure 21(b)). Bart *et al* used the method of NPoM to track the evolution of the Raman spectrum of molecular tunneling junctions [242], which explored the redox process caused by the generation and transport of hot electrons (figure 21(c)).

The other type is dynamic molecular junction technology combined with SERS technique, mainly including STM-BJ-SERS and MCBJ-SERS. For MCBJ, the light path can be

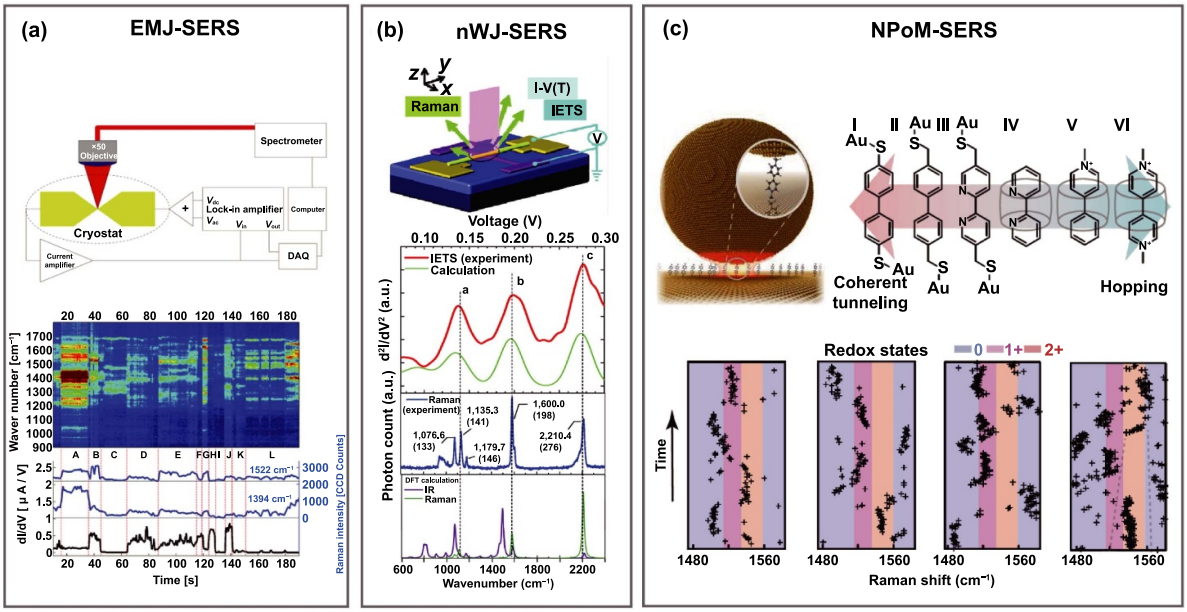

Figure 21. (a) Schematic of the EMJ-SERE setup (up) and waterfall plot of Raman spectrum and conduction measurements of bridging molecules (down). Reprinted with permission from [240]. Copyright (2008) American Chemical Society. (b) Schematic of the nWJ-SERE setup (up) and comparison of the Raman spectra to the IETS and DFT calculation of the bridging molecules (down). Reprinted with permission from [241]. Copyright (2010) American Chemical Society. (c) Schematic of the NPoM-SERS setup (up) and redox states peak positions of bridging molecule in Raman spectrum(down). Reproduced from [242], with permission from Springer Nature.

easily introduced from a perpendicular direction. Tian *et al* first combined SERS with MCBJ to detect the enhanced Raman signal of BDT molecular junction (figure 22(a)) [98]. It is found that the Raman signal of the molecular junction increases with the decrease of the gap width, which indicates that the enhanced Raman signal does come from the molecular junction in the nanogap under the excitation of a specific wavelength. The polarization dependence of Raman signal and incident laser further confirmed that the Raman signal is enhanced greatly when the polarization direction of incident laser is parallel to the electrode, while the vertical polarization has a significant inhibition effect on the Raman signal. Konishi *et al* monitored the thermal motion of a single BPY molecular junction through simultaneous Raman and conductance measurements in the MCBJ-SERS system (figure 22(b)) [239]. The analysis of the Raman bands revealed the dynamic mode switching between the vertical and tilted configurations of the bridging molecules in the nanogap. In 2018, Guo *et al* firstly reported that molecular orbital-gated SERS using MCBJ technology (figure 22(c)) [243]. They integrated a perpendicular side gate electrode to the source-drain electrodes into the MCBJ chip to exert a gating effect on the single molecule junction. Experiments shown that Raman scattering can be further enhanced by about 40% through molecular orbital gating. Moreover, Zhao *et al* studied the modulation of electron transport and Raman scattering by the atomic geometry of the electrode (figure 22(d)) [244]. Through pure mechanical operations, they manufactured both atomic-scale sharp and atomic-scale planar electrodes that can control the gap size with sub-angstrom precision. Experiments have found that the use of atomic-scale sharp electrodes can increase the conductivity of the amine-linked molecular junction by about 50%. While the atomic-scale planar electrodes are more advantageous in improving the response of Raman scattering to the size of the nano-gap.

For the combination use of STM-BJ and Raman spectroscopy, due to the vertical structure of STM-BJ, it is difficult to introduce light illumination on the tip. In recent years, a variety of efforts have been made to realize the combination of STM-BJ and Raman spectroscopy. Liu *et al* developed a 'fishing mode' tip-enhanced Raman spectroscopy (FM-TERS) to simultaneously obtain single-molecule *I–V* features and the corresponding Raman signals [97] (figure 22(e)). Bi *et al* modified the STM tip using a gold-covered tetrahedral glass (t-tip) so that the laser can be introduced inside the tetrahedral glass into the molecular junction [245] (figure 22(f)). Using this device, they demonstrated the effect of voltage-controlled conformational switching in molecular junctions. Kos *et al* introduced a transparent conductive cantilever beam in STM-BJ, which on the one hand can electrically contact the NPoM regime to connect the molecular junction, and on the other hand can maintain Raman observations of molecular junctions [246] (figure 22(g)). Real-time Raman measurements revealed that diphenylthiols molecular rings were distorted when bias was applied, which would affect the coupling between the molecule and the electrode. Domulevicz *et al* designed a transverse STM-BJ system, in which the tip and the oblique substrate were placed horizontally on both sides for better Raman signal acquisition [247] (figure 22(h)). By combining molecular electrical transport measurements with Raman spectroscopy, they extracted information about the configuration changes and dynamics of molecular junction under the electric field and during the stretching process.

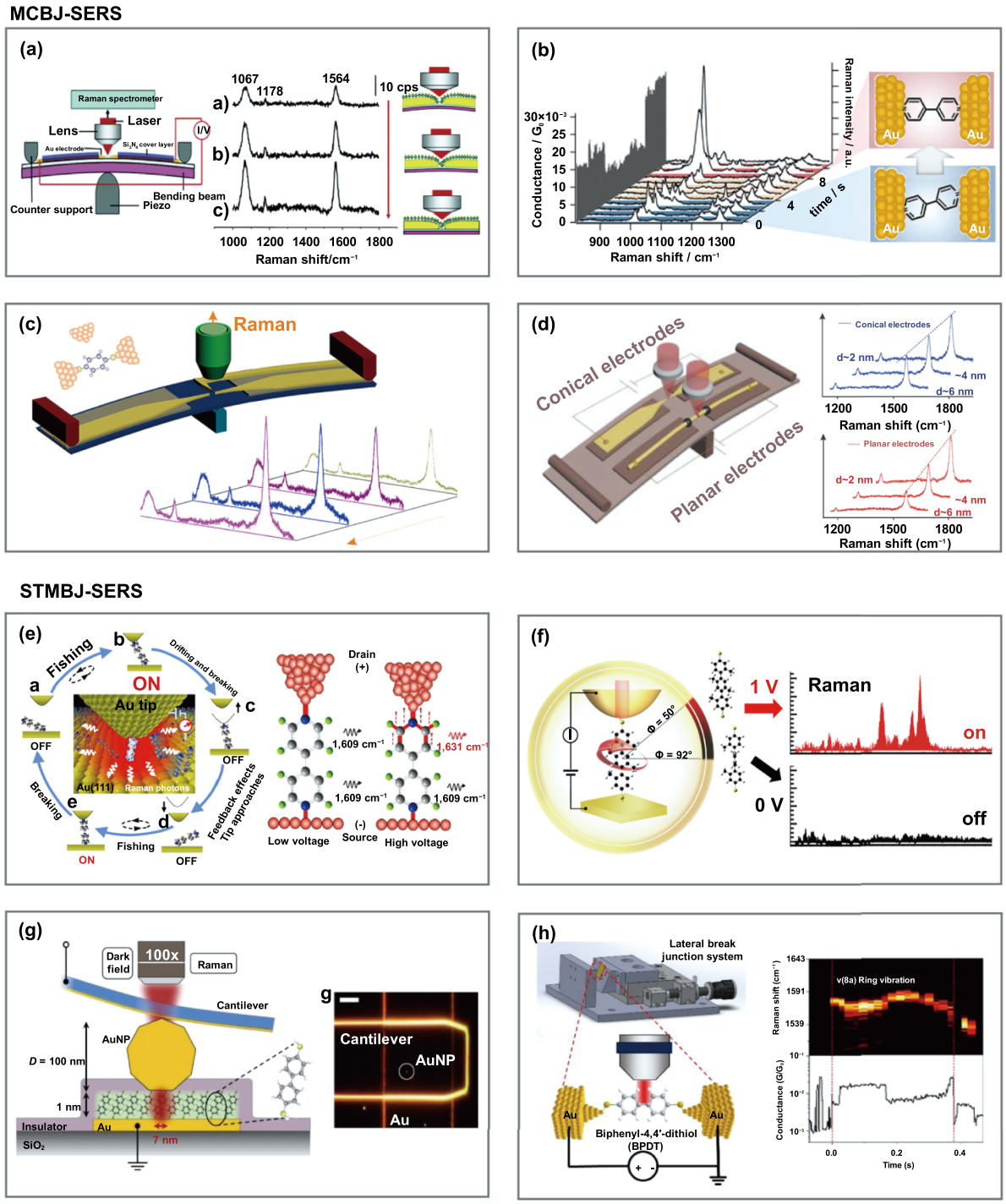

Figure 22. (a) Schematic of MCBJ-SERS setup (left) and Raman signal molecular junction with different gap width (right). Reprinted with permission from [98]. Copyright (2006) American Chemical Society. (b) SERS spectra of 4,4′-bipyridine molecule junctions with different molecular bridge states. Reprinted with permission from [239]. Copyright (2013) American Chemical Society. (c) Schematic of the measurement setup for side-gating Raman scattering and SERS spectra recorded upon different gate voltages. Reprinted with permission from [243]. Copyright (2018) American Chemical Society. (d) Schematic of the MCBJ experimental setup with both atomic-scale sharp and atomic-scale planar electrodes (left) and Raman spectroscopy of diaminobenzene upon different shape electrodes (right). [244] John Wiley & Sons. © 2018 WILEY-VCH Verlag GmbH & Co. KGaA, Weinheim. (e) Schematic of 'fishing mode' TERS. Reproduced from [97], with permission from Springer Nature. (f) Schematic of a molecular junction spectroscopy setup using a gold-covered tetrahedral glass as tip. Reprinted with permission from [245]. Copyright (2018) American Chemical Society. (g) Schematic of an Au nanoparticle on SAM (NPoM geometry) setup which is electrically contacted by a conductive transparent cantilever. Reproduced from [246]. CC BY 4.0. (h) Schematic of a transverse STM-BJ system. [247] John Wiley & Sons. © 2021 Wiley-VCH GmbH.

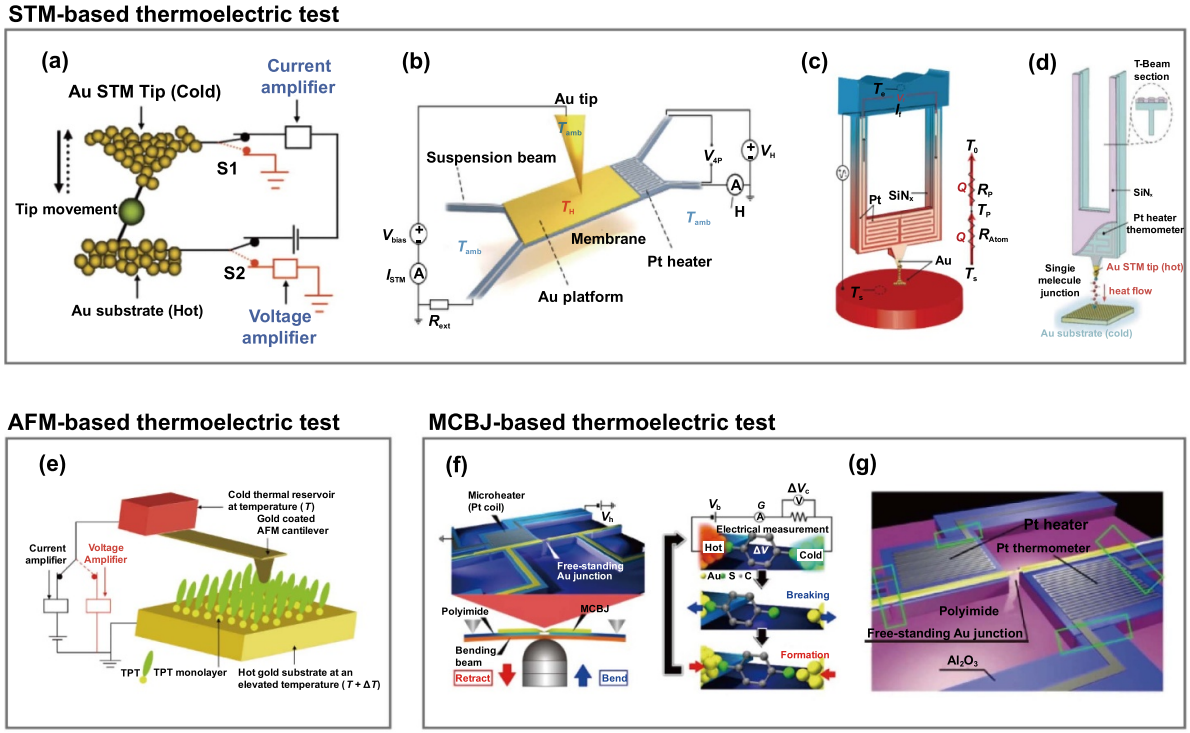

Figure 23. (a) Schematic of an STM-based thermoelectric test setup. From [249]. Reprinted with permission from AAAS. (b) Schematic of an ultra-high thermal resolution substrate chip. Reproduced from [75], with permission from Springer Nature. (c) Schematic of a C-SThM probe with a heated metallic substrate to construct a molecular junction. From [76]. Reprinted with permission from AAAS. (d) Schematic of the self-heating C-SThM set-up. Reproduced from [77], with permission from Springer Nature. (e) Schematic of an AFM-based thermoelectric test setup. Reprinted from [250], with the permission of AIP Publishing. (f) Schematic of a heater-embedded MCBJ chip. Reproduced from [78]. CC BY 4.0. (g) Schematic of an MCBJ chip modified with a heater and a thermometer. Reproduced from [81]. CC BY-NC-SA 3.0.

4.3. Thermoelectric characterization

Understanding the transport, dissipation and conversion of heat in molecular junctions is important for further high-efficient energy conversion. In addition, the study of the thermal transport properties of molecular junctions can provide new insights into the scope of characterizations of classical models and theorems [248]. Several research groups have experimentally quantified the thermoelectric properties of molecular junctions. The following will briefly discuss the experimental techniques used to measure the thermoelectric properties of molecular junctions, which can measure the voltage output generated by trapping the molecular junction between hot and cold electrodes. Ludoph *et al* first reported experimental measurements of Seebeck coefficient and conductance in Au point contact at liquid helium temperature [248]. This work provides a method for thermoelectric measurements at molecular junctions. Subsequently, Reddy *et al* used STM-BJ technology to conduct an experimental study on the thermoelectric characteristics of molecular junctions [249]. To study the thermoelectric effect of the molecular junction, they modified the STM-BJ technology to create a temperature difference in the molecular junction. As shown in figure 23(a), by heating the substrate and keeping the tip at room temperature, the temperature difference between the tip and the substrate, ΔT, is established. The thermal voltage ΔV caused by ΔT is then monitored during the connection and disconnection of the molecular junction. The Seebeck coefficient of the junction can be obtained by $S = -\Delta V/\Delta T$. For the first time, they captured a molecule between two gold electrodes with a temperature difference and measured the Seebeck coefficient of the BDT molecular junctions.

In recent years, with the progress of micro-and nano-manufacturing, researchers have continuously integrated the temperature control and detection components into specially designed STM-BJ to build a platform for detecting the thermal transfer characteristics of atomic-scale systems. For example, Mosso *et al* modified the substrates for single-molecule thermoelectric measurements [75]. By manufacturing the substrate to integrate a suspended platinum microheater, they built a chip as the high-temperature end for single-molecule thermal transport measurement with ultra-high resolution (figure 23(b)). Using this method, they simultaneously measured the charge and heat transfer in Au atom contact, confirming the validity of the Wiedemann-Franz law on the atomic scale. In contrast, Cui *et al* optimized the tip, and developed a calorimetric scanning thermal microscopy (C-SThM) probe with a high-resolution Pt thermometer. The substrate is heated by an external heat source. Since the single-molecule and the ultra-high thermal resolution tip are connected in series in a heat path, the temperature of the tip when the molecular junction is connected can be used to measure the heat flow through

the single-molecule [76] (figure 23(c)). They investigated heat transfer in Au and Pt point contact respectively, and observed quantization of thermal conductivity at room temperature in Au atomic junctions. Further, they integrated Pt coils into the tip, using tip joule heat directly to form a hot end on itself. The molecular thermal conductivity can be obtained by detecting the change of resistance value caused by the slight change of tip temperature before and after molecular junction connection [77] (figure 23(d)). Their experiments on the thermal conductivity of Au-alkandithiol-Au junctions containing 2–10 carbon atoms confirmed that unlike the length-dependent property of electrical conductance, thermal conductance has almost nothing to do with molecular length.

In addition to the STM-BJ technology, Tan *et al* developed a thermoelectric technology based on AFM to study the thermoelectric effect in SAM junctions [250] (figure 23(e)). In this scheme, the thermoelectric potential test can determine the relative position of the molecular orbitals, and the electrical measuring scheme of transition voltage spectroscopy can further reveal the energy separation. Thus, by simultaneously measuring the thermoelectric potential and current–voltage characteristics of the molecular junction, they can determine the molecular orbital arrangement. MCBJ technology is another widely used experimental method to detect thermoelectric transport properties in molecular junctions. Tsutsui *et al* integrated a Pt heater unit into one side of the electrode on the MCBJ chip, to establish the temperature differences between molecular junctions. Using this method, they investigated the Seebeck coefficients of Au-BDT-Au junctions and reported that the electrical transport properties of BDT molecules are sensitive to geometric configuration [78] (figure 23(f)). Furthermore, they also integrated heaters and thermometers on both sides of the suspended gold nano bridge to study the reason for the asymmetric electrothermal effect in symmetric point contact [81] (figure 23(g)).

5. Functionalization of molecular junctions

The ultimate goal of molecular electronics is to design electronic components from the atomic and molecular levels, which can realize the same functions as silicon-based electronic devices. The molecular junctions, are unable to provide a research foundation for the preparation of functional molecular electronic devices through accurately manufactured, precisely characterized and elegantly controlled. Furthermore, researchers can control the charge transport capacity of molecular junction by changing the temperature, magnetic field, light illumination, external electric field and electrochemical potential of the molecular junction, so as to realize the construction of molecular devices with specific functions. In this part, we will summarize and discuss the research progress of single-molecule functional devices.

5.1. Rectifier

A rectifier is a type of electronic device that only allows current passing through in one direction. It has a wide range of applications in voltage stabilization and logic circuits. This feature is mainly derived from the asymmetry of the channel material structure, such as semiconductor p-n junction, semiconductor-metal heterojunction and so on. For single-molecule devices, there are usually four methods to realize the rectifier function of a molecular junction: (a) design a molecular skeleton with an asymmetric structure, such as donor-acceptor structure [251] (figure 24(a)), so that the electron transport process is unidirectional; (b) use an asymmetric anchor group. For example, one end is connected by the Au–S bond, and the other end is connected by the Au–C bond [252] (figure 24(b)). Due to the different coupling effects between different anchor groups and electrodes, the transfer efficiency of electrons in different directions is different; (c) use different kinds of electrode materials, such as carbon-based electrodes and metal electrodes [157] (figure 24(c)). Due to the different work functions of the electrodes at both ends, there is a Schottky barrier, which causes the rectification effect; (d) control the external environment of molecular junctions, such as using ionic solution to surround the molecules [253] (figure 24(d)). An electric double layer will be generated at the interface between the electrode and the solution, which will cause a pinning effect between the molecular orbital and the chemical potential of the substrate. The magnitude of the current is related to the polarity of the bias voltage.

5.2. Switch

The Switch is one of the most basic components in a circuit. Molecular switches have attracted extensive research interests as powerful candidates for future electronic components. Molecular switches require functional molecules to have two different states that exhibit different conductance states [254]. In molecular electronics, it has been proved that the bistable or even multiple states of molecules can be excited by applying external stimuli, such as light, electrical, thermal and mechanical forces. In this way, the reversible switch of single-molecule conductance can be realized by changing the properties of the molecule by changing the anchoring mode, configuration and spin state [16, 255]. In this section, we will focus on the progress of molecular switching by optical, mechanical force and electric field regulation.

5.2.1. Optical-controlled single-molecule switch. Optical switch is a kind of electronic device which realizes circuit turn on and off by responses of optical stimulation. Some organic molecules with photoactive groups will change their conformation, chemical and electronic structure under light illumination, which will affect their electric transport properties. This type of work can usually be used in the design of single-molecule optical switching devices. Dulic *et al* first experimented with light-controlled molecular switches in 2003 [256]. They used photochromic dithienylethene molecules linked to a gold electrode via a sulfhydryl group. The closed-loop/open-loop molecular switches were then obtained by ultraviolet/visible irradiation respectively. Subsequently, a large number of dithienylethene molecular junctions have

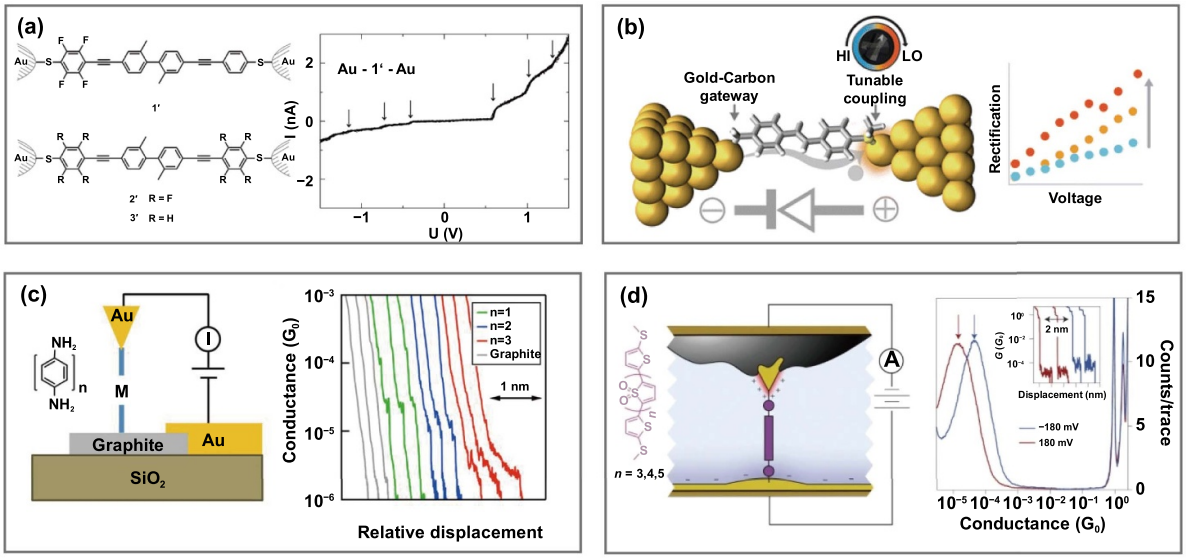

Figure 24. (a) Rectifier with molecular skeleton of asymmetric structure (left) and *I*–*V* curve of molecular(right). Copyright (2005) National Academy of Sciences. (b) Rectifier with asymmetric anchoring groups. Reprinted with permission from [252]. Copyright (Year) American Chemical Society. (c) Rectifier with different kinds of electrode materials (left) and sample conductance versus displacement traces (right). Copyright (2014) National Academy of Sciences. (d) Rectifier with molecules surrounded by ionic liquids (left) and log-binned conductance histograms of samples (right). Reproduced from [253], with permission from Springer Nature.

been reported, and their closed/opened conductance switching ratio can reach two orders of magnitude [257–260]. Subsequently, researchers have also developed a series of reversible optical switches with different molecular systems, such as azobenzene [261–264], diarylethenes [265–267], dimethyldihydropyrene/cyclophanediene [268], dihydroazulene/vinylheptafulvene [269–272], porphyrin [273, 274], spiropyran/merocyanine [275, 276] and other systems, as shown in figure 25(a).

How to obtain a higher switching ratio and a stable electrode interface is still the most challenging problem to fabricate a stable and repeatable single-molecule optical switch. However, in previous studies, light regulation is often irreversible (from an insulated open-loop to a conductive closed-loop with only one-way response, or vice versa). The reason for this unidirectional response is that the excited state of the molecule is easily quenched when interacting with electrode, which is caused by the strong molecular-electrode coupling between the anchor group of the molecule and the electrode. To overcome this problem, Guo's team implanted four methylene (CH_2) groups on each side of the diarylethenes skeleton, bridging between graphene electrodes to form stable molecular junction [265]. Due to the existence of methylene, the molecular-electrode coupling is significantly reduced, thus achieving a reversible optical switch, as shown in figure 25(b). As a result, they successfully constructed a completely reversible single-molecule optical switch, with switching ratio reaching 100, stability for more than one year and reproducibility exceeding more than 100 photosensitive cycles. It paved the way for the development of optoelectronic devices using molecular electronic properties.

5.2.2. Mechanical force-controlled single-molecule switch. The geometry of molecular junctions can also be manipulated by mechanical force to realize the conductance conversion of single molecular junctions [232, 278]. As mentioned in section 3.2, dynamic molecular junctions capture and release molecules by mechanically regulating the opening and closing of electrodes [24]. But at the same time, due to mechanical stretching, multiple conductance values often appear during the test, which arouses the attention of scientists.

How to obtain a stable single-molecule junction and regulate it mechanically? In 2009, Quek *et al* used STM-BJ technology to control the stretching and compression of molecular junctions and demonstrated a reversible binary switch based on BPY-gold single-molecule junction [232]. Specifically, they formed stable single junctions through repeated contact between the tip and the substrate and performed conductance tests. They found that the counts within the low G range occurred 2 Å after the gold point contact was disconnected. Thus, they modulated the tip-substrate separation with a sinusoidal motion of 2 Å amplitude during the measurement to switch the conductance between the two states. It can be clearly seen that the conductivity of the molecule is reversibly converted with the repeated stretching and compression of the nanoelectrode, as shown in figure 26(a). Subsequent theoretical studies have shown that different conductance states come from different contact geometries that change with the mechanical changes of the electrodes. In addition, Taniguchi *et al* reported a bistable mechanical switch of alkanedithiol based on MCBJ technology (figure 26(b)) [278]. After obtaining stable single molecular junctions using nanofabricated MCBJ chips, they applied sinusoidal motion to

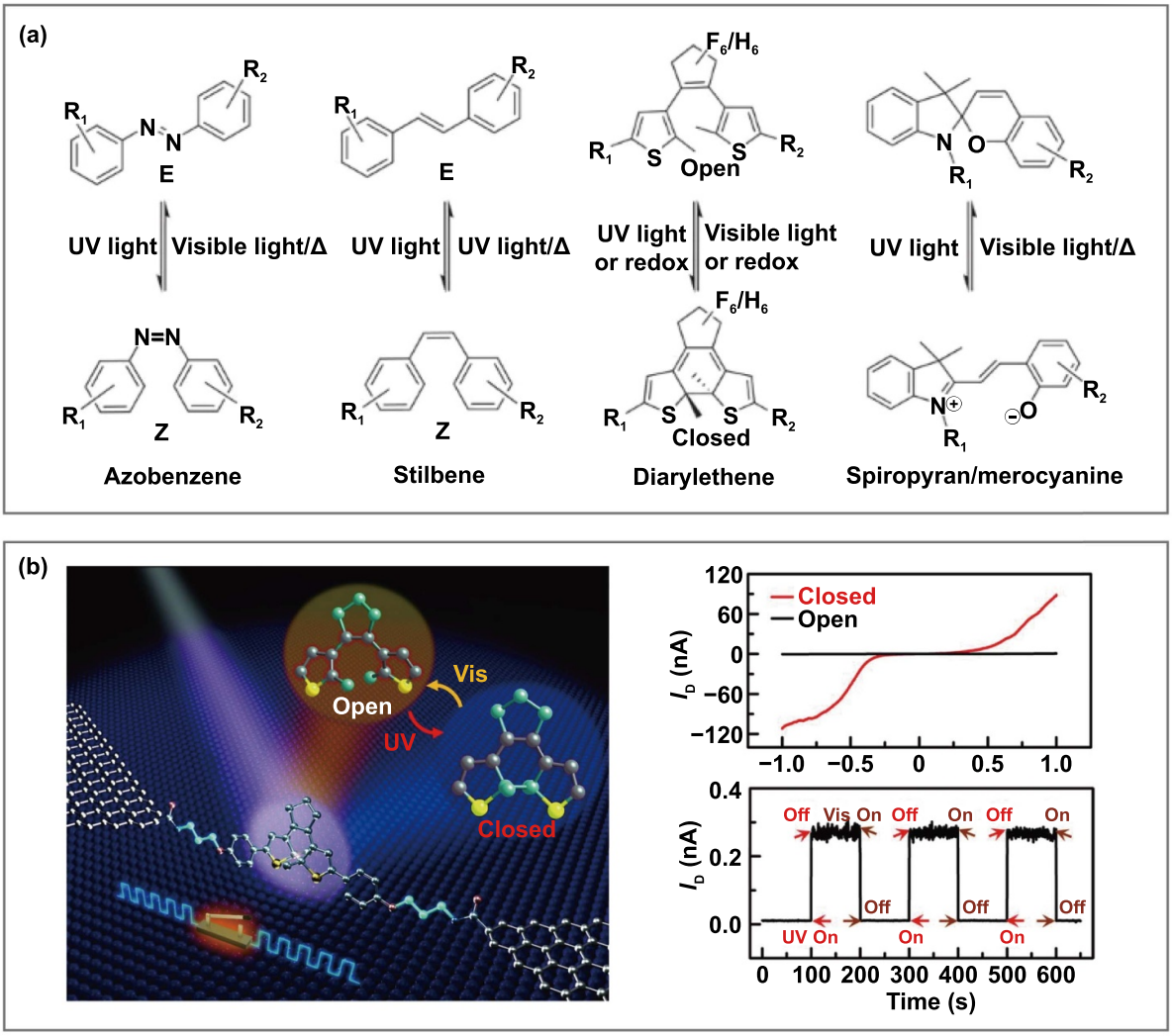

Figure 25. (a) Widely used photochromic molecule: azobenzene, stilbene, diarylethene, spiropyran. Reproduced from [277]. CC BY 4.0. (b) Schematic of a graphene-diarylethene-graphene reversible photoswitching molecular device (left) and *I*–*V* curve of open/closed state and photocurrent response curve (right). From [265]. Reprinted with permission from AAAS.

the piezoelectric actuator to achieve mechanical stretching/compression of the electrode. The molecular junction was observed to show a switch between high and low conductance by means of mechanical oscillating electrodes.

How does mechanical expansion achieve conductance control? It is mainly divided into several aspects. On the one hand, for systems with high rigidity, mechanical force manipulation mainly acts on the geometry of the electrode-molecule bond to affect the single-molecule level transport characteristics [232, 279–281]. For example, Ferri *et al* investigated the electromechanical behavior of molecular junctions in hemilabile ligands contact parts and found that the modulation of conductance results from the transition of molecular-metal contact parts from single-tooth/two-tooth ligand (figure 27(a)) [279]. In addition, Diez-Perez *et al* developed a method based on lateral coupling to mechanically and reversibly control the conductance of the single molecular junction by mechanically adjusting the angle between a single pentaphenylene bridged between two metal electrodes (figure 27(b)) [280].

On the other hand, for the flexible molecular system, the changes in molecular junction mainly come from changes in the configuration and conformation of the molecule itself [282–285]. For example, Wu *et al* imparted the molecule with mechanical sensitivity by introducing the flexible segment diketone part into the rigid molecular line. When the molecular junction is repeatedly compressed and relaxed, the molecule will fold along the flexible fragment and induce reversible conductance switch (figure 27(c)) [282]. For another example, Su *et al* reported for the first time a single-molecule switch operated by a stereoelectronic effect. By stretching and compressing the electrode, specific dihedral angles in permethyloligosilanes with aurophilic methylthiomethyl electrode contacts can be manipulated, thereby realizing the switching of different conductance states (figure 27(d)) [283].

In addition, for some flexible molecule systems, the conformational change will not only change the electron transport distance, but also accompany other phenomena, such as the change of molecular frontier orbital [286, 287] and QI

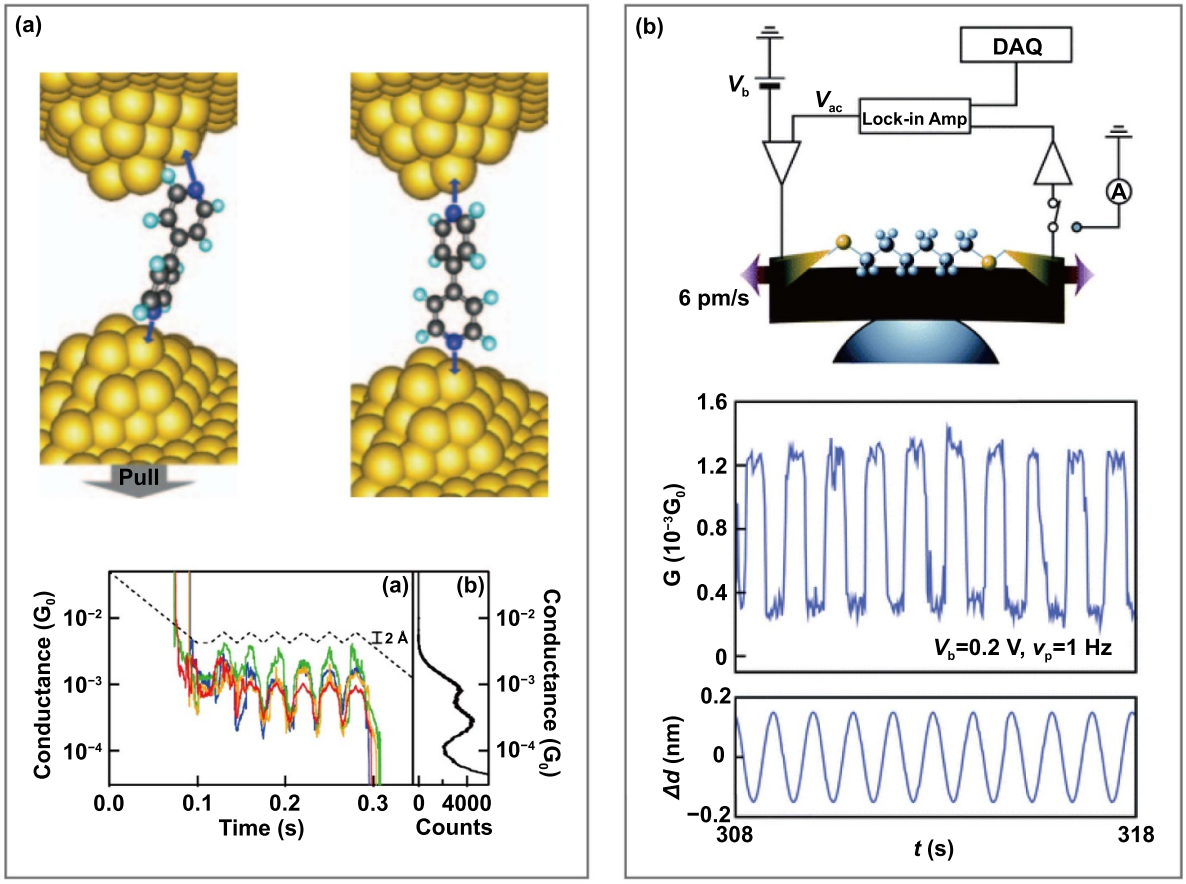

Figure 26. (a) Schematic of molecular junctions with the high and low conductance configurations (up) and high and low conduction state modulated by sinusoidal mechanical oscillation (down). Reproduced from [232], with permission from Springer Nature. (b) Schematic of MCBJ setup exploited for single molecule conductance and IETS measurements (up) and switching characteristics obtained under applied 1 Hz mechanical perturbations. Reproduced from [278] with permission of The Royal Society of Chemistry.

effect [43, 60, 288, 289]. These phenomena directly act on the electrical transport of molecules, and ultimately achieve high-efficiency regulation of molecular junction conductance. For example, Bruot *et al* used STM-BJ technology combined with IETS to study the conductance changes of BDT molecular junction during electrode stretching and compression, and confirmed that HOMO energy level caused by strain was closer to Fermi energy level of electrode, resulting in enhanced resonance conductance (figure 27(e)) [286]. For another example, Camarasa-Gómez *et al* studied the influence of the degree of freedom of configuration of ferrocene derivatives on the conductance of the single molecular junction, and found that the low conductance is the result of the DQI effect of Fano type controlled by mechanical force (figure 27(f)) [289].

5.2.3. Electric field-controlled single-molecule switch. Another way to regulate conductance switches of molecular junction is to use electric fields. Similar to mechanical force control, electric field can also control conductance switching by changing molecular anchor points [290], changing molecular conformation [245, 291–293], breaking chemical bonds [294, 295], and regulating molecular orbitals [296]. For example, Tang *et al* developed an electric-field-induced strategy to reversibly switch the connectivity of single molecular junction [290]. By controlling the bias voltage at both ends of the molecule, the anchor point of the pyridine ring and the electrode can be switched reversibly, leading to the switching of conductance. The conductance difference is about two orders of magnitude. Meng *et al* constructed asymmetric random conductivity switches caused by electric-field-induced isomerization of azobenzene based on graphene-molecular-graphene monolayers, achieving a switching ratio of about 2–2.46 [291]. It is noteworthy that this structure can also pass through a photoinduced conductance switch at low bias voltage. In terms of electric field breaking chemical bonds to modulate conductance, Godlewski *et al* reported that the covalent bond between trinaphthylene molecule and the DB dimer was broken through a high STM pulse bias voltage (>2.5 V) to achieve continuous conversion of high and low conductance states [294]. Recently, Na *et al* found that by applied gate electric fields, the LUMO and HOMO orbitals of ruthenium-diarylethene can move asymmetrically. This asymmetric movement can change the electrical transport properties of single molecules *in situ*. They used this feature to achieve a switching ratio of >100 on the graphene electrodes [296].

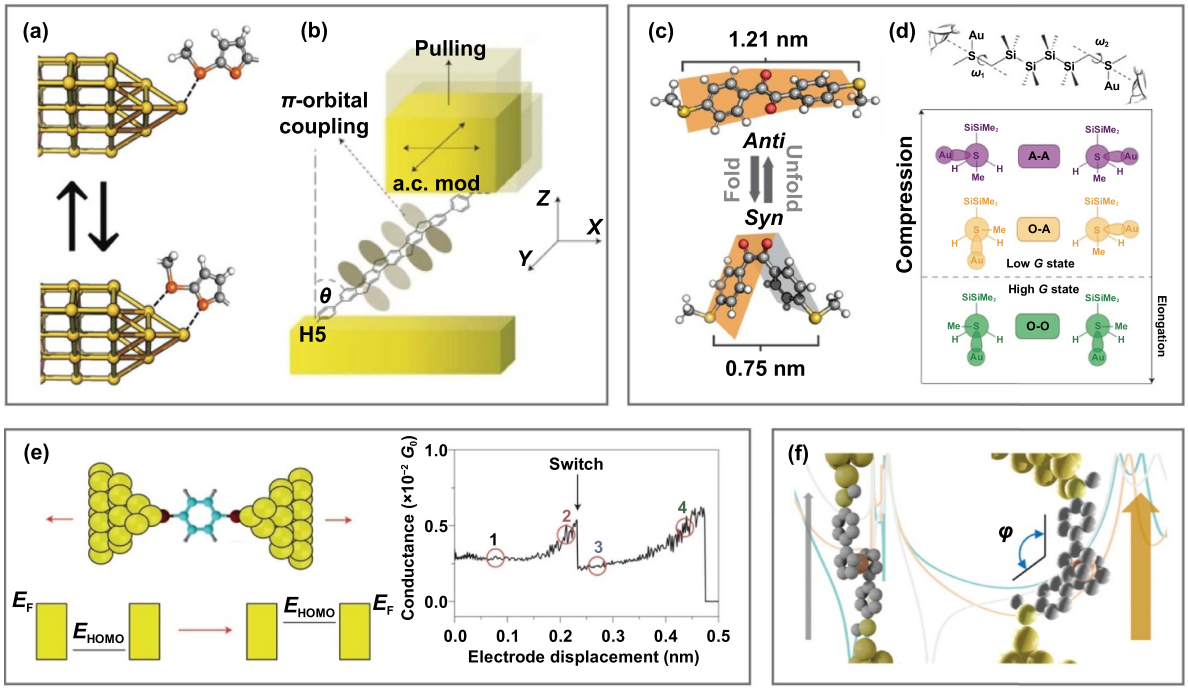

Figure 27. Examples for mechanical force manipulation regulate the geometry of the electrode-molecule bond: (a) the electromechanical behavior of molecular junctions in hemilabile ligands contact part and its monodentate and bidentate contact configurations at a Au electrode and (b) schematic of lateral coupling process; examples for mechanical force manipulation regulate the configuration and conformation of the molecule itself. (a) Reproduced from [279]. CC BY 4.0. (b) Reproduced from [280], with permission from Springer Nature. (c) Schematic of molecular folding along a flexible fragment and cycling between an anti and a syn conformation and (d) newman projections for the A-A (purple), O-A (yellow) and O-O (green) dihedral configurations from the perspective of the sulfur-methylene σ bond in the Au-Si4-Au system; examples for mechanical force manipulation leading to the change of molecular frontier orbital. (c) Reproduced from [282]. CC BY 4.0. (d) Reproduced from [283], with permission from Springer Nature. (e) Schematic of a molecular junction and energy diagram showing how the energy of the HOMO changes relative to E_F of the electrodes as electrode stretching (left) and conductance switching behavior of BDT junctions; examples for mechanical force manipulation leading to quantum interference effect. Reproduced from [286], with permission from Springer Nature. (f) Schematic of the change of configurational of a ferrocene derivative. Reprinted with permission from [289]. Copyright (2020) American Chemical Society.

5.3. Transistor

The feature size of CMOS-transistor has been continuously shrinking with the introduction of fin field-effect transistor (FinFET) to 16/14 nm [297, 298], turned into gate-all-around-FET (GAA-FET) when entering the 3–5 nm node [299, 300]. As described above, as the feature size continues to shrink, the gate's ability to control the channel is weakened, so new device structures must be introduced to meet the requirements of transistors. In molecular electronics, the molecules in the molecular junction can be analogous to the conductors inside the gate, and accordingly, the gated environment of the molecules is similar to GAA. Therefore, the study of molecular FET will contribute to extend research of the current type of GAA-FET architecture transistor devices, thus promoting the technological path forward.

5.3.1. Electrostatic gate control transistor. The single-molecule transistor can achieve the function of silicon-based transistors by regulating molecular orbitals through electrostatic gate. In 2009, Song *et al* reported a novel single-molecule transistor [48]. This transistor uses an approximately 3 nm thick aluminum oxide layer as the gate dielectric. They successfully adjusted the conductance of 1,4-BDT and 1,8-octanedithiol junctions by different gate voltages. When a voltage of 1 V was applied between the source/drain electrode with the gate electrode, the molecular orbital energy shifted by 0.25 eV, proving that there is a linear relationship between the gate voltage and the molecular orbital energy (figure 28(a)). In addition to using the substrate as the bottom gate, Xiang *et al* added a side gate electrode vertical to the electrodes pair in the MCBJ chip to regulate the electron transport of 1,4-BDT molecules, suggesting the possibility of directly regulating the charge transport properties in single-molecule junctions through this side gate [196] (figure 28(b)).

The electric field controlled by the gate electrode can change the molecular conformation and switch the conductance state of the molecule. In 2017, van der Zant *et al* reported a solid-state three-electrode device based on 2,4,6-hexakis-(pentachlorophenyl) mesitylene diradical molecule, manufactured using FBEM [301]. It has been proved that the gate voltage can be used to regulate the reversible and stable organic neutral diradical molecules from the neutral state to the reduced state. Meanwhile, due to the strong coupling with the electrode, the switch can reach sub-picosecond scale (figure 28(c)). Another example of molecular conformation changes is based on intramolecular proton transfer (PT). In this mechanism, the transfer of protons between different locations

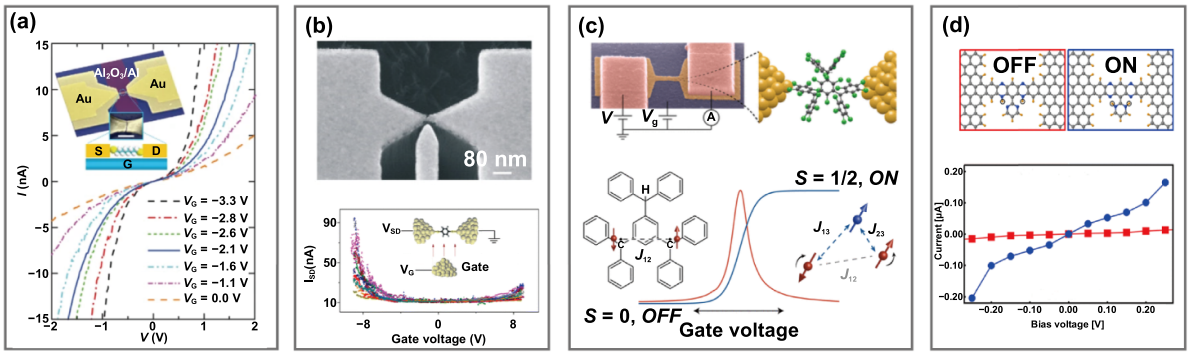

Figure 28. (a) Device structure and schematic diagram (inset) and I (V) curves of bridged molecules measured under different gate voltage. Reproduced from [48], with permission from Springer Nature. (b) SEM image of the MCBJ chip with independent side gate (up) and I (V) curves of the three-terminal molecular junction (down). Reprinted with permission from [196]. Copyright (2013) American Chemical Society. (c) SEM false-color image of molecular junction with AuPd/Al_2O_3 bottom gate (up) and schematic of gate voltage control spin state process (down). Reprinted with permission from [301]. Copyright (2017) American Chemical Society. (d) Schematic of molecular-graphene molecular junction in the form of OFF and ON (up) and corresponding I (V) curves (down). Reprinted with permission from [303]. Copyright (2021) American Chemical Society.

alters the electronic structure of the molecule and thus the conductance. In 2014, Hofmeister *et al* proved that the PT reaction in organic molecules could significantly change the molecular conductance, and the position of electrons can be effectively tuned by an external electric field [302]. In 2020, Weckbecker *et al* reported that a molecule-graphene junction could transfer two different conductive states through the PT process using theoretical simulation [303]. They demonstrated that the process could be controlled using an external electrostatic gate field to select the appropriate conductance state, confirming its potential for use in molecular transistors (figure 28(d)).

5.3.2. Electrochemical gate control transistor. Electrochemical gating can avoid the complicated solid-state three-terminal molecular device manufacturing process in electrostatic gating to realize effect conductance tuning, by using the double-layer potential existing at the metal-electrolyte interface as the gate. In addition, electrochemical gating can be performed at room temperature [304], the molecular redox state can be easily switched by electrochemical reaction.

Through the STM-BJ method, molecular junctions can be easily constructed in an electrochemical environment for studying transistor characteristics. The STM-BJ-based transistor schemes currently reported in the literature can be defined as two-electrode method, three-electrode method and four-electrode method according to the number of electrodes. As shown in figure 29(a) is a classic four-electrode electrochemical device: the STM tip and the substrate with a functional molecular layer are the working electrodes, and the potential difference between the two working electrodes is applied to drive the tunneling current. While the double potentiostat combines the counter electrode and the reference electrode to provide independent electrode potential control for the working electrode [19]. In 2003, Haiss *et al* constructed the first single-molecule electrochemical transistor using a four-electrode STM-BJ setup [29]. They observed the reversible conductivity change of the molecular junction, according to different supplied gate voltages. In 2014, Venkataraman's group first reported the three-electrode method [230]. The device is shown in figure 29(b), in which the encapsulated tip and the substrate are used as the working electrode, and the platinum electrode is used as the counter and also the gate electrode. The author found that when changing the gate voltage (V_g), the electric double layer on the working electrode would be affected, and therefore, molecular conductance can be regulated by changing V_g.

In 2015, Lovat *et al* developed a two-electrode single-molecule electrochemical transistor based on STM-BJ [305]. They proposed an asymmetric double layer model: due to the asymmetry of the electrode region exposed to polar/ionic solvents, a denser double layer forms on the coating tip compared to the substrate. In this case, molecular resonance can be regarded as being fixed on the chemical potential of the substrate, so that a bias-dependent shift of molecular resonance energy within the junction can be observed. This method provides a straightforward way to achieve the same effect as the electrochemical gate. Moreover, because the reaction occurs at the tip, the bias voltage of the electrochemical reaction is about five times larger than that of a traditional three-electrode electrochemical system (figure 29(c)).

In 2018, Xin *et al* demonstrated an effective method to adjust the molecular orbital energy level and the Fermi energy level of the graphene electrode by using ionic liquid as the gate dielectric, thereby realizing the controllable charge transport by the gate [306]. All of the three electrochemically inert aromatic chain junctions they studied exhibited gate-controlled conductance behavior. Since ionic liquids can keep their electrical double layer constant below their freezing point, this single-molecule transistor can be further used to explore gate-related quantum transport and new physical phenomena of single-molecule at low temperatures (figure 29(d)).

5.4. Spintronic device

Spintronics is one of the emerging scientific fields that study the electronics caused by the manipulation of the spin state of

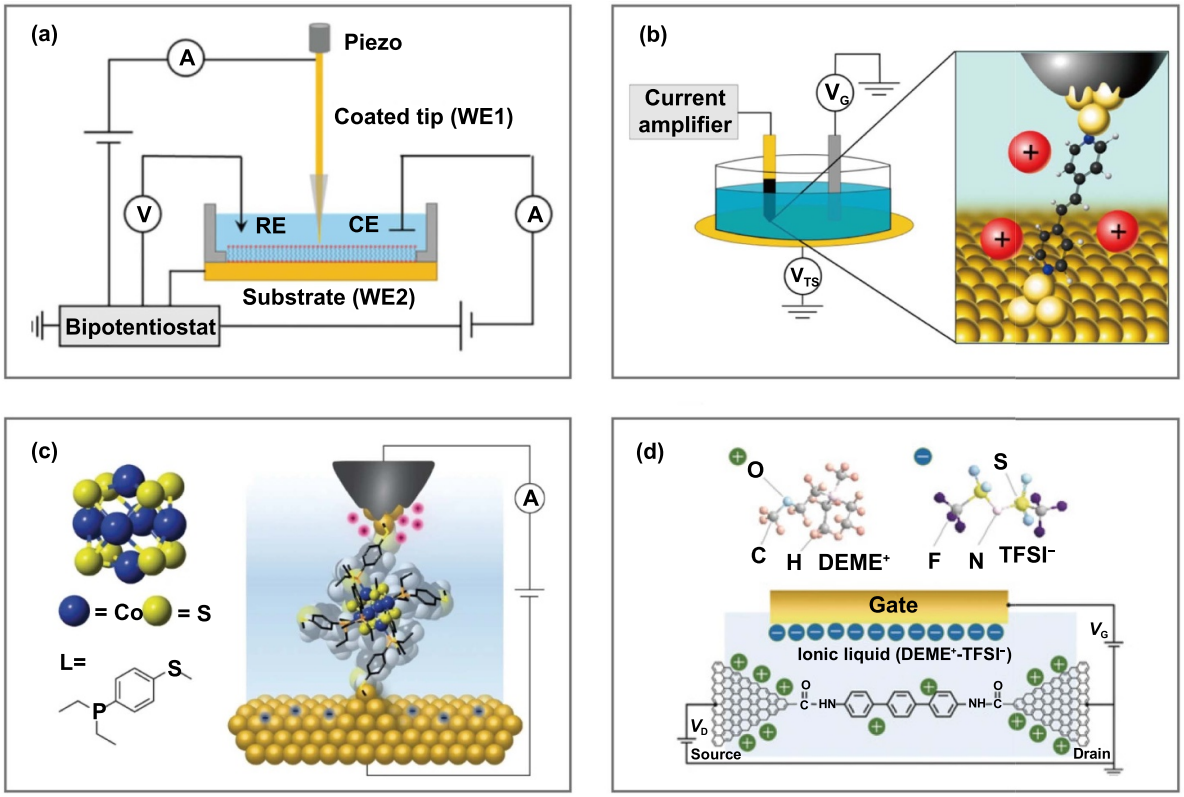

Figure 29. (a) Schematic of a four-electrode electrochemical STM-BJ setup. [19] John Wiley & Sons. © 2021 Wiley-VCH GmbH. (b) Schematic of a three-electrode electrochemical STM-BJ setup. Reprinted with permission from [230]. Copyright (2014) American Chemical Society. (c) Schematic of a two-electrode electrochemical STM-BJ setup in an ionic environment. Reproduced from [305], with permission from Springer Nature. (d) Schematic of graphene-molecule-graphene single-molecule junctions with ionic-liquid gate dielectric. [306] John Wiley & Sons. © 2018 Wiley-VCH Verlag GmbH & Co. KGaA, Weinheim.

electron. Molecular spintronics, which is a new and attractive field, has received considerable attention due to weak molecular spin-orbital coupling, long spin diffusion lengths and spin lifetimes relative to conventional metals or semi-conductors [307, 308]. Molecular spintronic devices, therefore, use the spin characteristics of electrons to realize functions such as sensing, information storage and transmission [309].

In 2002, Emberly *et al* observed theoretically possible spin-valve behavior in a molecular junction system of 1,4-BDT SAM bridged by Fe–Ni magnetic tips [82]. In 2004, Pasupathy *et al* fabricated single-molecule spintronic devices for the first time in laboratory-based on electromigrated break junction, and demonstrated the Kondo assisted tunneling of C_{60} molecules in contact with ferronickel electrodes [69] (figure 30(a)).

With the development of molecular electron spin theory, many functional molecular spintronic devices have been manufactured and studied experimentally and theoretically. For example, in 2015, Brooke *et al* prepared BPY molecular junctions with Ni and Au contacts based on STM-BJ technology. They found that the molecular junction exhibits single-molecule transistor behavior. Theoretical calculations showed that this behavior is caused by interference with charge transport due to strong hybridization of the spin-polarized ferromagnetic Ni d electrons with the LUMO of BPY molecules [310] (figure 30(b)). For another example, Li *et al* designed a square planar nickel (II) porphyrin derivative (NiTPPF) and studied its spin-state induced conductance switching using STM-BJ technology. They found that the addition of an off-axis ligand could trigger the spin states transition of this molecule, which can realize the reversible conductance switch function at room temperature [311].

Recent theoretical and experimental data clearly show that ordered films of chiral organic molecules on the surface can act as electron spin filters at room temperature. This effect is called chiral-induced spin selectivity (CISS). The CISS effect opens up the probability of utilizing chiral molecules in spintronics and demonstrates the potential of molecular spintronic devices as switches [312]. Based on this, in 2019, Suda *et al* developed a light-triggered molecular spin switch using the CISS effect. As shown in figure 30(c), the device functions as a single-molecule spin device of overcrowded alkenes (OCAs) molecule by using light stimulation to realize the chiral reversal of a molecular motor [313].

In addition, molecular spin sensors based on spin signals have attracted wide attention because of their small size, high selectivity, high sensitivity and low energy consumption. In 2018, Zou *et al* conducted a theoretical study on the transition metal phthalocyanine molecular junction adsorbed by gas molecules and confirmed its potential as a gas sensor [314] (figure 30(d)).

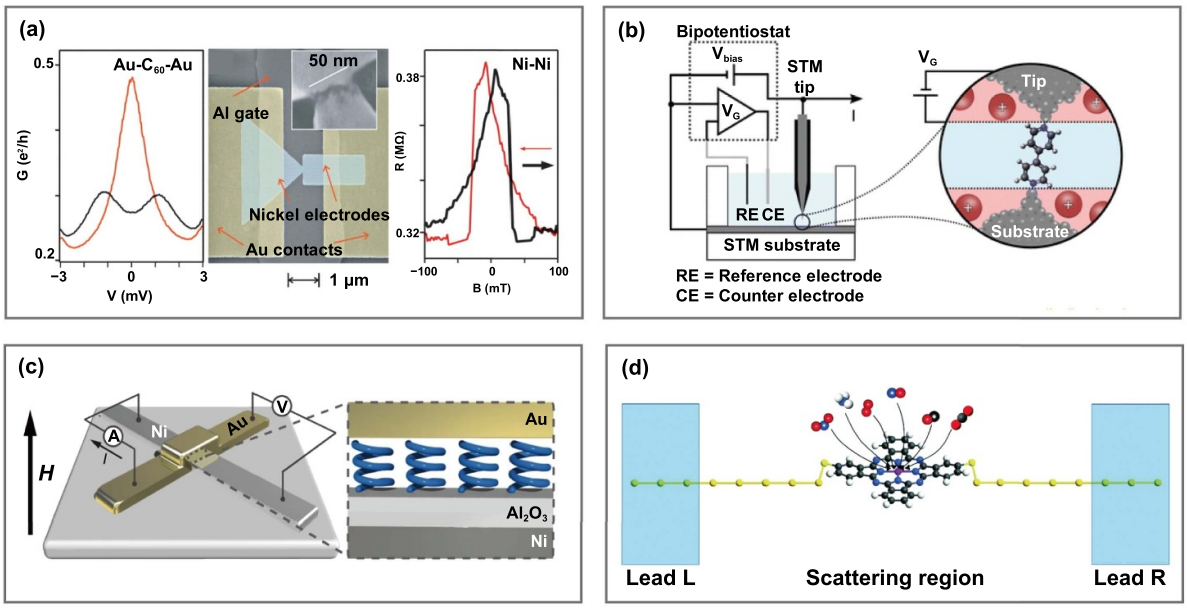

Figure 30. (a) Conductance signal of C60 molecular junction (left) and SEM of electromigrated molecular junction (center) and tunnel reluctance of Ni contact after electromigration without C_{60} (right). From [69]. Reprinted with permission from AAAS. (b) Schematic of a four-electrode STM-BJ setup and an enlarged view of an electric double layer. Reprinted with permission from [310]. Copyright (2015) American Chemical Society. (c) Schematic of a crossbar tunnel junction device and an enlarged view of molecule detail. Reproduced from [313], with permission from Springer Nature. (d) Schematic of phthalocyanine-based molecular junction for gas sensor. Reproduced from [314] with permission of The Royal Society of Chemistry.

6. Summary and perspectives

Beneficial from the advances in nanotechnology, it is becoming increasingly feasible to fabricate molecular junctions with atomic-level precision and characterize and regulate their properties. In this review, we always focus on molecular junctions, the basic model in the field of molecular electronics. We summarized the most advanced methods of molecular junction fabrication and discuss the molecular level characterization and regulation by using molecular junction. In addition, we also emphasized that the ultimate aim of molecular electronics is achieving molecular assembly of logic circuits, and summarized various existing functional molecular devices.

On the one hand, although molecular electronics has made great progresses in recent years, there are still many challenges involved in precise machining and fine regulation down to molecular even near atomic scale. First, it is necessary to optimize and perfect the existing fabrication characterization methods [25]. By combining the most advanced micro- and nano-manufacturing equipment, a molecular junction can be obtained with a processing accuracy close to a single atom and the increased manufacturing stability. The second is to make more complex configurations of molecular junctions to achieve multifunctional detection and regulation. In addition to its own development, molecular electronics can also be used as a research tool to be compatible and mutually promoted with the development of other disciplines [14]. Thirdly, starting from the ultimate goal of molecular electronics, how to implement the prototypical molecular junctions into functional circuit components is the core problem in future exploration [94]. How to form a stable and reliable molecular junction with an adjustable molecule-electrode interface is still the key challenge, whereas the molecular electronic device can really be moving forward into application after well solved. Therefore, the next crucial step for molecular electronics is to develop manufacturing technologies to realize the construction of integrated molecular electronic devices with high stability and reproducibility.

On the other hand, since molecular electronics investigates the relationships between molecular structure and electric performance, and thus to regulate and adopt those relationship into application. Looking forward to the future, first, focusing on some cutting-edge scientific issues at the single-molecule and even quantum scales can realize the observation and regulation of novel light and electron phenomena induced by size confinement effects. For example, the characterization and control of single-molecule junctions can not only help us understand the coupling and interaction between tunneling electrons and molecules [224, 232], but also further promote to study the dynamics of molecule-scale chemical reactions in nano-confined spaces [65] and the effects of external electric fields [315]. Second, some new electron transport theories will provide some new working modes for the design of molecular electronic devices, especially in the fields of quantum computing [316, 317], superconductivity [318] and other transformative quantum technologies [319]. With the introduction of electron spin into molecular electronics, quantum operations can be achieved by manipulating the spin in response to electrical signals to realize the memristor [320]. Therefore, future opportunities for the vision of 'Beyond CMOS' by molecular electronics may come true.

Acknowledgments

This work was supported by the National Natural Science Foundation of China (Nos. 22173075, 21933012, 31871877), the National Key Research and Development Program of China (2017YFA0204902) and the Fundamental Research Funds for the Central Universities (Nos. 20720200068, 20720190002).

ORCID iDs

Junyang Liu https://orcid.org/0000-0002-7252-1900
Wenjing Hong https://orcid.org/0000-0003-4080-6175

References

[1] Moore G E 1998 Cramming more components onto integrated circuits *Proc. IEEE* **86** 82–5
[2] Salahuddin S, Ni K and Datta S 2018 The era of hyper-scaling in electronics *Nat. Electron.* **1** 442–50
[3] Chen Y, Shu Z, Zhang S, Zeng P, Liang H, Zheng M and Duan H 2021 Sub-10 nm fabrication: methods and applications *Int. J. Extreme Manuf.* **3** 032002
[4] Yang Y, Gu C and Li J 2019 Sub-5 nm metal nanogaps: physical properties, fabrication methods, and device applications *Small* **15** e1804177
[5] Fang F, Zhang N, Guo D, Ehmann K, Cheung B, Liu K and Yamamura K 2019 Towards atomic and close-to-atomic scale manufacturing *Int. J. Extreme Manuf.* **1** 012001
[6] Luo S, Mancini A, Berte R, Hoff B H, Maier S A and de Mello J C 2021 Massively parallel arrays of size-controlled metallic nanogaps with gap-widths down to the sub-3-nm level *Adv. Mater.* **33** e2100491
[7] Luo S, Hoff B H, Maier S A and de Mello J C 2021 Scalable fabrication of metallic nanogaps at the sub-10 nm level *Adv. Sci.* **8** 2102756
[8] Liu J *et al* 2019 Transition from tunneling leakage current to molecular tunneling in single-molecule junctions *Chemistry* **5** 390–401
[9] Peercy P S 2000 The drive to miniaturization *Nature* **406** 1023–6
[10] van Ruitenbeek J M 2016 Molecular electronics: a brief overview of the status of the field *Single-Molecule Electronics: An Introduction to Synthesis, Measurement and Theory* ed M Kiguchi (Singapore: Springer Singapore) pp 1–23
[11] Xiang D, Wang X L, Jia C C, Lee T and Guo X F 2016 Molecular-scale electronics: from concept to function *Chem. Rev.* **116** 4318–440
[12] Xin N, Guan J, Zhou C, Chen X, Gu C, Li Y, Ratner M A, Nitzan A, Stoddart J F and Guo X 2019 Concepts in the design and engineering of single-molecule electronic devices *Nat. Rev. Phys.* **1** 211–30
[13] Su T A, Neupane M, Steigerwald M L, Venkataraman L and Nuckolls C 2016 Chemical principles of single-molecule electronics *Nat. Rev. Mater.* **1** 16002
[14] Chen H L and Stoddart J F 2021 From molecular to supramolecular electronics *Nat. Rev. Mater.* **6** 804–28
[15] Gehring P, Thijssen J M and van der Zant H S J 2019 Single-molecule quantum-transport phenomena in break junctions *Nat. Rev. Phys.* **1** 381–96
[16] Sun L, Diaz-Fernandez Y A, Gschneidtner T A, Westerlund F, Lara-Avila S and Moth-Poulsen K 2014 Single-molecule electronics: from chemical design to functional devices *Chem. Soc. Rev.* **43** 7378–411
[17] Cui A, Dong H and Hu W 2015 Nanogap electrodes towards solid state single-molecule transistors *Small* **11** 6115–41
[18] Tsutsui M and Taniguchi M 2012 Single molecule electronics and devices *Sensors* **12** 7259–729
[19] Bai J, Li X, Zhu Z, Zheng Y and Hong W 2021 Single-molecule electrochemical transistors *Adv. Mater.* **33** 2005883
[20] Hong C, Yang S and Ndukaife J C 2020 Stand-off trapping and manipulation of sub-10 nm objects and biomolecules using opto-thermo-electrohydrodynamic tweezers *Nat. Nanotechnol.* **15** 908–13
[21] Wang T and Nijhuis C A 2016 Molecular electronic plasmonics *Appl. Mater. Today* **3** 73–86
[22] Chen L J, Feng A N, Wang M N, Liu J Y, Hong W J, Guo X F and Xiang D 2018 Towards single-molecule optoelectronic devices *Sci. China-Chem.* **61** 1368–84
[23] Barla P, Joshi V K and Bhat S 2021 Spintronic devices: a promising alternative to CMOS devices *J. Comput. Electron.* **20** 805–37
[24] Komoto Y, Fujii S, Iwane M and Kiguchi M 2016 Single-molecule junctions for molecular electronics *J. Mater. Chem.* C **4** 8842–58
[25] Lu Z, Zheng J, Shi J, Zeng B-F, Yang Y, Hong W and Tian Z-Q 2021 Application of micro/nanofabrication techniques to on-chip molecular electronics *Small Methods* **5** 2001034
[26] Evers F, Korytár R, Tewari S and van Ruitenbeek J M 2020 Advances and challenges in single-molecule electron transport *Rev. Mod. Phys.* **92** 035001
[27] Makk P, Tomaszewski D, Martinek J, Balogh Z, Csonka S, Wawrzyniak M, Frei M, Venkataraman L and Halbritter A 2012 Correlation analysis of atomic and single-molecule junction conductance *ACS Nano* **6** 3411–23
[28] Haiss W, Nichols R J, van Zalinge H, Higgins S J, Bethell D and Schiffrin D J 2004 Measurement of single molecule conductivity using the spontaneous formation of molecular wires *Phys. Chem. Chem. Phys.* **6** 4330–7
[29] Haiss W, van Zalinge H, Higgins S J, Bethell D, Höbenreich H, Schiffrin D J and Nichols R J 2003 Redox state dependence of single molecule conductivity *J. Am. Chem. Soc.* **125** 15294–5
[30] Xu B and Tao N 2003 Measurement of single-molecule resistance by repeated formation of molecular junctions *Science* **301** 1221–3
[31] Venkataraman L, Klare J E, Nuckolls C, Hybertsen M S and Steigerwald M L 2006 Dependence of single-molecule junction conductance on molecular conformation *Nature* **442** 904–7
[32] Garner M H *et al* 2018 Comprehensive suppression of single-molecule conductance using destructive sigma-interference *Nature* **558** 415–9
[33] Huang Z, Xu B, Chen Y, Ventra M D and Tao N 2006 Measurement of current-induced local heating in a single molecule junction *Nano Lett.* **6** 1240–4
[34] Xu B, Xiao X and Tao N J 2003 Measurements of single-molecule electromechanical properties *J. Am. Chem. Soc.* **125** 16164–5
[35] Frei M, Aradhya S V, Hybertsen M S and Venkataraman L 2012 Linker dependent bond rupture force measurements in single-molecule junctions *J. Am. Chem. Soc.* **134** 4003–6
[36] Aradhya S V, Frei M, Hybertsen M S and Venkataraman L 2012 Van der Waals interactions at metal/organic interfaces at the single-molecule level *Nat. Mater.* **11** 872–6
[37] Lumbroso O S, Simine L, Nitzan A, Segal D and Tal O 2018 Electronic noise due to temperature differences in atomic-scale junctions *Nature* **562** 240–4

[38] Hong W, Li H, Liu S, Fu Y, Li J, Kaliginedi V, Decurtins S and Wandlowski T 2012 Trimethylsilyl-terminated oligo(phenylene ethynylene)s: an approach to single-molecule junctions with covalent Au-C sigma-bonds *J. Am. Chem. Soc.* **134** 19425–31

[39] Reed M A, Zhou C, Muller C J, Burgin T P and Tour J M 1997 Conductance of a molecular junction *Science* **278** 252–4

[40] Zhou C, Muller C J, Deshpande M R, Sleight J W and Reed M A 1995 Microfabrication of a mechanically controllable break junction in silicon *Appl. Phys. Lett.* **67** 1160–2

[41] Huber R *et al* 2008 Electrical conductance of conjugated oligomers at the single molecule level *J. Am. Chem. Soc.* **130** 1080–4

[42] Dubois V, Raja S N, Gehring P, Caneva S, van der Zant H S J, Niklaus F and Stemme G 2018 Massively parallel fabrication of crack-defined gold break junctions featuring sub-3 nm gaps for molecular devices *Nat. Commun.* **9** 3433

[43] Frisenda R, Janssen V A E C, Grozema F C, van der Zant H S J and Renaud N 2016 Mechanically controlled quantum interference in individual π-stacked dimers *Nat. Chem.* **8** 1099–104

[44] Lörtscher E, Ciszek J W, Tour J and Riel H 2006 Reversible and controllable switching of a single-molecule junction *Small* **2** 973–7

[45] Lörtscher E, Gotsmann B, Lee Y, Yu L, Rettner C and Riel H 2012 Transport properties of a single-molecule diode *ACS Nano* **6** 4931–9

[46] Jeong H, Domulevicz L K and Hihath J 2021 Design and fabrication of a MEMS-based break junction device for mechanical strain-correlated optical characterization of a single-molecule *J. Microelectromech. Syst.* **30** 126–36

[47] Jeong H, Li H B, Domulevicz L and Hihath J 2020 An on-chip break junction system for combined single-molecule conductance and Raman spectroscopies *Adv. Funct. Mater.* **30** 2000615

[48] Song H, Kim Y, Jang Y H, Jeong H, Reed M A and Lee T 2009 Observation of molecular orbital gating *Nature* **462** 1039–43

[49] Hoffmann-Vogel R 2017 Electromigration and the structure of metallic nanocontacts *Appl. Phys. Rev.* **4** 031302

[50] Kim Y, Ang C H, Ang K and Chang S W 2021 Electromigrated nanogaps: a review on the fabrications and applications *J. Vac. Sci. Technol.* B **39** 010802

[51] Park H, Lim A K L, Alivisatos A P, Park J and McEuen P L 1999 Fabrication of metallic electrodes with nanometer separation by electromigration *Appl. Phys. Lett.* **75** 301–3

[52] Ward D R, Corley D A, Tour J M and Natelson D 2011 Vibrational and electronic heating in nanoscale junctions *Nat. Nanotechnol.* **6** 33–38

[53] Qin L, Park S, Huang L and Mirkin Chad A 2005 On-wire lithography *Science* **309** 113–5

[54] Guo X *et al* 2006 Covalently bridging gaps in single-walled carbon nanotubes with conducting molecules *Science* **311** 356

[55] Guo X and Nuckolls C 2009 Functional single-molecule devices based on SWNTs as point contacts *J. Mater. Chem.* **19** 5470–3

[56] Qi P, Javey A, Rolandi M, Wang Q, Yenilmez E and Dai H 2004 Miniature organic transistors with carbon nanotubes as quasi-one-dimensional electrodes *J. Am. Chem. Soc.* **126** 11774–5

[57] Wei D, Liu Y, Cao L, Wang Y, Zhang H and Yu G 2008 Real time and *in situ* control of the gap size of nanoelectrodes for molecular devices *Nano Lett.* **8** 1625–30

[58] Cao Y, Dong S, Liu S, He L, Gan L, Yu X, Steigerwald M L, Wu X, Liu Z and Guo X 2012 Building high-throughput molecular junctions using indented graphene point contacts *Angew. Chem., Int. Ed.* **51** 12228–32

[59] Prins F, Barreiro A, Ruitenberg J W, Seldenthuis J S, Aliaga-Alcalde N, Vandersypen L M K and van der Zant H S J 2011 Room-temperature gating of molecular junctions using few-layer graphene nanogap electrodes *Nano Lett.* **11** 4607–11

[60] Caneva S, Gehring P, García-Suárez V M, García-Fuente A, Stefani D, Olavarria-Contreras I J, Ferrer J, Dekker C and van der Zant H S J 2018 Mechanically controlled quantum interference in graphene break junctions *Nat. Nanotechnol.* **13** 1126–31

[61] Chen F, Li X, Hihath J, Huang Z and Tao N 2006 Effect of anchoring groups on single-molecule conductance: comparative study of thiol-, amine-, and carboxylic-acid-terminated molecules *J. Am. Chem. Soc.* **128** 15874–81

[62] Hong W, Manrique D Z, Moreno-García P, Gulcur M, Mishchenko A, Lambert C J, Bryce M R and Wandlowski T 2012 Single molecular conductance of tolanes: experimental and theoretical study on the junction evolution dependent on the anchoring group *J. Am. Chem. Soc.* **134** 2292–304

[63] Di Ventra M and Taniguchi M 2016 Decoding DNA, RNA and peptides with quantum tunnelling *Nat. Nanotechnol.* **11** 117–26

[64] Guo C, Yu X, Refaely-Abramson S, Sepunaru L, Bendikov T, Pecht I, Kronik L, Vilan A, Sheves M and Cahen D 2016 Tuning electronic transport via hepta-alanine peptides junction by tryptophan doping *Proc. Natl Acad. Sci. USA* **113** 10785

[65] Yang C *et al* 2021 Electric field–catalyzed single-molecule Diels-Alder reaction dynamics *Sci. Adv.* **7** eabf0689

[66] Li P, Jia C and Guo X 2021 Structural transition dynamics in carbon electrode-based single-molecule junctions *Chin. J. Chem.* **39** 223–31

[67] Schoonveld W A, Wildeman J, Fichou D, Bobbert P A, van Wees B J and Klapwijk T M 2000 Coulomb-blockade transport in single-crystal organic thin-film transistors *Nature* **404** 977–80

[68] Park J *et al* 2002 Coulomb blockade and the Kondo effect in single-atom transistors *Nature* **417** 722–5

[69] Pasupathy A N, Bialczak R C, Martinek J, Grose J E, Donev L A K, McEuen P L and Ralph D C 2004 The Kondo effect in the presence of ferromagnetism *Science* **306** 86–89

[70] Bai J *et al* 2019 Anti-resonance features of destructive quantum interference in single-molecule thiophene junctions achieved by electrochemical gating *Nat. Mater.* **18** 364–9

[71] Huang B *et al* 2018 Controlling and observing sharp-valleyed quantum interference effect in single molecular junctions *J. Am. Chem. Soc.* **140** 17685–90

[72] Li Y *et al* 2019 Gate controlling of quantum interference and direct observation of anti-resonances in single molecule charge transport *Nat. Mater.* **18** 357–63

[73] Liu J, Huang X, Wang F and Hong W 2019 Quantum interference effects in charge transport through single-molecule junctions: detection, manipulation, and application *Acc. Chem. Res.* **52** 151–60

[74] Lee W, Kim K, Jeong W, Zotti L A, Pauly F, Cuevas J C and Reddy P 2013 Heat dissipation in atomic-scale junctions *Nature* **498** 209–12

[75] Mosso N, Drechsler U, Menges F, Nirmalraj P, Karg S, Riel H and Gotsmann B 2017 Heat transport through atomic contacts *Nat. Nanotechnol.* **12** 430–3

[76] Cui L, Jeong W, Hur S, Matt M, Klöckner J C, Pauly F, Nielaba P, Cuevas J C, Meyhofer E and Reddy P 2017

Quantized thermal transport in single-atom junctions *Science* **355** 1192–5
[77] Cui L, Hur S, Akbar Z A, Klöckner J C, Jeong W, Pauly F, Jang S-Y, Reddy P and Meyhofer E 2019 Thermal conductance of single-molecule junctions *Nature* **572** 628–33
[78] Tsutsui M, Morikawa T, He Y, Arima A and Taniguchi M 2015 High thermopower of mechanically stretched single-molecule junctions *Sci. Rep.* **5** 11519
[79] Morikawa T, Arima A, Tsutsui M and Taniguchi M 2014 Thermoelectric voltage measurements of atomic and molecular wires using microheater-embedded mechanically-controllable break junctions *Nanoscale* **6** 8235–41
[80] Tsutsui M, Morikawa T, Arima A and Taniguchi M 2013 Thermoelectricity in atom-sized junctions at room temperatures *Sci. Rep.* **3** 3326
[81] Tsutsui M, Kawai T and Taniguchi M 2012 Unsymmetrical hot electron heating in quasi-ballistic nanocontacts *Sci. Rep.* **2** 217
[82] Emberly E G and Kirczenow G 2002 Molecular spintronics: spin-dependent electron transport in molecular wires *Chem. Phys.* **281** 311–24
[83] Li H, Shi W, Song J, Jang H-J, Dailey J, Yu J and Katz H E 2019 Chemical and biomolecule sensing with organic field-effect transistors *Chem. Rev.* **119** 3–35
[84] Zhang C, Chen P and Hu W 2015 Organic field-effect transistor-based gas sensors *Chem. Soc. Rev.* **44** 2087–107
[85] Reecht G, Scheurer F, Speisser V, Dappe Y J, Mathevet F and Schull G 2014 Electroluminescence of a polythiophene molecular wire suspended between a metallic surface and the tip of a scanning tunneling microscope *Phys. Rev. Lett.* **112** 047403
[86] Schwarz F and Lörtscher E 2014 Break-junctions for investigating transport at the molecular scale *J. Phys.-Condes. Matter* **26** 474201
[87] Khoo K H, Chen Y, Li S and Quek S Y 2015 Length dependence of electron transport through molecular wires—a first principles perspective *Phys. Chem. Chem. Phys.* **17** 77–96
[88] McCreery R L 2004 Molecular electronic junctions *Chem. Mater.* **16** 4477–96
[89] Scholes G D *et al* 2017 Using coherence to enhance function in chemical and biophysical systems *Nature* **543** 647–56
[90] Fano U 1961 Effects of configuration interaction on intensities and phase shifts *Phys. Rev.* **124** 1866–78
[91] Hong W, Valkenier H, Mészáros G, Manrique D Z, Mishchenko A, Putz A, García P M, Lambert C J, Hummelen J C and Wandlowski T 2011 An MCBJ case study: the influence of π-conjugation on the single-molecule conductance at a solid/liquid interface *Beilstein J. Nanotechnol.* **2** 699–713
[92] Yang G *et al* 2017 Protonation tuning of quantum interference in azulene-type single-molecule junctions *Chem. Sci.* **8** 7505–9
[93] Zhang Y-P *et al* 2018 Distinguishing diketopyrrolopyrrole isomers in single-molecule junctions via reversible stimuli-responsive quantum interference *J. Am. Chem. Soc.* **140** 6531–5
[94] Jeong H, Kim D, Xiang D and Lee T 2017 High-yield functional molecular electronic devices *ACS Nano* **11** 6511–48
[95] Vilan A, Aswal D and Cahen D 2017 Large-area, ensemble molecular electronics: motivation and challenges *Chem. Rev.* **117** 4248–86
[96] Zheng H, Jiang F, He R, Yang Y, Shi J and Hong W 2019 Charge transport through peptides in single-molecule electrical measurements *Chin. J. Chem.* **37** 1083–96
[97] Liu Z *et al* 2011 Revealing the molecular structure of single-molecule junctions in different conductance states by fishing-mode tip-enhanced Raman spectroscopy *Nat. Commun.* **2** 305
[98] Tian J H, Liu B, Li X, Yang Z L, Ren B, Wu S T, Tao N and Tian Z Q 2006 Study of molecular junctions with a combined surface-enhanced Raman and mechanically controllable break junction method *J. Am. Chem. Soc.* **128** 14748–9
[99] Akkerman H B, Blom P W M, de Leeuw D M and de Boer B 2006 Towards molecular electronics with large-area molecular junctions *Nature* **441** 69–72
[100] Holmlin R E, Haag R, Chabinyc M L, Ismagilov R F, Cohen A E, Terfort A, Rampi M A and Whitesides G M 2001 Electron transport through thin organic films in metal−insulator−metal junctions based on self-assembled monolayers *J. Am. Chem. Soc.* **123** 5075–85
[101] Chiechi R C, Weiss E A, Dickey M D and Whitesides G M 2008 Eutectic gallium–indium (EGaIn): a moldable liquid metal for electrical characterization of self-assembled monolayers *Angew. Chem., Int. Ed.* **47** 142–4
[102] Feldman A K, Steigerwald M L, Guo X and Nuckolls C 2008 Molecular electronic devices based on single-walled carbon nanotube electrodes *Acc. Chem. Res.* **41** 1731–41
[103] Ghasemi S and Moth-Poulsen K 2021 Single molecule electronic devices with carbon-based materials: status and opportunity *Nanoscale* **13** 659–71
[104] Jia C, Ma B, Xin N and Guo X 2015 Carbon electrode–molecule junctions: a reliable platform for molecular electronics *Acc. Chem. Res.* **48** 2565–75
[105] Black J R 1969 Electromigration—a brief survey and some recent results *IEEE Trans. Electron Devices* **16** 338–47
[106] Houck A A, Labaziewicz J, Chan E K, Folk J A and Chuang I L 2005 Kondo effect in electromigrated gold break junctions *Nano Lett.* **5** 1685–8
[107] Esen G and Fuhrer M S 2005 Temperature control of electromigration to form gold nanogap junctions *Appl. Phys. Lett.* **87** 263101
[108] Strachan D R, Smith D E, Johnston D E, Park T H, Therien M J, Bonnell D A and Johnson A T 2005 Controlled fabrication of nanogaps in ambient environment for molecular electronics *Appl. Phys. Lett.* **86** 043109
[109] Hoffmann R, Weissenberger D, Hawecker J and Stöffler D 2008 Conductance of gold nanojunctions thinned by electromigration *Appl. Phys. Lett.* **93** 043118
[110] Campbell J M and Knobel R G 2013 Feedback-controlled electromigration for the fabrication of point contacts *Appl. Phys. Lett.* **102** 023105
[111] Johnston D E, Strachan D R and Johnson A T C 2007 Parallel fabrication of nanogap electrodes *Nano Lett.* **7** 2774–7
[112] Suga H, Suzuki H, Otsu K, Abe T, Umeta Y, Tsukagoshi K, Sumiya T, Shima H, Akinaga H and Naitoh Y 2020 Feedback electromigration assisted by alternative voltage operation for the fabrication of facet-edge nanogap electrodes *ACS Appl. Nano Mater.* **3** 4077–83
[113] O'Neill K, Osorio E A and van der Zant H S J 2007 Self-breaking in planar few-atom Au constrictions for nanometer-spaced electrodes *Appl. Phys. Lett.* **90** 133109
[114] Prins F, Hayashi T, de Vos van Steenwijk B J A, Gao B, Osorio E A, Muraki K and van der Zant H S J 2009 Room-temperature stability of Pt nanogaps formed by self-breaking *Appl. Phys. Lett.* **94** 123108
[115] Wheeler P J, Chen R and Natelson D 2013 Noise in electromigrated nanojunctions *Phys. Rev.* B **87** 155411
[116] Kanamaru Y, Ando M and Shirakashi J-I 2014 Ultrafast feedback-controlled electromigration using a field-programmable gate array *J. Vac. Sci. Technol.* B **33** 02B106

[117] Xiang A, Hou S and Liao J 2014 Tuning the local temperature during feedback controlled electromigration in gold nanowires *Appl. Phys. Lett.* **104** 223113

[118] Rothemund P, Morris Bowers C, Suo Z and Whitesides G M 2018 Influence of the contact area on the current density across molecular tunneling junctions measured with EGaIn top-electrodes *Chem. Mater.* **30** 129–37

[119] Karuppannan S K, Hongting H, Troadec C, Vilan A and Nijhuis C A 2019 Ultrasmooth and photoresist-free micropore-based EGaIn molecular junctions: fabrication and how roughness determines voltage response *Adv. Funct. Mater.* **29** 1904452

[120] Nijhuis C A, Reus W F, Barber J R, Dickey M D and Whitesides G M 2010 Charge transport and rectification in arrays of SAM-based tunneling junctions *Nano Lett.* **10** 3611–9

[121] Nijhuis C A, Reus W F, Barber J R and Whitesides G M 2012 Comparison of SAM-based junctions with Ga_2O_3/EGaIn top electrodes to other large-area tunneling junctions *J. Phys. Chem.* C **116** 14139–50

[122] Wan A, Jiang L, Sangeeth C S S and Nijhuis C A 2014 Reversible soft top-contacts to yield molecular junctions with precise and reproducible electrical characteristics *Adv. Funct. Mater.* **24** 4442–56

[123] Zhu Z, Daniel T A, Maitani M, Cabarcos O M, Allara D L and Winograd N 2006 Controlling gold atom penetration through alkanethiolate self-assembled monolayers on Au{111} by adjusting terminal group intermolecular interactions *J. Am. Chem. Soc.* **128** 13710–9

[124] Kim T-W, Wang G, Lee H and Lee T 2007 Statistical analysis of electronic properties of alkanethiols in metal–molecule–metal junctions *Nanotechnology* **18** 315204

[125] Haick H and Cahen D 2008 Contacting organic molecules by soft methods: towards molecule-based electronic devices *Acc. Chem. Res.* **41** 359–66

[126] Ulgut B and Abruña H D 2008 Electron transfer through molecules and assemblies at electrode surfaces *Chem. Rev.* **108** 2721–36

[127] Khoshmanesh K, Tang S-Y, Zhu J Y, Schaefer S, Mitchell A, Kalantar-zadeh K and Dickey M D 2017 Liquid metal enabled microfluidics *Lab Chip* **17** 974–93

[128] Peng Z-L, Chen Z-B, Zhou X-Y, Sun -Y-Y, Liang J-H, Niu Z-J, Zhou X-S and Mao B-W 2012 Single molecule conductance of carboxylic acids contacting Ag and Cu electrodes *J. Phys. Chem.* C **116** 21699–705

[129] Aradhya S V, Frei M, Halbritter A and Venkataraman L 2013 Correlating structure, conductance, and mechanics of silver atomic-scale contacts *ACS Nano* **7** 3706–12

[130] Ternes M, González C, Lutz C P, Hapala P, Giessibl F J, Jelínek P and Heinrich A J 2011 Interplay of conductance, force, and structural change in metallic point contacts *Phys. Rev. Lett.* **106** 016802

[131] Li X *et al* 2009 Large-area synthesis of high-quality and uniform graphene films on copper foils *Science* **324** 1312

[132] Novoselov K S, Geim A K, Morozov S V, Jiang D, Zhang Y, Dubonos S V, Grigorieva I V and Firsov A A 2004 Electric field effect in atomically thin carbon films *Science* **306** 666

[133] Dai H 2002 Carbon nanotubes: synthesis, integration, and properties *Acc. Chem. Res.* **35** 1035–44

[134] Avouris P 2002 Molecular electronics with carbon nanotubes *Acc. Chem. Res.* **35** 1026–34

[135] Tsukagoshi K, Yagi I and Aoyagi Y 2004 Pentacene nanotransistor with carbon nanotube electrodes *Appl. Phys. Lett.* **85** 1021–3

[136] Collins P G, Hersam M, Arnold M, Martel R and Avouris P 2001 Current saturation and electrical breakdown in multiwalled carbon nanotubes *Phys. Rev. Lett.* **86** 3128–31

[137] Javey A, Guo J, Paulsson M, Wang Q, Mann D, Lundstrom M and Dai H 2004 High-field quasiballistic transport in short carbon nanotubes *Phys. Rev. Lett.* **92** 106804

[138] Collins P G, Arnold M S and Avouris P 2001 Engineering carbon nanotubes and nanotube circuits using electrical breakdown *Science* **292** 706–9

[139] Whalley A C, Steigerwald M L, Guo X and Nuckolls C 2007 Reversible switching in molecular electronic devices *J. Am. Chem. Soc.* **129** 12590–1

[140] Thiele C *et al* 2014 Fabrication of carbon nanotube nanogap electrodes by helium ion sputtering for molecular contacts *Appl. Phys. Lett.* **104** 103102

[141] Roy S, Vedala H, Roy A D, Kim D-H, Doud M, Mathee K, Shin H-K, Shimamoto N, Prasad V and Choi W 2008 Direct electrical measurements on single-molecule genomic DNA using single-walled carbon nanotubes *Nano Lett.* **8** 26–30

[142] Geim A K and Novoselov K S 2007 The rise of graphene *Nat. Mater.* **6** 183–91

[143] Nef C, Pósa L, Makk P, Fu W, Halbritter A, Schönenberger C and Calame M 2014 High-yield fabrication of nm-size gaps in monolayer CVD graphene *Nanoscale* **6** 7249–54

[144] Mol J A, Lau C S, Lewis W J M, Sadeghi H, Roche C, Cnossen A, Warner J H, Lambert C J, Anderson H L and Briggs G A D 2015 Graphene-porphyrin single-molecule transistors *Nanoscale* **7** 13181–5

[145] Sadeghi H, Mol J A, Lau C S, Briggs G A D, Warner J and Lambert C J 2015 Conductance enlargement in picoscale electroburnt graphene nanojunctions *Proc. Natl Acad. Sci. USA* **112** 2658

[146] Lau C S, Mol J A, Warner J H and Briggs G A D 2014 Nanoscale control of graphene electrodes *Phys. Chem. Chem. Phys.* **16** 20398–401

[147] Zhu Y, Tan Z and Hong W 2021 Simultaneous electrical and mechanical characterization of single-molecule junctions using AFM-BJ technique *ACS Omega* **6** 30873–88

[148] Zhou X-S, Liang J-H, Chen Z-B and Mao B-W 2011 An electrochemical jump-to-contact STM-break junction approach to construct single molecular junctions with different metallic electrodes *Electrochem. Commun.* **13** 407–10

[149] Wang Y-H, Zhou X-Y, Sun -Y-Y, Han D, Zheng J-F, Niu Z-J and Zhou X-S 2014 Conductance measurement of carboxylic acids binding to palladium nanoclusters by electrochemical jump-to-contact STM break junction *Electrochim. Acta* **123** 205–10

[150] Li X-M, Wang Y-H, Seng J-W, Zheng J-F, Cao R, Shao Y, Chen J-Z, Li J-F, Zhou X-S and Mao B-W 2021 z-Piezo pulse-modulated STM break junction: toward single-molecule rectifiers with dissimilar metal electrodes *ACS Appl. Mat. Interfaces* **13** 8656–63

[151] Vezzoli A, Brooke R J, Ferri N, Brooke C, Higgins S J, Schwarzacher W and Nichols R J 2018 Charge transport at a molecular GaAs nanoscale junction *Faraday Discuss.* **210** 397–408

[152] Vezzoli A, Brooke R J, Ferri N, Higgins S J, Schwarzacher W and Nichols R J 2017 Single-molecule transport at a rectifying GaAs contact *Nano Lett.* **17** 1109–15

[153] Vezzoli A, Brooke R J, Higgins S J, Schwarzacher W and Nichols R J 2017 Single-molecule photocurrent at a metal–molecule–semiconductor junction *Nano Lett.* **17** 6702–7

[154] Aragonès A C, Darwish N, Ciampi S, Sanz F, Gooding J J and Díez-Pérez I 2017 Single-molecule electrical contacts on silicon electrodes under ambient conditions *Nat. Commun.* **8** 15056

[155] Peiris C R, Ciampi S, Dief E M, Zhang J, Canfield P J, Le Brun A P, Kosov D S, Reimers J R and Darwish N 2020

Spontaneous S–Si bonding of alkanethiols to Si(111)–H: towards Si–molecule–Si circuits *Chem. Sci.* **11** 5246–56
[156] Peiris C R, Vogel Y B, Le Brun A P, Aragonès A C, Coote M L, Díez-Pérez I, Ciampi S and Darwish N 2019 Metal–single-molecule–semiconductor junctions formed by a radical reaction bridging gold and silicon electrodes *J. Am. Chem. Soc.* **141** 14788–97
[157] Kim T, Liu Z-F, Lee C, Neaton J B and Venkataraman L 2014 Charge transport and rectification in molecular junctions formed with carbon-based electrodes *Proc. Natl Acad. Sci. USA* **111** 10928
[158] Rudnev A V, Kaliginedi V, Droghetti A, Ozawa H, Kuzume A, Haga M-A, Broekmann P and Rungger I 2017 Stable anchoring chemistry for room temperature charge transport through graphite-molecule contacts *Sci. Adv.* **3** e1602297
[159] Liu L *et al* 2016 Charge transport through dicarboxylic-acid-terminated alkanes bound to graphene–gold nanogap electrodes *Nanoscale* **8** 14507–13
[160] Tao S *et al* 2019 Graphene-contacted single molecular junctions with conjugated molecular wires *ACS Appl. Nano Mater.* **2** 12–18
[161] Zhang Q, Liu L, Tao S, Wang C, Zhao C, González C, Dappe Y J, Nichols R J and Yang L 2016 Graphene as a promising electrode for low-current attenuation in nonsymmetric molecular junctions *Nano Lett.* **16** 6534–40
[162] He C, Zhang Q, Fan Y, Zhao C, Zhao C, Ye J, Dappe Y J, Nichols R J and Yang L 2019 Effect of asymmetric anchoring groups on electronic transport in hybrid metal/molecule/graphene single molecule junctions *ChemPhysChem* **20** 1830–6
[163] He C, Zhang Q, Gao T, Liu C, Chen Z, Zhao C, Zhao C, Nichols R J, Dappe Y J and Yang L 2020 Charge transport in hybrid platinum/molecule/graphene single molecule junctions *Phys. Chem. Chem. Phys.* **22** 13498–504
[164] He C, Zhang Q, Tao S, Zhao C, Zhao C, Su W, Dappe Y J, Nichols R J and Yang L 2018 Carbon-contacted single molecule electrical junctions *Phys. Chem. Chem. Phys.* **20** 24553–60
[165] Xiang D, Jeong H, Lee T and Mayer D 2013 Mechanically controllable break junctions for molecular electronics *Adv. Mater.* **25** 4845–67
[166] Moreland J and Ekin J W 1985 Electron tunneling experiments using Nb-Sn 'break' junctions *J. Appl. Phys.* **58** 3888–95
[167] Muller C J, van Ruitenbeek J M and de Jongh L J 1992 Experimental observation of the transition from weak link to tunnel junction *Physica* C **191** 485–504
[168] Muller C J, van Ruitenbeek J M and de Jongh L J 1992 Conductance and supercurrent discontinuities in atomic-scale metallic constrictions of variable width *Phys. Rev. Lett.* **69** 140–3
[169] Li R *et al* 2017 Switching of charge transport pathways via delocalization changes in single-molecule metallacycles junctions *J. Am. Chem. Soc.* **139** 14344–7
[170] Liu J *et al* 2017 Radical-enhanced charge transport in single-molecule phenothiazine electrical junctions *Angew. Chem., Int. Ed.* **56** 13061–5
[171] Boussaad S and Tao N J 2002 Atom-size gaps and contacts between electrodes fabricated with a self-terminated electrochemical method *Appl. Phys. Lett.* **80** 2398–400
[172] He H X, Boussaad S, Xu B Q, Li C Z and Tao N J 2002 Electrochemical fabrication of atomically thin metallic wires and electrodes separated with molecular-scale gaps *J. Electroanal. Chem.* **522** 167–72
[173] Li C Z, He H X and Tao N J 2000 Quantized tunneling current in the metallic nanogaps formed by electrodeposition and etching *Appl. Phys. Lett.* **77** 3995–7
[174] Liu B, Xiang J, Tian J-H, Zhong C, Mao B-W, Yang F-Z, Chen Z-B, Wu S-T and Tian Z-Q 2005 Controllable nanogap fabrication on microchip by chronopotentiometry *Electrochim. Acta* **50** 3041–7
[175] Mészáros G, Kronholz S, Karthäuser S, Mayer D and Wandlowski T 2007 Electrochemical fabrication and characterization of nanocontacts and nm-sized gaps *Appl. Phys.* A **87** 569–75
[176] Tian J-H *et al* 2010 The fabrication and characterization of adjustable nanogaps between gold electrodes on chip for electrical measurement of single molecules *Nanotechnology* **21** 274012
[177] Yang Y, Chen Z, Liu J, Lu M, Yang D, Yang F and Tian Z 2011 An electrochemically assisted mechanically controllable break junction approach for single molecule junction conductance measurements *Nano Res.* **4** 1199–207
[178] Yang Y, Liu J, Feng S, Wen H, Tian J, Zheng J, Schöllhorn B, Amatore C, Chen Z and Tian Z 2016 Unexpected current–voltage characteristics of mechanically modulated atomic contacts with the presence of molecular junctions in an electrochemically assisted–MCBJ *Nano Res.* **9** 560–70
[179] Zheng J-T *et al* 2016 Electrochemically assisted mechanically controllable break junction studies on the stacking configurations of oligo(phenylene ethynylene)s molecular junctions *Electrochim. Acta* **200** 268–75
[180] Yang Y *et al* 2011 Conductance histogram evolution of an EC–MCBJ fabricated Au atomic point contact *Nanotechnology* **22** 275313
[181] Yi Z, Banzet M, Offenhäusser A and Mayer D 2010 Fabrication of nanogaps with modified morphology by potential-controlled gold deposition *Phys. Status Solidi* **4** 73–75
[182] van Ruitenbeek J M, Alvarez A, Piñeyro I, Grahmann C, Joyez P, Devoret M H, Esteve D and Urbina C 1996 Adjustable nanofabricated atomic size contacts *Rev. Sci. Instrum.* **67** 108–11
[183] Arroyo C R, Frisenda R, Moth-Poulsen K, Seldenthuis J S, Bjørnholm T and van der Zant H S J 2013 Quantum interference effects at room temperature in OPV-based single-molecule junctions *Nanoscale Res. Lett.* **8** 234
[184] Kim Y *et al* 2012 Charge transport characteristics of diarylethene photoswitching single-molecule junctions *Nano Lett.* **12** 3736–42
[185] Schirm C, Matt M, Pauly F, Cuevas J C, Nielaba P and Scheer E 2013 A current-driven single-atom memory *Nat. Nanotechnol.* **8** 645–8
[186] Stefani D, Guo C, Ornago L, Cabosart D, El Abbassi M, Sheves M, Cahen D and van der Zant H S J 2021 Conformation-dependent charge transport through short peptides *Nanoscale* **13** 3002–9
[187] Zhang S *et al* 2021 *In-situ* control of on-chip angstrom gaps, atomic switches, and molecular junctions by light irradiation *Nano Today* **39** 101226
[188] Yang Y, Liu J, Zheng J, Lu M, Shi J, Hong W, Yang F and Tian Z 2017 Promising electroplating solution for facile fabrication of Cu quantum point contacts *Nano Res.* **10** 3314–23
[189] Tan Z *et al* 2019 Atomically defined angstrom-scale all-carbon junctions *Nat. Commun.* **10** 1748
[190] Zhao S *et al* 2020 Cross-plane transport in a single-molecule two-dimensional van der Waals heterojunction *Sci. Adv.* **6** eaba6714
[191] Champagne A R, Pasupathy A N and Ralph D C 2005 Mechanically adjustable and electrically gated single-molecule transistors *Nano Lett.* **5** 305–8

[192] Martin C A, Smit R H M, van der Zant H S J and van Ruitenbeek J M 2009 A nanoelectromechanical single-atom switch *Nano Lett.* **9** 2940–5
[193] Martin C A, van Ruitenbeek J M and van der Zant H S J 2010 Sandwich-type gated mechanical break junctions *Nanotechnology* **21** 265201
[194] Perrin M L, Verzijl C J O, Martin C A, Shaikh A J, Eelkema R, van Esch J H, van Ruitenbeek J M, Thijssen J M, van der Zant H S J and Dulić D 2013 Large tunable image-charge effects in single-molecule junctions *Nat. Nanotechnol.* **8** 282–7
[195] Mangin A, Anthore A, Della Rocca M L, Boulat E and Lafarge P 2009 Transport through metallic nanogaps in an in-plane three-terminal geometry *J. Appl. Phys.* **105** 014313
[196] Xiang D, Jeong H, Kim D, Lee T, Cheng Y, Wang Q and Mayer D 2013 Three-terminal single-molecule junctions formed by mechanically controllable break junctions with side gating *Nano Lett.* **13** 2809–13
[197] Arima A, Tsutsui M, Morikawa T, Yokota K and Taniguchi M 2014 Fabrications of insulator-protected nanometer-sized electrode gaps *J. Appl. Phys.* **115** 114310
[198] Muthusubramanian N, Galan E, Maity C, Eelkema R, Grozema F C and van der Zant H S J 2016 Insulator-protected mechanically controlled break junctions for measuring single-molecule conductance in aqueous environments *Appl. Phys. Lett.* **109** 013102
[199] Zhao Z, Guo C, Ni L, Zhao X, Zhang S and Xiang D 2021 *In situ* photoconductivity measurements of imidazole in optical fiber break-junctions *Nanoscale Horiz.* **6** 386–92
[200] Benner D, Boneberg J, Nürnberger P, Waitz R, Leiderer P and Scheer E 2014 Lateral and temporal dependence of the transport through an atomic gold contact under light irradiation: signature of propagating surface plasmon polaritons *Nano Lett.* **14** 5218–23
[201] Fischer A C, Forsberg F, Lapisa M, Bleiker S J, Stemme G, Roxhed N and Niklaus F 2015 Integrating MEMS and ICs *Microsyst. Nanoeng.* **1** 15005
[202] Karipidou Z *et al* 2016 Ultrarobust thin-film devices from self-assembled metal–terpyridine oligomers *Adv. Mater.* **28** 3473–80
[203] Kushmerick J G, Naciri J, Yang J C and Shashidhar R 2003 Conductance scaling of molecular wires in parallel *Nano Lett.* **3** 897–900
[204] Snider G, Kuekes P, Hogg T and Williams R S 2005 Nanoelectronic architectures *Appl. Phys.* A **80** 1183–95
[205] Stan M R, Franzon P D, Goldstein S C, Lach J C and Ziegler M M 2003 Molecular electronics: from devices and interconnect to circuits and architecture *Proc. IEEE* **91** 1940–57
[206] Green J E *et al* 2007 A 160-kilobit molecular electronic memory patterned at 1011 bits per square centimetre *Nature* **445** 414–7
[207] Park S, Wang G, Cho B, Kim Y, Song S, Ji Y, Yoon M-H and Lee T 2012 Flexible molecular-scale electronic devices *Nat. Nanotechnol.* **7** 438–42
[208] Morteza Najarian A, Szeto B, Tefashe U M and McCreery R L 2016 Robust all-carbon molecular junctions on flexible or semi-transparent substrates using 'process-friendly' fabrication *ACS Nano* **10** 8918–28
[209] Puebla-Hellmann G, Venkatesan K, Mayor M and Lörtscher E 2018 Metallic nanoparticle contacts for high-yield, ambient-stable molecular-monolayer devices *Nature* **559** 232–5
[210] Kos D, Assumpcao D R, Guo C and Baumberg J J 2021 Quantum tunneling induced optical rectification and plasmon-enhanced photocurrent in nanocavity molecular junctions *ACS Nano* **15** 14535–43
[211] Wan A, Suchand Sangeeth C S, Wang L, Yuan L, Jiang L and Nijhuis C A 2015 Arrays of high quality SAM-based junctions and their application in molecular diode based logic *Nanoscale* **7** 19547–56
[212] Luo Y *et al* 2002 Two-dimensional molecular electronics circuits *ChemPhysChem* **3** 519–25
[213] Melosh N A, Boukai A, Diana F, Gerardot B, Badolato A, Petroff P M and Heath J R 2003 Ultrahigh-density nanowire lattices and circuits *Science* **300** 112–5
[214] Kaliginedi V, Moreno-García P, Valkenier H, Hong W, García-Suárez V M, Buiter P, Otten J L H, Hummelen J C, Lambert C J and Wandlowski T 2012 Correlations between molecular structure and single-junction conductance: a case study with oligo(phenylene-ethynylene)-type wires *J. Am. Chem. Soc.* **134** 5262–75
[215] Huang C, Rudnev A V, Hong W and Wandlowski T 2015 Break junction under electrochemical gating: testbed for single-molecule electronics *Chem. Soc. Rev.* **44** 889–901
[216] Choi S H, Risko C, Delgado M C R, Kim B, Brédas J-L and Frisbie C D 2010 Transition from tunneling to hopping transport in long, conjugated oligo-imine wires connected to metals *J. Am. Chem. Soc.* **132** 4358–68
[217] Hines T, Diez-Perez I, Hihath J, Liu H, Wang Z-S, Zhao J, Zhou G, Müllen K and Tao N 2010 Transition from tunneling to hopping in single molecular junctions by measuring length and temperature dependence *J. Am. Chem. Soc.* **132** 11658–64
[218] Ho Choi S, Kim B and Frisbie C D 2008 Electrical resistance of long conjugated molecular wires *Science* **320** 1482–6
[219] Lu Q, Liu K, Zhang H, Du Z, Wang X and Wang F 2009 From tunneling to hopping: a comprehensive investigation of charge transport mechanism in molecular junctions based on oligo(p-phenylene ethynylene)s *ACS Nano* **3** 3861–8
[220] Moreno-García P *et al* 2013 Single-molecule conductance of functionalized oligoynes: length dependence and junction evolution *J. Am. Chem. Soc.* **135** 12228–40
[221] Zhao X, Huang C, Gulcur M, Batsanov A S, Baghernejad M, Hong W, Bryce M R and Wandlowski T 2013 Oligo(aryleneethynylene)s with terminal pyridyl groups: synthesis and length dependence of the tunneling-to-hopping transition of single-molecule conductances *Chem. Mater.* **25** 4340–7
[222] Wang W, Lee T and Reed M A 2003 Mechanism of electron conduction in self-assembled alkanethiol monolayer devices *Phys. Rev.* B **68** 035416
[223] Venkataraman L, Klare J E, Tam I W, Nuckolls C, Hybertsen M S and Steigerwald M L 2006 Single-molecule circuits with well-defined molecular conductance *Nano Lett.* **6** 458–62
[224] Li X, He J, Hihath J, Xu B, Lindsay S M and Tao N 2006 Conductance of single alkanedithiols: conduction mechanism and effect of molecule−electrode contacts *J. Am. Chem. Soc.* **128** 2135–41
[225] Park Y S, Whalley A C, Kamenetska M, Steigerwald M L, Hybertsen M S, Nuckolls C and Venkataraman L 2007 Contact chemistry and single-molecule conductance: a comparison of phosphines, methyl sulfides, and amines *J. Am. Chem. Soc.* **129** 15768–9
[226] Quinn J R, Foss F W, Venkataraman L and Breslow R 2007 Oxidation potentials correlate with conductivities of aromatic molecular wires *J. Am. Chem. Soc.* **129** 12376–7
[227] Liu K, Wang X and Wang F 2008 Probing charge transport of ruthenium-complex-based molecular wires at the single-molecule level *ACS Nano* **2** 2315–23
[228] Wen H-M, Yang Y, Zhou X-S, Liu J-Y, Zhang D-B, Chen Z-B, Wang J-Y, Chen Z-N and Tian Z-Q 2013

Electrical conductance study on 1,3-butadiyne-linked dinuclear ruthenium(ii) complexes within single molecule break junctions *Chem. Sci.* **4** 2471–7
[229] Algethami N, Sadeghi H, Sangtarash S and Lambert C J 2018 The conductance of porphyrin-based molecular nanowires increases with length *Nano Lett.* **18** 4482–6
[230] Capozzi B, Chen Q, Darancet P, Kotiuga M, Buzzeo M, Neaton J B, Nuckolls C and Venkataraman L 2014 Tunable charge transport in single-molecule junctions via electrolytic gating *Nano Lett.* **14** 1400–4
[231] Li C, Pobelov I, Wandlowski T, Bagrets A, Arnold A and Evers F 2008 Charge transport in single Au | alkanedithiol | Au junctions: coordination geometries and conformational degrees of freedom *J. Am. Chem. Soc.* **130** 318–26
[232] Quek S Y, Kamenetska M, Steigerwald M L, Choi H J, Louie S G, Hybertsen M S, Neaton J B and Venkataraman L 2009 Mechanically controlled binary conductance switching of a single-molecule junction *Nat. Nanotechnol.* **4** 230–4
[233] Vonlanthen D, Mishchenko A, Elbing M, Neuburger M, Wandlowski T and Mayor M 2009 Chemically controlled conductivity: torsion-angle dependence in a single-molecule biphenyldithiol junction *Angew. Chem., Int. Ed.* **48** 8886–90
[234] You S, J-T L, Guo J and Jiang Y 2017 Recent advances in inelastic electron tunneling spectroscopy *Adv. Phys.* X **2** 907–36
[235] Smit R H M, Noat Y, Untiedt C, Lang N D, van Hemert M C and van Ruitenbeek J M 2002 Measurement of the conductance of a hydrogen molecule *Nature* **419** 906–9
[236] Stipe B C, Rezaei M A and Ho W 1998 Single-molecule vibrational spectroscopy and microscopy *Science* **280** 1732–5
[237] Kim Y, Song H, Strigl F, Pernau H-F, Lee T and Scheer E 2011 Conductance and vibrational states of single-molecule junctions controlled by mechanical stretching and material variation *Phys. Rev. Lett.* **106** 196804
[238] Long D P, Lazorcik J L, Mantooth B A, Moore M H, Ratner M A, Troisi A, Yao Y, Ciszek J W, Tour J M and Shashidhar R 2006 Effects of hydration on molecular junction transport *Nat. Mater.* **5** 901–8
[239] Konishi T, Kiguchi M, Takase M, Nagasawa F, Nabika H, Ikeda K, Uosaki K, Ueno K, Misawa H and Murakoshi K 2013 Single molecule dynamics at a mechanically controllable break junction in solution at room temperature *J. Am. Chem. Soc.* **135** 1009–14
[240] Ward D R, Halas N J, Ciszek J W, Tour J M, Wu Y, Nordlander P and Natelson D 2008 Simultaneous measurements of electronic conduction and Raman response in molecular junctions *Nano Lett.* **8** 919–24
[241] Yoon H P, Maitani M M, Cabarcos O M, Cai L, Mayer T S and Allara D L 2010 Crossed-nanowire molecular junctions: a new multispectroscopy platform for conduction−structure correlations *Nano Lett.* **10** 2897–902
[242] de Nijs B *et al* 2017 Plasmonic tunnel junctions for single-molecule redox chemistry *Nat. Commun.* **8** 994
[243] Guo C *et al* 2018 Molecular orbital gating surface-enhanced Raman scattering *ACS Nano* **12** 11229–35
[244] Zhao Z *et al* 2018 Shaping the atomic-scale geometries of electrodes to control optical and electrical performance of molecular devices *Small* **14** 1703815
[245] Bi H, Palma C-A, Gong Y, Hasch P, Elbing M, Mayor M, Reichert J and Barth J V 2018 Voltage-driven conformational switching with distinct Raman signature in a single-molecule junction *J. Am. Chem. Soc.* **140** 4835–40
[246] Kos D, Di Martino G, Boehmke A, de Nijs B, Berta D, Földes T, Sangtarash S, Rosta E, Sadeghi H and Baumberg J J 2020 Optical probes of molecules as nano-mechanical switches *Nat. Commun.* **11** 5905
[247] Domulevicz L, Jeong H, Paul N K, Gomez-Diaz J S and Hihath J 2021 Multidimensional characterization of single-molecule dynamics in a plasmonic nanocavity *Angew. Chem., Int. Ed.* **60** 16436–41
[248] Ludoph B and Ruitenbeek J M V 1999 Thermopower of atomic-size metallic contacts *Phys. Rev.* B **59** 12290–3
[249] Reddy P, Jang S-Y, Segalman Rachel A and Majumdar A 2007 Thermoelectricity in molecular junctions *Science* **315** 1568–71
[250] Tan A, Sadat S and Reddy P 2010 Measurement of thermopower and current-voltage characteristics of molecular junctions to identify orbital alignment *Appl. Phys. Lett.* **96** 013110
[251] Elbing M, Ochs R, Koentopp M, Fischer M, von Hänisch C, Weigend F, Evers F, Weber H B and Mayor M 2005 A single-molecule diode *Proc. Natl Acad. Sci. USA* **102** 8815
[252] Batra A, Darancet P, Chen Q, Meisner J S, Widawsky J R, Neaton J B, Nuckolls C and Venkataraman L 2013 Tuning rectification in single-molecular diodes *Nano Lett.* **13** 6233–7
[253] Capozzi B, Xia J, Adak O, Dell E J, Liu Z-F, Taylor J C, Neaton J B, Campos L M and Venkataraman L 2015 Single-molecule diodes with high rectification ratios through environmental control *Nat. Nanotechnol.* **10** 522–7
[254] Ke G, Duan C, Huang F and Guo X 2020 Electrical and spin switches in single-molecule junctions *InfoMat* **2** 92–112
[255] Song H, Reed M A and Lee T 2011 Single molecule electronic devices *Adv. Mater.* **23** 1583–608
[256] Dulić D, van der Molen S J, Kudernac T, Jonkman H T, de Jong J J D, Bowden T N, van Esch J, Feringa B L and van Wees B J 2003 One-way optoelectronic switching of photochromic molecules on gold *Phys. Rev. Lett.* **91** 207402
[257] Odell A, Delin A, Johansson B, Rungger I and Sanvito S 2010 Investigation of the conducting properties of a photoswitching dithienylethene molecule *ACS Nano* **4** 2635–42
[258] Pärs M, Hofmann C C, Willinger K, Bauer P, Thelakkat M and Köhler J 2011 An organic optical transistor operated under ambient conditions *Angew. Chem., Int. Ed.* **50** 11405–8
[259] He J *et al* 2005 Switching of a photochromic molecule on gold electrodes: single-molecule measurements *Nanotechnology* **16** 695–702
[260] Meng F, Hervault Y-M, Shao Q, Hu B, Norel L, Rigaut S and Chen X 2014 Orthogonally modulated molecular transport junctions for resettable electronic logic gates *Nat. Commun.* **5** 3023
[261] Cao Y, Dong S, Liu S, Liu Z and Guo X 2013 Toward functional molecular devices based on graphene–molecule junctions *Angew. Chem., Int. Ed.* **52** 3906–10
[262] Kumar A S, Ye T, Takami T, Yu B-C, Flatt A K, Tour J M and Weiss P S 2008 Reversible photo-switching of single azobenzene molecules in controlled nanoscale environments *Nano Lett.* **8** 1644–8
[263] Pakula C, Zaporojtchenko V, Strunskus T, Zargarani D, Herges R and Faupel F 2010 Reversible light-controlled conductance switching of azobenzene-based metal/polymer nanocomposites *Nanotechnology* **21** 465201
[264] Smaali K, Lenfant S, Karpe S, Oçafrain M, Blanchard P, Deresmes D, Godey S, Rochefort A, Roncali J and Vuillaume D 2010 High on−off conductance switching ratio in optically-driven self-assembled conjugated molecular systems *ACS Nano* **4** 2411–21

[265] Jia C *et al* 2016 Covalently bonded single-molecule junctions with stable and reversible photoswitched conductivity *Science* **352** 1443–5

[266] Jia C, Wang J, Yao C, Cao Y, Zhong Y, Liu Z, Liu Z and Guo X 2013 Conductance switching and mechanisms in single-molecule junctions *Angew. Chem., Int. Ed.* **52** 8666–70

[267] Tsuji Y and Hoffmann R 2014 Frontier orbital control of molecular conductance and its switching *Angew. Chem., Int. Ed.* **53** 4093–7

[268] Roldan D, Kaliginedi V, Cobo S, Kolivoska V, Bucher C, Hong W, Royal G and Wandlowski T 2013 Charge transport in photoswitchable dimethyldihydropyrene-type single-molecule junctions *J. Am. Chem. Soc.* **135** 5974–7

[269] Broman S L, Lara-Avila S, Thisted C L, Bond A D, Kubatkin S, Danilov A and Nielsen M B 2012 Dihydroazulene photoswitch operating in sequential tunneling regime: synthesis and single-molecule junction studies *Adv. Funct. Mater.* **22** 4249–58

[270] Lara-Avila S, Danilov A V, Kubatkin S E, Broman S L, Parker C R and Nielsen M B 2011 Light-triggered conductance switching in single-molecule dihydroazulene/vinylheptafulvene junctions *J. Phys. Chem.* C **115** 18372–7

[271] Li T *et al* 2013 Ultrathin reduced graphene oxide films as transparent top-contacts for light switchable solid-state molecular junctions *Adv. Mater.* **25** 4164–70

[272] Seo S, Min M, Lee S M and Lee H 2013 Photo-switchable molecular monolayer anchored between highly transparent and flexible graphene electrodes *Nat. Commun.* **4** 1920

[273] Battacharyya S, Kibel A, Kodis G, Liddell P A, Gervaldo M, Gust D and Lindsay S 2011 Optical modulation of molecular conductance *Nano Lett.* **11** 2709–14

[274] Orbelli Biroli A *et al* 2011 A multitechnique physicochemical investigation of various factors controlling the photoaction spectra and of some aspects of the electron transfer for a series of push–pull Zn(II) porphyrins acting as dyes in DSSCs *J. Phys. Chem.* C **115** 23170–82

[275] Klajn R 2014 Spiropyran-based dynamic materials *Chem. Soc. Rev.* **43** 148–84

[276] Cai S *et al* 2019 Light-driven reversible intermolecular proton transfer at single-molecule junctions *Angew. Chem., Int. Ed.* **58** 3829–33

[277] Zhang X, Hou L and Samorì P 2016 Coupling carbon nanomaterials with photochromic molecules for the generation of optically responsive materials *Nat. Commun.* **7** 11118

[278] Taniguchi M, Tsutsui M, Yokota K and Kawai T 2010 Mechanically-controllable single molecule switch based on configuration specific electrical conductivity of metal–molecule–metal junctions *Chem. Sci.* **1** 247–53

[279] Ferri N, Algethami N, Vezzoli A, Sangtarash S, McLaughlin M, Sadeghi H, Lambert C J, Nichols R J and Higgins S J 2019 Hemilabile ligands as mechanosensitive electrode contacts for molecular electronics *Angew. Chem., Int. Ed.* **58** 16583–9

[280] Diez-Perez I, Hihath J, Hines T, Wang Z-S, Zhou G, Müllen K and Tao N 2011 Controlling single-molecule conductance through lateral coupling of π orbitals *Nat. Nanotechnol.* **6** 226–31

[281] Meisner J S, Kamenetska M, Krikorian M, Steigerwald M L, Venkataraman L and Nuckolls C 2011 A single-molecule potentiometer *Nano Lett.* **11** 1575–9

[282] Wu C, Bates D, Sangtarash S, Ferri N, Thomas A, Higgins S J, Robertson C M, Nichols R J, Sadeghi H and Vezzoli A 2020 Folding a single-molecule junction *Nano Lett.* **20** 7980–6

[283] Su T A, Li H, Steigerwald M L, Venkataraman L and Nuckolls C 2015 Stereoelectronic switching in single-molecule junctions *Nat. Chem.* **7** 215–20

[284] Franco I, George C B, Solomon G C, Schatz G C and Ratner M A 2011 Mechanically activated molecular switch through single-molecule pulling *J. Am. Chem. Soc.* **133** 2242–9

[285] Walkey M C *et al* 2019 Chemically and mechanically controlled single-molecule switches using spiropyrans *ACS Appl. Mat. Interfaces* **11** 36886–94

[286] Bruot C, Hihath J and Tao N 2012 Mechanically controlled molecular orbital alignment in single molecule junctions *Nat. Nanotechnol.* **7** 35–40

[287] Li Y, Haworth N L, Xiang L, Ciampi S, Coote M L and Tao N 2017 Mechanical stretching-induced electron-transfer reactions and conductance switching in single molecules *J. Am. Chem. Soc.* **139** 14699–706

[288] Stefani D, Weiland K J, Skripnik M, Hsu C, Perrin M L, Mayor M, Pauly F and van der Zant H S J 2018 Large conductance variations in a mechanosensitive single-molecule junction *Nano Lett.* **18** 5981–8

[289] Camarasa-Gómez M, Hernangómez-Pérez D, Inkpen M S, Lovat G, Fung E D, Roy X, Venkataraman L and Evers F 2020 Mechanically tunable quantum interference in ferrocene-based single-molecule junctions *Nano Lett.* **20** 6381–6

[290] Tang C *et al* 2020 Electric-field-induced connectivity switching in single-molecule junctions *iScience* **23** 100770

[291] Meng L *et al* 2019 Side-group chemical gating via reversible optical and electric control in a single molecule transistor *Nat. Commun.* **10** 1450

[292] Alemani M, Peters M V, Hecht S, Rieder K-H, Moresco F and Grill L 2006 Electric field-induced isomerization of azobenzene by STM *J. Am. Chem. Soc.* **128** 14446–7

[293] Li H B, Tebikachew B E, Wiberg C, Moth-Poulsen K and Hihath J 2020 A memristive element based on an electrically controlled single-molecule reaction *Angew. Chem., Int. Ed.* **59** 11641–6

[294] Godlewski S, Kawai H, Kolmer M, Zuzak R, Echavarren A M, Joachim C, Szymonski M and Saeys M 2016 Single-molecule rotational switch on a dangling bond dimer bearing *ACS Nano* **10** 8499–507

[295] Zhang L *et al* 2018 Electrochemical and electrostatic cleavage of alkoxyamines *J. Am. Chem. Soc.* **140** 766–74

[296] Xin N *et al* 2021 Tunable symmetry-breaking-induced dual functions in stable and photoswitched single-molecule junctions *J. Am. Chem. Soc.* **143** 20811–7

[297] Fahad H M, Hu C and Hussain M M 2015 Simulation study of a 3D device integrating FinFET and UTBFET *IEEE Trans. Electron Devices* **62** 83–87

[298] Yadav C, Kushwaha P, Khandelwal S, Duarte J P, Chauhan Y S and Hu C 2014 Modeling of GaN-based normally-off FinFET *IEEE Electron Device Lett.* **35** 612–4

[299] Lee B-H, Hur J, Kang M-H, Bang T, Ahn D-C, Lee D, Kim K-H and Choi Y-K 2016 A vertically integrated junctionless nanowire transistor *Nano Lett.* **16** 1840–7

[300] Lee B-H, Kang M-H, Ahn D-C, Park J-Y, Bang T, Jeon S-B, Hur J, Lee D and Choi Y-K 2015 Vertically integrated multiple nanowire field effect transistor *Nano Lett.* **15** 8056–61

[301] Gaudenzi R, de Bruijckere J, Reta D, Moreira I D P R, Rovira C, Veciana J, van der Zant H S J and Burzurí E 2017 Redox-induced gating of the exchange interactions in a single organic diradical *ACS Nano* **11** 5879–83

[302] Hofmeister C, Härtle R, Rubio-Pons Ó, Coto P B, Sobolewski A L and Thoss M 2014 Switching the conductance of a molecular junction using a proton transfer reaction *J. Mol. Model.* **20** 2163

[303] Weckbecker D, Coto P B and Thoss M 2021 Molecular transistor controlled through proton transfer *J. Phys. Chem. Lett.* **12** 413–7
[304] Zhang J, Kuznetsov A M, Medvedev I G, Chi Q, Albrecht T, Jensen P S and Ulstrup J 2008 Single-molecule electron transfer in electrochemical environments *Chem. Rev.* **108** 2737–91
[305] Lovat G, Choi B, Paley D W, Steigerwald M L, Venkataraman L and Roy X 2017 Room-temperature current blockade in atomically defined single-cluster junctions *Nat. Nanotechnol.* **12** 1050–4
[306] Xin N, Li X, Jia C, Gong Y, Li M, Wang S, Zhang G, Yang J and Guo X 2018 Tuning charge transport in aromatic-ring single-molecule junctions via ionic-liquid gating *Angew. Chem., Int. Ed.* **57** 14026–31
[307] Sanvito S 2011 Molecular spintronics *Chem. Soc. Rev.* **40** 3336–55
[308] Naaman R and Waldeck D H 2015 Spintronics and chirality: spin selectivity in electron transport through chiral molecules *Annu. Rev. Phys. Chem.* **66** 263–81
[309] Senthil Kumar K and Ruben M 2017 Emerging trends in spin crossover (SCO) based functional materials and devices *Coord. Chem. Rev.* **346** 176–205
[310] Brooke R J, Jin C, Szumski D S, Nichols R J, Mao B-W, Thygesen K S and Schwarzacher W 2015 Single-molecule electrochemical transistor utilizing a nickel-pyridyl spinterface *Nano Lett.* **15** 275–80
[311] Li J, Wu Q, Xu W, Wang H-C, Zhang H, Chen Y, Tang Y, Hou S, Lambert C J and Hong W 2021 Room-temperature single-molecule conductance switch via confined coordination-induced spin-state manipulation *CCS Chem.* 1744–52
[312] Naaman R and Waldeck D H 2012 Chiral-induced spin selectivity effect *J. Phys. Chem. Lett.* **3** 2178–87
[313] Suda M, Thathong Y, Promarak V, Kojima H, Nakamura M, Shiraogawa T, Ehara M and Yamamoto H M 2019 Light-driven molecular switch for reconfigurable spin filters *Nat. Commun.* **10** 2455
[314] Zou D, Zhao W, Cui B, Li D and Liu D 2018 Adsorption of gas molecules on a manganese phthalocyanine molecular device and its possibility as a gas sensor *Phys. Chem. Chem. Phys.* **20** 2048–56
[315] Huang X *et al* 2019 Electric field–induced selective catalysis of single-molecule reaction *Sci. Adv.* **5** eaaw3072
[316] Moreno-Pineda E, Klyatskaya S, Du P, Damjanović M, Taran G, Wernsdorfer W and Ruben M 2018 Observation of cooperative electronic quantum tunneling: increasing accessible nuclear states in a molecular qudit *Inorg. Chem.* **57** 9873–9
[317] Wernsdorfer W and Ruben M 2019 Synthetic Hilbert space engineering of molecular qudits: isotopologue chemistry *Adv. Mater.* **31** 1806687
[318] Winkelmann C B, Roch N, Wernsdorfer W, Bouchiat V and Balestro F 2009 Superconductivity in a single-C60 transistor *Nat. Phys.* **5** 876–9
[319] Goswami S *et al* 2020 Charge disproportionate molecular redox for discrete memristive and memcapacitive switching *Nat. Nanotechnol.* **15** 380–9
[320] Thiele S, Balestro F, Ballou R, Klyatskaya S, Ruben M and Wernsdorfer W 2014 Electrically driven nuclear spin resonance in single-molecule magnets *Science* **344** 1135–8